UNIVERSIDAD DE INVESTIGACIÓN DE TECNOLOGÍA EXPERIMENTAL YACHAY

Escuela de Ciencias de la Tierra, Energía y Ambiente

TÍTULO: MAGNETOMETRY SURVEY APPLIED TO GEOTHERMAL EXPLORATION IN CHACHIMBIRO, NORTHERN OF ECUADOR

Trabajo de integración curricular presentado como requisito para la obtención del título de Geólogo

Autor:

Javier Ricardo Pauta Ordóñez

Tutor:

PhD. Celine Mandon

Urcuquí, septiembre 2021

Urcuquí, 7 de septiembre de 2021

SECRETARÍA GENERAL
(Vicerrectorado Académico/Cancillería)
ESCUELA DE CIENCIAS DE LA TIERRA, ENERGÍA Y AMBIENTE
CARRERA DE GEOLOGÍA
ACTA DE DEFENSA No. UITEY-GEO-2021-00010-AD

A los 7 días del mes de septiembre de 2021, a las 09:00 horas, de manera virtual mediante videoconferencia, y ante el Tribunal Calificador, integrado por los docentes:

Presidente Tribunal de Defensa	Dra. FOSTER ANNA ELIZABETH , Ph.D.
Miembro No Tutor	Dr. SOLTANI DEHNAVI, AZAM , Ph.D.
Tutor	Dra. MANDON CELINE LUCIE , Ph.D.

El(la) señor(ita) estudiante **PAUTA ORDOÑEZ, JAVIER RICARDO**, con cédula de identidad No. **1104777626**, de la **ESCUELA DE CIENCIAS DE LA TIERRA, ENERGÍA Y AMBIENTE**, de la Carrera de **GEOLOGÍA**, aprobada por el Consejo de Educación Superior (CES), mediante Resolución **RPC-SE-10-No.031-2016**, realiza a través de videoconferencia, la sustentación de su trabajo de titulación denominado: **MAGNETOMETRY SURVEY APPLIED TO GEOTHERMAL EXPLORATION IN CHACHIMBIRO, NORTHERN OF ECUADOR**, previa a la obtención del título de **GEÓLOGO/A**.

El citado trabajo de titulación, fue debidamente aprobado por el(los) docente(s):

Tutor	Dra. MANDON CELINE LUCIE , Ph.D.

Y recibió las observaciones de los otros miembros del Tribunal Calificador, las mismas que han sido incorporadas por el(la) estudiante.

Previamente cumplidos los requisitos legales y reglamentarios, el trabajo de titulación fue sustentado por el(la) estudiante y examinado por los miembros del Tribunal Calificador. Escuchada la sustentación del trabajo de titulación a través de videoconferencia, que integró la exposición de el(la) estudiante sobre el contenido de la misma y las preguntas formuladas por los miembros del Tribunal, se califica la sustentación del trabajo de titulación con las siguientes calificaciones:

Tipo	Docente	Calificación
Miembro Tribunal De Defensa	Dr. SOLTANI DEHNAVI, AZAM , Ph.D.	9,8
Presidente Tribunal De Defensa	Dra. FOSTER ANNA ELIZABETH , Ph.D.	9,5
Tutor	Dra. MANDON CELINE LUCIE , Ph.D.	9,3

Lo que da un promedio de: **9.5 (Nueve punto Cinco)**, sobre 10 (diez), equivalente a: **APROBADO**

Para constancia de lo actuado, firman los miembros del Tribunal Calificador, el/la estudiante y el/la secretario ad-hoc.

Certifico que *en cumplimiento del Decreto Ejecutivo 1017 de 16 de marzo de 2020, la defensa de trabajo de titulación (o examen de grado modalidad teórico práctica) se realizó vía virtual, por lo que las firmas de los miembros del Tribunal de Defensa de Grado, constan en forma digital.*

PAUTA ORDOÑEZ, JAVIER RICARDO
Estudiante

Dra. FOSTER ANNA ELIZABETH , Ph.D.
Presidente Tribunal de Defensa

ANNA ELIZABETH FOSTER
Digitally signed by ANNA ELIZABETH FOSTER
Date: 2021.09.08 09:01:02 -05'00'

Dra. MANDON CELINE LUCIE , Ph.D.
Tutor

CELINE LUCIE MANDON
2021.09.07 13:35:20 -05'00'

UNIVERSIDAD YACHAY TECH

Dr. SOLTANI DEHNAVI, AZAM , Ph.D.
Miembro No Tutor

AZAM SOLTANI DEHNAVI

Firmado digitalmente por AZAM SOLTANI DEHNAVI
Fecha: 2021.09.07 11:53:31 -05'00'

TERÁN ROSALES, ANDREA YOLANDA
Secretario Ad-hoc

ANDREA YOLANDA TERAN ROSALES

Firmado digitalmente por ANDREA YOLANDA TERAN ROSALES
Fecha: 2021.09.07 11:37:51 -05'00'

AUTORÍA

Yo, **Javier Ricardo Pauta Ordóñez**, con cédula de identidad 1104777626, declaro que las ideas, juicios, valoraciones, interpretaciones, consultas bibliográficas, definiciones y conceptualizaciones expuestas en el presente trabajo; así cómo, los procedimientos y herramientas utilizadas en la investigación, son de absoluta responsabilidad de el/la autora (a) del trabajo de integración curricular. Así mismo, me acojo a los reglamentos internos de la Universidad de Investigación de Tecnología Experimental Yachay.

Urcuquí, septiembre 2021.

Firmado electrónicamente por:
JAVIER RICARDO
PAUTA ORDONEZ

____

Javier Ricardo Pauta Ordóñez
CI: 1104777626

AUTORIZACIÓN DE PUBLICACIÓN

Yo, **Javier Ricardo Pauta Ordóñez,** con cédula de identidad 1104777626, cedo a la Universidad de Investigación de Tecnología Experimental Yachay, los derechos de publicación de la presente obra, sin que deba haber un reconocimiento económico por este concepto. Declaro además que el texto del presente trabajo de titulación no podrá ser cedido a ninguna empresa editorial para su publicación u otros fines, sin contar previamente con la autorización escrita de la Universidad.

Asimismo, autorizo a la Universidad que realice la digitalización y publicación de este trabajo de integración curricular en el repositorio virtual, de conformidad a lo dispuesto en el Art. 144 de la Ley Orgánica de Educación Superior

Urcuquí, septiembre 2021.

Firmado electrónicamente por:
JAVIER RICARDO
PAUTA ORDONEZ

____

Javier Ricardo Pauta Ordóñez
CI: 1104777626

Dedication

To my beloved family, which always have been there to give me their unconditional love and support. Especially my grandparents Pepito and Catita, my parents Jhon and Marlene, and my brothers and sister David, Verónica and Pablo.

Javier Ricardo Pauta Ordóñez

Acknowledgments

I am very grateful to all the people that have been part of my life during this path. Infinite thanks to all the teachers that I met since the start of the university and turned on my passion and love for science, included Nicola Di Teodoro, Juan Lobos, Victor Vilas, and many more teachers that passed through the university when I was in Tronco común.

Thanks to all the teachers that belong to the Geology school, those who are gone and those who stay. Thanks in especial to Edwin and Alejandra that remembered my admiration for life and living beings which made me to take the decision to choose geology as career.

Thanks in especial to the best teachers I ever met and my thesis advisors Celine and Elisa. Work whit them has been one of the best and inspiring experiences of Yachay Tech. They always supported me not only in the academics but also in my emotional life. It wouldn´t be possible to finish my thesis without them.

I also would like to thank INPC for teach me and provide the magnetometer used in this work and to CELEC for helping me with the access to the area and previous studies published from Chachimbiro.

Finally, I would like to say thanks to all the people that in a way to another have been and essential part of my life. Thanks to friends María, Gissel, Nico, Jair, Juan, Cristina, Carlos, Erika and Alex, for being my second family. To my geofamily and all the classmates that I had during the career, they are amazing people that taught me a lot and I will always remember. Also, thanks to Daniela for having been a part of my life and helping me to keep in the university.

Javier Ricardo Pauta Ordóñez

Resumen

Los estudios geofísicos son una forma eficiente de obtener información de las estructuras bajo la superficie. El método magnético es especialmente útil para detectar estructuras poco profundas y cambios en la magnetización debido a varios procesos, tales como el fallamiento y las alteraciones hidrotermales. A pesar de la riqueza de recursos geotérmicos en América del Sur, su uso para generación de energía eléctrica es muy limitado. En Ecuador, la mayoría de los proyectos geotérmicos están en fases de prospección y exploración inicial. Chachimbiro, ubicado al norte del Ecuador, es uno de los sitios con mayor potencial a convertirse en una planta de energía geotérmica. El objetivo de este trabajo es el de realizar estudios complementarios para mejorar el modelo existente del sistema geotérmico. Para esto, realizamos un estudio magnético de alta resolución con un distanciamiento de ~30 m entre puntos, alrededor del área del pozo Chachimbiro 1, y así comprender mejor las estructuras poco profundas que están sobre el reservorio, de la misma forma se realizaron dos líneas de estudio con un distanciamiento de ~5 m entre puntos y perpendicularmente a las fallas locales. Luego se compararon estos resultados con datos magnetelúricos y gravimétricos, que son menos precisos para detectar rasgos poco profundos. La comparación con estudios previos mostro que las fallas y la distribución de anomalías magnéticas de este estudio se ajustan con lo descrito en estudios previos. Nuestro estudio magnético fue útil para diferenciar las anomalías magnéticas relacionadas con topografía, fallamiento y alteraciones hidrotermales. Además, este estudio contribuirá a tener un mejor entendimiento del área, lo que es necesario para realizar futuras perforaciones en el área, que es potencialmente la primera planta de energía geotérmica del país.

Palabras Clave: Magnetometría, métodos Geofísicos, sistemas Geotermales, volcán Chachimbiro, Deteccion de fallas.

Abstract

Geophysical surveys are efficient ways to obtain information on subsurface structures. The magnetic method is especially useful to detect shallow structures and changes in magnetization due to several processes, such as faulting and hydrothermal alterations. Despite the richness of available geothermal resources in South America, their use for electricity production is very limited. In Ecuador, geothermal projects in Ecuador are still at very initial phases of prospection and exploration. Chachimbiro, in northern Ecuador, is one of the potential site for developing a geothermal power plant. The objective of this project is to provide complementary studies to improve the existing model. We performed high resolution magnetometry survey with ~30 m spacing between points around the drilling area to get a better understanding of the shallow structure above the reservoir, as well as two survey lines with ~5 m spacing perpendicular to local faults. We then compared our results with existing magnetotelluric and gravimetric data, which are less precise for shallow structural features. Comparison with previous works shown that faults location and low magnetic anomalies distribution of this study fits with the locations described in previous studies. Our magnetic survey was usefulness to differentiate magnetic anomalies related to topography, faulting and hydrothermal alterations. Our study thus contributes to a better knowledge of the area, needed for future drilling planning of potentially, the first geothermal power plant of the country.

Keywords: Magnetometry, Geophysical methods, Geothermal systems, Chachimbiro volcano, Fault detection.

Table of Contents

Table of Figures

1. Introduction

1.1. Fossil fuels and environmental impacts

Energy is a fundamental pillar in the development of the economy and technology. Nowadays, the principal sources of energy are fossil fuels, petroleum, coal, and natural gas. These sources are located under the ground and are a product of organic matter accumulation in anoxic conditions.

The main problem related to fossil fuel use is that their combustion releases several toxic gases (CO_2, NO_x, SO_x, and CH_4, also known as greenhouse gases) and other small particles (10 micrometers or less) to the atmosphere, causing environmental damage (Withagen, 1994; Williams, 2002). A significant accumulation of these gases leads to greater retention of the solar radiation that enters the Earth's atmosphere inducing global warming, what is known as the greenhouse effect. It is a natural process that would normally occur in periods of hundreds of thousands of years but is currently accelerating due to the increased use of these fuels (e.g. Al-Ghussain, 2019). Scientists have shown that this effect is linked to other environmental impacts such as melting of ice in the poles, rise of sea levels, acidification of oceans, among others (e.g. Karl and Trenberth, 2003). Moreover, fossil fuels are also considered finite resources, with estimates that they would run out by the middle to the end of the 21th century (e.g. Hoel, 1996; Dincer and Rosen, 1999). This concern has created the need to search for alternative energy sources that generate fewer pollutants to the environment, clean energies that can be exploited, generating significantly lower greenhouse gas emissions than fossil fuels. A good example of success in using alternative energy sources is Iceland, with almost 86% of its energy generation coming from renewable sources (68% geothermal, 18% hydropower). They use geothermal energy directly in industry, house heating, farming, and more (Ragnarsson, 2015).

Furthermore, these energies should be renewable, meaning that they will not be exhausted during human time scales. These new energies currently in use are the wind energy, hydraulic, solar, geothermal, and biomass. The largest inconvenience for the exploitation of renewable energies at a great scale is the high costs in comparison to fossil fuels. During the last decades, the prices have become more competitive, allowing the implementation of power plants that cover farms and houses' energetic needs, even for towns and cities. In some countries, renewable energies are the cheapest alternative because of the abundance or prevalence of local energy sources (Dincer and Rosen, 1999).

Geothermal energy is the heat contained within the Earth. This energy, available almost everywhere on Earth's surface, can be recovered and exploited for human use. Geothermal heat mainly results from radioactive decay of potassium, thorium, and uranium in the crust (~50 %), with a small contribution from the friction along continental margins and remnant energy accumulated during primordial accretion. Earth is slowly cooling from its hot interior outwards to the cold atmosphere. The geothermal gradient is the average increase of the Earth's temperature with increasing depth. The average geothermal gradient of the Earth is about 2.5 – 3 ºC every 100 m (Dickson and Fanelli, 2004). This average geothermal gradient is representative of most places on Earth while others, such as volcanoes, have higher gradients. The rocks' temperature increases much faster with depth at these locations, allowing hot water reservoirs to form at much more shallow depths.

1.2. Geothermal systems

Geothermal systems can be found in different parts of the world, but only those with a normal or abnormally high gradient are the most exploitable, generally related to tectonic margins. These systems are characterized by their temperature; low-temperature systems up to 100 ºC and high-temperature systems range from 100 to >400 ºC (Dickson and Fanelli, 2004). Three elements are essential to form a geothermal system: a heat source, a reservoir, and a fluid. The heat source can be magmatic intrusions that are relatively shallow (~10 km) or magmatic chambers at dormant volcanoes, from which the heat is conducted up to the overlying rocks. The reservoir is formed by a layer of porous rocks in which the fluids are accumulated. It is overlain by a layer of impermeable rocks (also called the cap rock) and connected to the surface by faults where water can be expelled. An efficient geothermal system requires replenishing the system's fluid with meteoric water (i.e., rainwater). Once heated, the geothermal water interacts with rocks increasing the number of cations, and can become acidic if the magmatic source releases magmatic gases. The mechanism that controls geothermal systems is fluid convection, occurring due to changes in fluid density. The heat from the source causes the thermal expansion of fluids, making them less dense. These fluids with low-density rise and are replaced by cooler and thereby denser fluids.

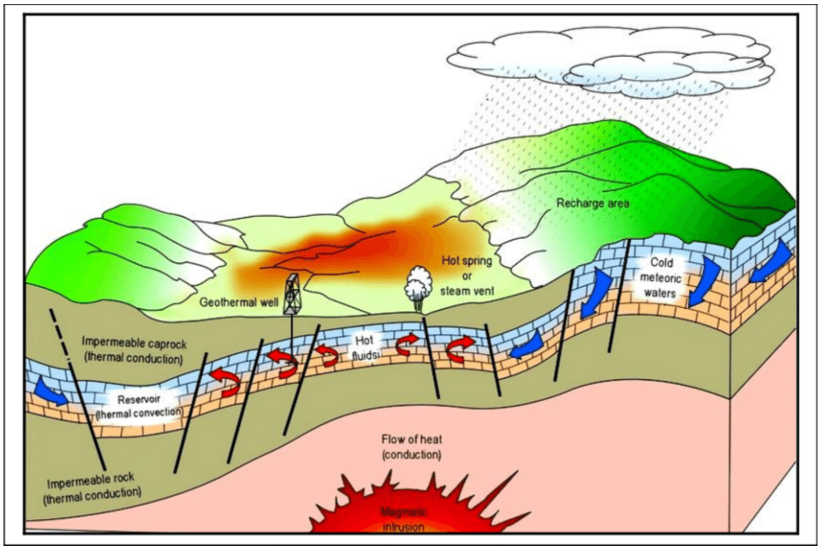

Figure 1: Schematic representation of an ideal geothermal system, image from Syukri et al., (2018).

The system can be explained as infiltrated meteoric water being heated by hot rocks and stored in a permeable reservoir. Convecting water transfers heat from the source to the surface, the reservoir being further refilled with meteoric water. An ideal geothermal system is represented in Figure 1 as a schematic model. Geothermal systems can be classified considering a variety of characteristics. Figure 2 shows a classification based on temperature, enthalpy, and physical state (Saemundsson et al., 2011).

Low-temperature (LT) systems with reservoir temperature at 1 km depth below 150°C. Often characterized by hot or boiling springs.	***Low-enthalpy*** geothermal systems with reservoir fluid enthalpies less than 800 kJ/kg, corresponding to temperatures less than about 190ºC.	***Liquid-dominated*** geothermal reservoirs with the water temperature at, or below, the boiling point at the prevailing pressure and the water phase controls the pressure in the reservoir. Some steam may be present.
Medium-temperature (MT) systems with reservoir temperature at 1 km depth between 150- 200°C.		
High-temperature (HT) systems with reservoir temperature at 1 km depth above 200°C. Characterized by fumaroles, steam vents, mud pools and highly altered ground.	***High-enthalpy*** geothermal systems with reservoir fluid enthalpies greater than 800 kJ/kg.	***Two-phase*** geothermal reservoirs where steam and water co-exist and the temperature and pressure follow the boiling point curve.
		Vapour-dominated *reservoirs* where temperature is at, or above, boiling at the prevailing pressure and the steam phase controls the pressure in the reservoir. Some liquid water may be present.

Figure 2: Geothermal systems classification based on temperature, enthalpy, and physical state, according to Saemundsson et al. (2011).

Saemundsson (2011) also provide another classification based on the geological setting: 1) Volcanic geothermal systems (e.g geothermal field north of San Francisco, Surtsey, Iceland) in which the flow is mainly controlled by fractures and fault zones, associated with volcanic activity and located close to or inside volcanic complexes; 2) Convective fracture-controlled systems (e.g Soultz-sous-Forêts in France) with a heat source from crust at depth in tectonically active areas. Geothermal water flows at depths more than 1 km, mainly through vertical fractures; 3) Sedimentary geothermal systems (e.g. geothermal systems found along United States pacific coast, such Appalachia) present in several major sedimentary basins worldwide in zones with an anomalous geothermal gradient. This type of system is primarily conductive, but some convective systems may be contained in sedimentary rocks; 4) Geo-pressured systems related to oil and gas reservoirs (e.g. Texas and Luisiana gulf coasts) where fluids caught in stratigraphic traps have lithographic pressure; 5) Hot dry rock (HDR) or engineered geothermal systems (EGS) (e.g. some systems in Japan, Australia, France, Germany), consisting of the volume of rock heated by high heat flow or volcanism with relatively low or no permeability; 6) Shallow resources, referring to the usual heat flux in near-surface formations and thermal energy that is stored in rocks and warm groundwater systems near the surface.

This variety of geothermal systems implies that the Earth's available thermal energy is immense, but people can use only a modest fraction. Human use is limited to areas where geological conditions permit a carrier (water in the liquid phase or steam) to transfer the heat from deep hot zones to or near the surface (Lund and Boyd, 2016). The amount of usable energy from geothermal sources varies with depth and by extraction method. Figure 3 shows some of the worldwide uses of geothermal energy.

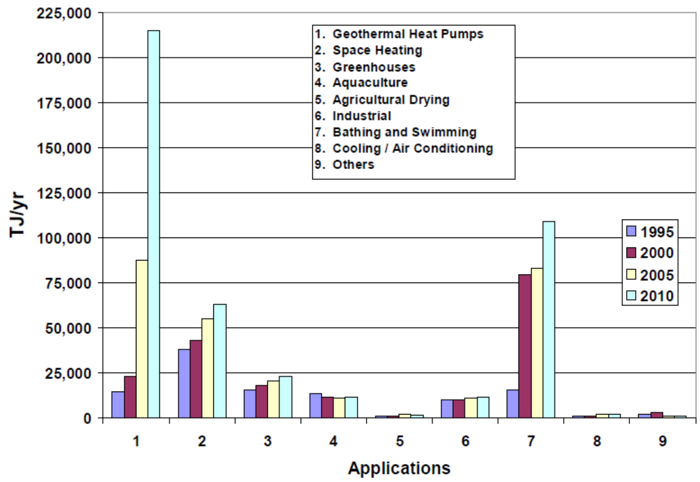

Figure 3: Comparison of worldwide geothermal energy utilization in TJ/year for 1995, 2000, 2005, and 2010. Image from Lund et al., (2010).

1.3. Geothermal prospection

The primary purpose of geothermal exploration is to define the reservoir's location, volume, shape, and structure and determine its characteristics such as fluid type, temperature, and how much energy can be produced. Exploration can be performed using geological, geochemical, and geophysical data. Geological prospection is usually the first step in geothermal prospection. It starts with observations of surface features like fumaroles, geysers, hot springs or steaming ground, or any other feature that can give information about the system and map faults and hydrothermal alteration regions (Gupta and Roy, 2006).

1.3.1. Geochemical prospection

Geochemical prospection relies on the chemical analysis of liquids and gases from a geothermal system to determine the nature and temperature of fluids in the reservoir. According to Óskarsson and Ármannsson (2015), geothermometry (fluid temperature estimate based on chemical composition) is based on the following assumptions: 1) The fluid reached the local equilibrium with secondary minerals in the reservoir at a specific temperature. The chemical equilibria have to be sensitive to temperature. 2) The composition of the fluids does not change during their rise to the surface. Solute geothermometry is based on minerals' solubility in the water and is measured by the concentration or activity, commonly utilizing silica geothermometers for it. 3) Finally, gas geothermometry assumes the gases equilibrium and uses gas geothermometers to estimate temperatures from gas concentration in steam. The most common gases used are the geothermal gases CO_2, H_2S, H_2, and CH_4. Phuong et al. (2012) used geothermal fluids applied in geothermal prospection in Indonesia. They did a soil gas survey for radon (Rn), thoron (Tn), CO_2, mercury (Hg), and the chemical analysis of the hot spring waters in the Ungaran geothermal field. Chemical analysis showed a water temperature range from ~18 ºC to ~56 ºC, while the gas soil survey revealed several fault systems trending NNE-SSW and WNW-ESE. The presence of these same gases (Rn, Tn and CO_2) also helped identify a fracture zone that is allowing the fluids to migrate to the surface (Phuong et al., 2012).

1.3.2. Geophysical prospection

Geophysical surveys are the only way to obtain a detailed delineation of the subsurface structures, other than drilling (Gupta and Roy, 2006). These methods take into consideration the physical properties of the Earth. A geophysical survey may be helpful to delineate the geothermal area, and locate aquifers and other geological structures. Some of the physical factors with importance in a geothermal system are temperature, porosity, permeability, fluid salinity, and pressure (Georgsson, 2009). Direct geophysical methods applied to the Earth's surface cannot measure these properties. However, some methods may give indirect information about the geothermal systems: electrical conductivity, propagation of seismic waves, density, magnetic susceptibility (Dickson and Fanelli, 2004). According to Georgsson, one should distinguish between direct and indirect methods. Direct methods provide information on the factors affected by geothermal activity and include thermal, electromagnetic, electrical methods, and self-potential. On the other hand, passive methods give information that may reveal structures and geological bodies that would help understand the system, including magnetic surveys, gravity surveys, active seismic methods, and passive seismic monitoring.

Thermal methods consist of taking direct measurements in the field to determine temperature. These methods would help to determine the Earth's surface temperature, thermal inertia and thermal radiation from Earth's surface. It is limited to shallow depths (~10 m). Drilling is an active method that can be combined with measurements of the ground temperature, but it is usually expensive (Domra Kana et al., 2015).

The transient electromagnetic method (TEM) creates a grounded dipole that emits a constant magnetic field. A secondary induced field decays through time and it is monitored by measuring the voltage on the surface. TEM measurements allow the study of structures at depths from 1-1.5 km. Studies in Iceland helped to create maps down to 600 m depth, showing a low-resistivity-body with a high-resistivity core that reaches temperatures above 250 ºC (Georgsson, 2009). Magnetotelluric method (MT) measures the Earth's natural electric field and magnetic field in orthogonal directions, both being dependent on the subsurface resistivity (Sircar et al., 2015). MT detects resistivity anomalies associated with faults, or the presence of a cap rock (i.e. low conductivity materials) and is thus useful to deduce the subsurface geology. MT studies from Sircar et al., (2015) in Arabia Saudi helped create 2D and 3D models which show the structure of the reservoir, composed by a shale/sandstone body between two layers of high-resistivity basalts. Electrical methods the principle says that the distribution of electrical potential in the ground around a current-carrying electrode depends on the electrical resistivities and distribution of the surrounding soils and rocks. This is useful because the electrical properties of the rocks are affected also by for example temperature and water content (Manzella, 1999). Electrical surveys show anomalies with low resistivity associated to a subsurface reservoir. The self-potential (SP) method is useful to understand the groundwater movement in the system.

The seismic method uses seismic waves that travel along the surface and subsurface through different rock material, and that are refracted or reflected by discontinuities. This allows a user to measure the velocity distribution, anomalies and attenuation of seismic waves. The method can be employed in a passive or active way (Domra Kana et al., 2015). Active methods use hammers or explosions to create seismic waves, and the information that can be obtained are the density of the formations, porosity, texture, boundaries and discontinuities. Passive methods use natural seismic activity and are useful to delineate active faults and permeable zones, as well as predict locations of hot bodies.

The gravimetric method consists of measurements of gravity anomalies in the Earth's surface derived from the density differences of the rocks in the subsurface. This method allows to determine masses of rock with high or low density which is possible by comparing it with the gravitational field measured (Georgsson, 2009). It also allows to search small, local, geological structures (Hammer, 1939). Studies from Hochstein and Hunt, (1970) in New Zealand helped to provide the approximate depth of the greywacke basement beneath the Broadlands area.

Magnetic methods measure the Earth's magnetic field intensity, usually vertical magnetic gradient or total magnetic field. Anomalies in the magnetic field are due to differences in magnetic susceptibilities (i.e. differences in magnetizations) and they are often produced by remanent magnetism, carried by a ferrous body. The magnetic method is useful to locate intrusive bodies, tracing individual buried dykes and faults or estimating their depth (Bjornsson, 1980). Common sources of anomalies include dykes, faults, lava flows or iron-rich sediments (Chandra, 2015). Magnetic anomalies are useful to delineate high-temperature hydrothermal/geothermal systems; this is possible because several geothermal processes may alter the rock magnetization, going through a demagnetization of minerals or altering them to a less magnetic mineral (Caratori Tontini et al., 2016). Magnetic studies in Mahallat, Iran shows a 3D model of the area with an igneous body at a depth of approximately 1 km (Mohammadzadeh-Moghaddam et al., 2012).

1.4. State of geothermal prospection in Ecuador

To this day, geothermal energy in Ecuador has been exploited for direct uses only, such as bathing resorts and swimming pools, despite the fact that geothermal exploration started in 1978 under the supervision of the former Instituto Nacional de Electrification (INECEL) with the help of several specialists in geology, geochemistry and geophysics. This group explored several areas with recent volcanic activity or with surficial features like hot springs. In 1980 they determined priority geothermal areas, based on location, volcanic features (intensity, volume, frequency and age), hydrological conditions and surficial chemical characteristics. Following this, a collaborative study with Colombia to determine the viability of the Tufiño-Chiles-Cerro Negro area was initiated in 1983, and several geophysical studies were done in 1989 in Chachimbiro, in the northern part of Ecuador. All geothermal projects in the country ended in 1993 and were abandoned until 2007 (Piedra Lara, 2011). In 2008, there was a new proposal to change the productive and energetic matrix of the country, leading to studies in geothermal areas again. From 2010 until today, the Corporación Eléctrica del Ecuador (CELEC EP) has carried out studies in several geothermal areas of the country (Villacreses Baque et al., 2017).

In the last years, government policies have aimed for the development of renewable resources such as wind, solar, biomass and geothermal to reduce the use of fossil fuels and related gases emission. During the last decade, a geothermal plan was launched for electricity generation based on 11 potential geothermal sites: Chachimbiro, Chalpatán, Chacana-Jamanco, Chalupas, Guapán, Chacana-Cachiyacu, Tufiño, Chimborazo, Chacana-Oyacachi, Baños de Cuenca and Salcedo (Beate and Urquizo, 2015). Geological, geophysical and geochemical measurements have been done for Chachimbiro, Chacana-Jamanco and Chacana-Oyacachi projects (Beate and Urquizo, 2015). However, the only progressing project to date is that of Chachimbiro, with the first prospection well drilled in 2017 and more planned for the coming years.

2. Problem statement

Ecuador is a country with high volcanic activity. Previous government studies with assistance of foreign programs determined a geothermal potential at 1700 Megawatts electric (MWe) in 1999. Despite this great potential, there are still no geothermal power plants in Ecuador, nor an extensive use of this resource. One of the reasons, besides the investment problem, could be the lack of knowledge on how to use various tools for geothermal exploration and how to interpret the data. In Chachimbiro, the geothermal potential is estimated to be 81 MWe (Lloret and Labus, 2014). Several geophysical and geochemical surveys have been done, starting with a pre-drilling stage in 2012 and a drill stage in 2017. The methods used in that stage were magnetotellurics, gravimetry and magnetometry. However, many of these studies were led by foreign entities, without creating the local capacity to continue or expand these prospection surveys. The present study aims at being a complementary study of the main focus area in Chachimbiro, utilizing magnetometry to try to determine hydrothermal alteration zones, cap rocks and fault locations in the drilling area.

3. Objectives

- Collect the available geophysical and geological information.
- Perform a large-scale ground magnetometry survey with an evenly spaced grid in the area of the drilling sites.
- Analyze the magnetometry data to add knowledge about the subsurface geology of the area.
- Compare it with the newly collected data to understand the area's shallow geology.
- Determine the usefulness of magnetometry to locate faults in geothermally altered terrain.

4. Chachimbiro volcanic complex

4.1. Geological setting

The interaction of the Nazca, the South American and Cocos Plates is the main cause of the volcanism and tectonism in Ecuador. This resulted in the formation of the Andean Cordillera, which is conformed of two mountain ranges, the Cordillera Occidental to the west and the Cordillera Real to the east, with the Inter-Andean Valley depression in between (Figure 4A).

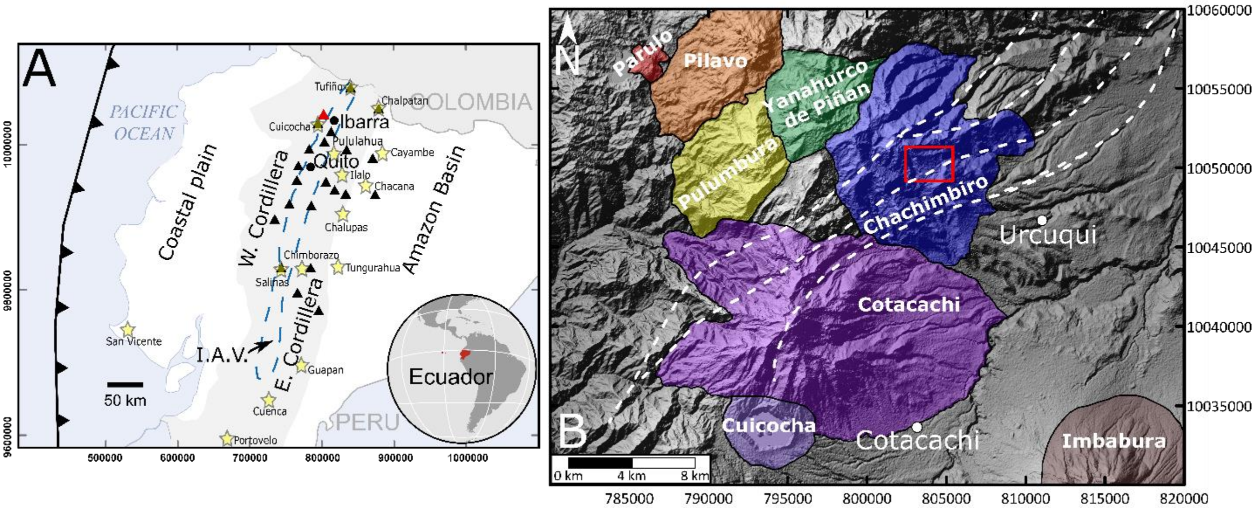

Figure 4: Location map. A) geologic map of Ecuador with the location of the study area in red square; black triangles are Quaternary volcanos while red triangle is the Chachimbiro volcano. Yellow stars show the location of other geothermal areas in Ecuador. B) Geologic map of the area with the principal volcanic complexes close to Chachimbiro; white dots show Urcuqui and Cotacachi towns and dashed lines represent major faults in the zone. Red square represents the study area.

The Chachimbiro volcanic complex is located in Northern Ecuador within the Imbabura province (Figure 4B), marking the limit between the Western Andean Range and the Inter-Andean Valley. The average elevation around the Chachimbiro complex is 2560 m, and the topography is dominated by the Cotacachi and Yanaurcu de Piñan stratovolcanoes. Chachimbiro, alongside Cotacachi, Cuicocha, Pulumbura, Yanaurcu de Piñan and Pilavo volcanoes, belongs to the Andean Volcanic front of Ecuador. Except for Cuicocha, all the volcanoes in this zone are considered dormant volcanoes.

The volcanic edifice of Chachimbiro has a diameter of ~12 km, rising 1500 m above the Inter-Andean Valley. The basement of the Chachimbiro complex comprises Cretaceous rocks accreted in a subduction zone. To the west of the complex, the basement is composed mainly of basic and intermediate volcanic rocks, emplaced in a submarine environment and covered by discontinuous turbidite deposits, pyroclastic and epiclastic continental deposits that belong to Silante formation (Granda, 2011), deposited during the Late Cretaceous to Early Miocene (Vallejo Cruz, 2007). To the east, the basement is composed of distal volcanic deposits covering sedimentary deposits from Miocene and Pliocene, which are affected by active NNE and NE faults with sinistral movement (Bernard et al., 2009), which determine the deposition zone during eruptive events. These faults are also zones of high degassing (Bellver-Baca et al., 2019). The Pallatanga formation, mainly composed of basaltic rocks, is considered the volcanic basement of the Western Cordillera. The Rio Cala Group overlays the Pallatanga formation and is mainly composed of massive basaltic to andesitic lavas, volcanic breccias, and volcanoclastic sandstones. The Natividad formation is related to the Rio Cala Group, composed of sedimentary rocks of the complex, correlated with turbidites deposited during the Eocene. This formation is exposed on the southeastern flank of the complex (Granda, 2011).

The eruptive history of Chachimbiro is described by Bernard et al., 2009. According to this study, the eruptive history is divided into four periods; three of them formed the volcano's domes. The first activity started forming the Huanguillaro dome during the Middle Pleistocene, mainly composed of calc-alkaline andesitic lava. The dome subsequently was destroyed by a giant landslide, depositing debris-avalanche deposits up to 25 km away from the source and leaving a caldera at the edges of the Huanguillaro and Conrayaro. The Tumbatu edifice formation characterizes the second period, growing within the depression of the collapsed Huanguillaro during the Late Pleistocene. Three main stages are responsible for the formation of this edifice; the first stage is characterized by the extrusion of dacitic domes producing large pyroclastic flows, resulting in block and ash flow deposits. More acidic lavas and explosive activity characterize the second stage, dated approximately 44 kyr. The corresponding units are ash and pumice flow deposits, reaching a thickness of 70 cm and traveling as far as 25 km from the source. The last stage is characterized by Plinian-type eruptions followed by new dacitic dome extrusions with block and ash flows and later emissions of andesitic tephra. This edifice also suffered a landslide related to an explosive event, forming a debris-avalanche deposit that even reached the Chota valley. The third period is characterized by the extrusion of several dacitic domes. One of the major eruptions resulted in the 3640 – 3510 BC blast, during which a dome located at the foot of La

Viuda peak violently exploded in a blast directed towards the south (Bernard et al., 2014). This extruded rhyodacite dome was formed by magma originating from two magmatic reservoirs emplaced at ~14.4 and 8 km depth, with temperatures of ~940 ºC and ~860 ºC, respectively. The last activity was the formation the Huga dome, accompanied by emission of andesitic tephras. Then, the volcano had a quiet period with high erosion in the volcanic edifice and a later remobilization of volcanic slope during a final dacitic tephra emission stage associated with Loma Albuji.

Previous studies observed several hydrothermal alterations which are: mesothermal propylitic (chlorite-epidote-calcite); which affected basaltic rocks not related with current thermal activity; Epithermal propylitic (smectite-chlorite), related with acid fluids and current thermal activity; argillic (smectite-kaolinite), related with hot springs and fumaroles in the area, also considered to be related with the current thermal activity; Advanced argillic (opal-smectite-kaolinite), which is related with fumaroles with high H_2S concentrations, and also considered related with the current argillic alteration; Carbonization, related with carbonate minerals deposited along structures where CO_2 gas is released (Pilicita, 2016).

4.2. Chachimbiro geothermal system

Previous works, such as the magnetotelluric (MT) studies from Pilicita (2016), determined that hydrothermal alteration is controlled by the right lateral strike - slip Azufral fault system (which includes the Pijumbi fault), trending NE-SW, and the Chachimbiro fault system and NW-SE lineaments. CO_2 and H_2S emissions are found close to the areas with hydrothermal alterations. Gas flow and alteration disappear in the NW direction from this point and no hot springs exist further than the Pijumbi and Azufral stream intersection. This may suggest that the Pijumbi fault is the boundary for the geothermal system. In terms of fluid geochemistry, studies showed springs with mixed chloride-bicarbonate composition and maximum temperature reaching 61 ºC, indicating reservoir temperature of between ~235 and ~265 ºC at the deepest part of the reservoir (Aguilera et al., 2005; Inguaggiato et al., 2010; Gherardi and Spycher, 2014). The main stress of the regional structural system is oriented in an E-W direction, creating a subparallel fault system oriented NE-SW, including two contemporaneous structures, theAzufral fault and Chachimbiro fault systems. This would allow the upward movement of fluids in the system.

Also, Bernard et al. in 2014 studied the last volcanic eruption between 3640 – 3510 years BC resulting in an extruded rhyodicite dome in between ~650 m wide and ~225 m high. Two reservoirs located 6.3 km east from the magma chamber were emplaced at ~14.4 and 8 km depth. The temperatures estimated were ~940 ºC and ~860 ºC. The depth of the clay minerals is described by Guillén, (2020), which estimate a smectite layer around ~200 m and an illite layer around ~250 m depth.

4.2.1. *Previous geophysical studies*

Several geophysical studies were carried out in the geothermal area of Chachimbiro, including Magnetotellurics (MT), Transient Electromagnetic Method (TEM), and resistivity method. Those studies helped to have an idea of the geothermal system of Chachimbiro, the estimated depth of the cap rock, and the degree of hydrothermal alteration in the geothermal area of Chachimbiro.

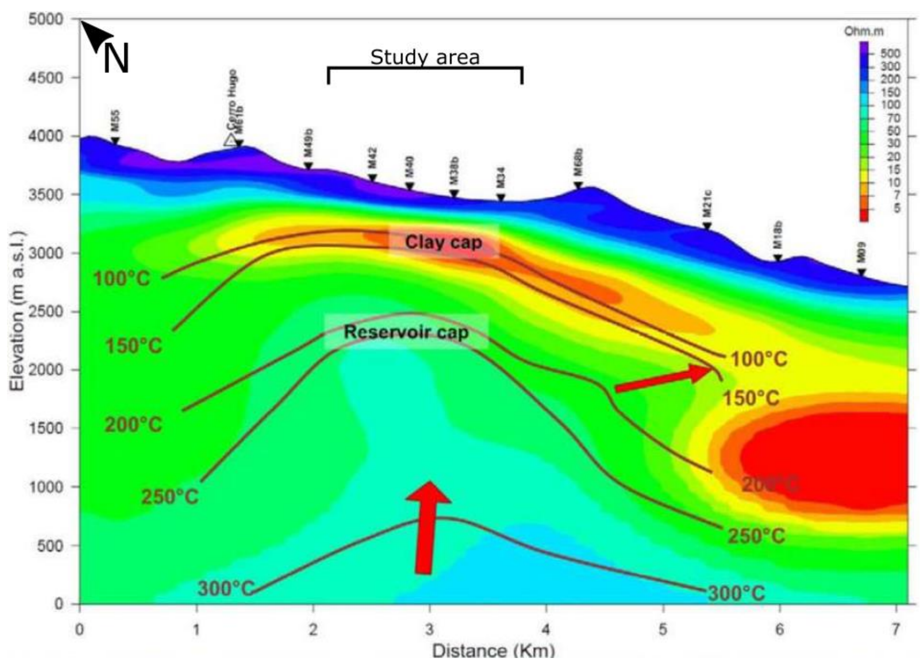

Figure 5: NW-SE resistivity cross-section, modified after Torres Calderón, (2014).

The study from Torres Calderón from 2014 combined two geophysical methods to generate a conceptual model of the geothermal system. Magnetotelluric (MT) data was collected using 70 stations and arranged in a grid of 150 m x 150 m x 15-100 m, while the Transient Electromagnetic Method (TEM) was applied using 36 stations. Figure 5 presents the final inversion model combining the two methods showing resistivity cross-sections. These are interpreted to show a high-temperature system with a low-resistivity cap above a high-resistivity core. Isotherms were sketched using the TEM resistivities and geochemical data.

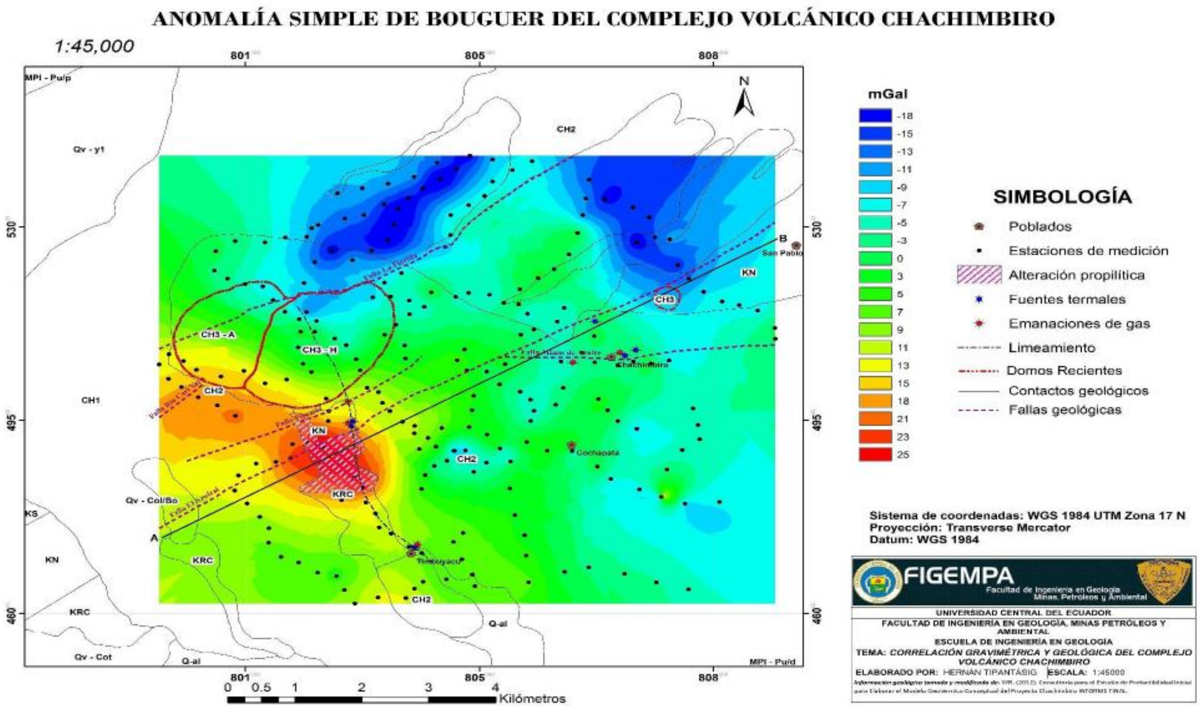

Figure 6: Correlation of the gravimetric results with structural and geological information from the Chachimbiro volcanic Complex, image from Córdova Tipantásig, (2017).

Córdova Tipantásig (2017) used the gravimetric method by measuring relative gravity from 234 stations georeferenced with a GPS. The parameters taken into account for the study were location, topography, accessibility and a distance between stations of ~250 m. The northern area shows an abrupt change between low and intermediate gravimetric values, while, the middle part shows changes between high and intermediate values. This changes in the gravimetric values may indicate a density change of related rocks and the presence of a lineament NE-SW direction and other with NW-SE direction.

Figure 6 shows a simple Bouguer anomaly map, suggesting that high anomaly areas could be related to high density from basement rocks with hydrothermal alteration. Also, the author suggests that an intrusive body is related to previous volcanism of the volcanic complex. High densities can be related to propylitic alteration generated by the fluids that filled rock cavities, reducing its permeability and increasing cohesion. On the other hand, intermediate gravimetric values could be related to lower densities from a mixture of low cohesive materials from debris avalanche of the Chachimbiro 1 and 2. Finally, the author takes into consideration geological data from the surface. From this, they interpret low gravimetric values to be related to low density materials, likely sedimentary rocks and volcanic deposits, suggesting the basement is located at great depth.

Pilicita (2014) used Magnetotelluric (MT) data collected in 2011 by WesternGeco Integrated EM CoE. In total 70 stations were located on an irregular grid with a spacing ~0.35 km between them. The study was carried with eleven profiles in total. Several cross-sections were done with the data collected. The author identifies three anomalies separated from each other by a fault, two of them cover large areas. A shallow anomaly may correspond to the cap rock and covers 11.07 km^2 with an average thickness of ~388 m.

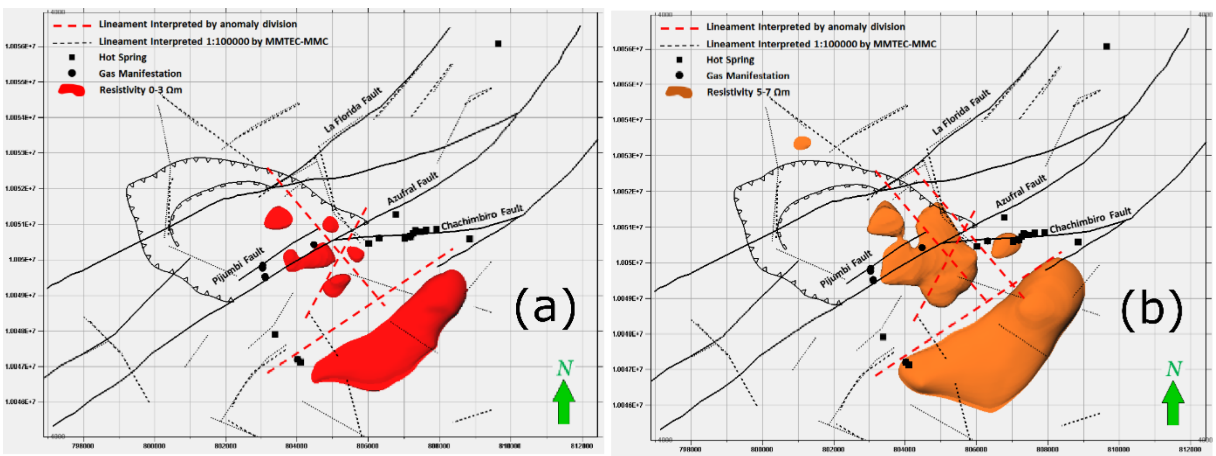

Figure 7: Low resistivity anomalies, faults and fractures in the Chachimbiro geothermal area. a) Resistivity anomalies between 0 to 3 Ωm. B) Resistivity anomalies between 5 to 7 Ωm. Image from Pilicita (2016).

Figure 7 (a) show the moderately low resistivity anomalies appear to be offset or separated by the Azufral and Pijumbi faults; this anomaly may be the cap rock. While (b) present the Azufral, Chachimbiro, Pijumbi faults and a lineament passing through the anomalies. A lineament in NW-SE direction is shown close to the borders of 5 to 7 Ωm resistivity anomaly. Lineaments increase permeability of the system and outer boundaries. Another lineament is subparallel to the Azufral fault that divides two anomalies. Resistivity distribution shows several layers; a shallow part with a high resistivity of >160 Ωm, corresponding to Quaternary volcanic rocks and tills; a lower resistivity zone <10 Ωm which are possibly related to the cap rock, formed by smectite, and has been described in other technical reports. Below this low resistivity anomaly, resistivity values increase from 10 to 160 Ωm, forming a medium resistivity zone that includes a high resistivity core of 60 – 160 Ωm.

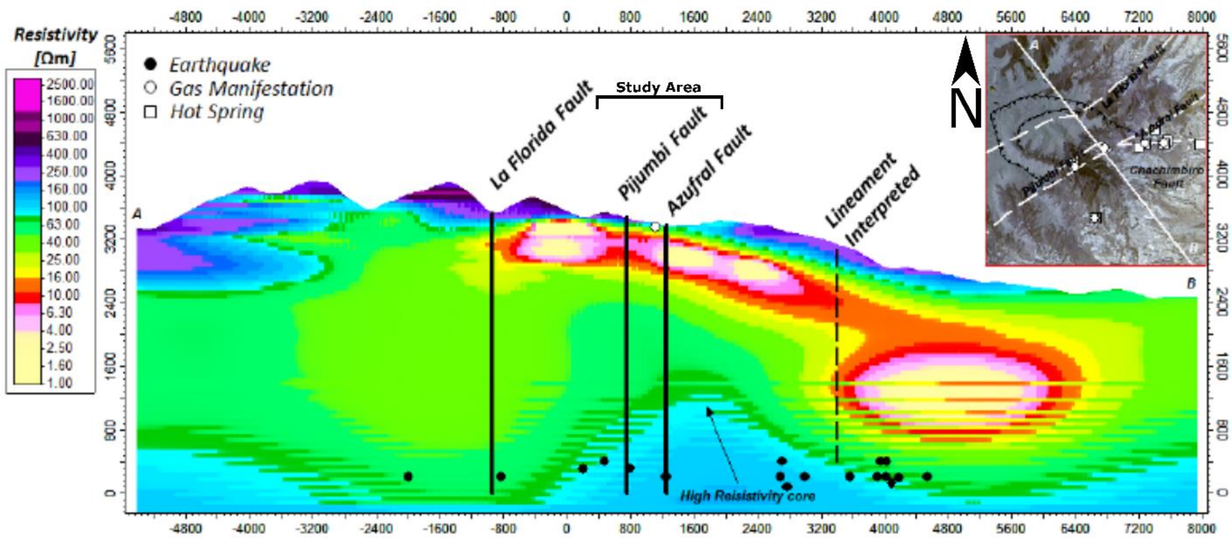

Figure 8: Resistivity cross-section showing the high resistivity core and the relation between the interpreted lineament, earthquakes, fault, gas manifestation and resistivity anomalies. Figure from Pilicita (2016).

Figure 8 shows the cross-section from the MT data collected, with a projection of the faults, reaching the high resistivity core. Hot springs and gas emissions are located along the faults, indicating that the core's fluids have connection with the surface through the faults.

Previous studies helped to create several models of the Chachimbiro's geothermal system, which allowed them to estimate the approximate depths of the reservoir and the cap rock. Córdova Tipantásig (2017) determined an approximate depth of the cap rock around ~600 m, while the reservoir top is approximately at ~2000 to ~2100 m. The Torres Calderón (2014) model shows the estimated depth of the cap rock is around ~300 to ~600 m, and reservoir top at ~1500 m depth. The Pilicita (2016) model shows a similar estimated depth of cap rock around ~300 to ~600 m with a thickness ~388 m, and a reservoir top at ~1500 m depth. As for the heat source, Bernard et al., (2014) showed magmatic reservoirs at ~14.4 and 8 km depth.

5. Methods

5.1. Magnetic theory

Magnetic fluxes exist in a magnet, going from the positive pole (north pole) to the negative pole (south pole), both poles having the same intensities but different sign. The direction and intensity of the magnetic field vary from point to point at the Earth's surface because the Earth behaves on average as a giant magnet. The force F between two magnetic poles of magnitude m_1 and m_2 separated by a distance r is given by:

$$\boldsymbol{F} = \frac{\mu_0 m_1 m_2}{4\pi\mu_R r^2} \qquad (\mathbf{1})$$

Where μ_0 is the magnetic permeability of free space which has a value of $4\pi*10^{-7}$ [$WbA^{-1}m^{-1}$] and $\boldsymbol{\mu_R}$ denotes relative permeability, that is the ratio of the permeability of a specific medium to the permeability of free space.

$$\mu_R = \frac{\mu}{\mu_0} \qquad (\mathbf{2})$$

In terms of magnetic susceptibility

$$\mu_R = 1 + k \qquad (\mathbf{3})$$

Where k is the magnetic susceptibility, which is dimensionless

The force is attractive when the poles have different signs and repulsive if the poles have the same sign. μ_R is dimensionless.

The magnetic field B is a consequence of the current flux lines between two poles per unit area. The units of magnetic field are the Tesla ($T = Wb^1m^{-2}$). The magnetic field is given by:

$$B = \frac{\mu_0 m}{4\pi\mu_R r^2} \qquad (\mathbf{4})$$

The magnetic field is represented by force lines and its direction and intensity correspond to the number of lines per unit area.

The magnetic moment is the strength and orientation of a magnet or any other object that has a magnetic field, given by:

$$m = pr \qquad (\mathbf{5})$$

Where m is a vector with the direction of unit vector r that extends from a negative magnetic pole to a positive magnetic pole p

When a material is located within a magnetic field, it can acquire a magnetization in the same direction as the applied magnetic field, which it will lose if the object is removed from the applied field, which is lost if it is removed. This phenomenon is called induced magnetization or magnetic polarization and result from the dipole alignment to the field direction within a material. The induced magnetic intensity J_i of a material is defined as the sum of all dipole moments m per volume unit V, given by:

$$J_i = \frac{\sum m}{V} \qquad (\mathbf{6})$$

The induced magnetization intensity is proportional to the magnetization force H of the inducing field:

$$J_i = kH \qquad (\mathbf{7})$$

Where H is the surrounding magnetic field.

The total magnetic field including the magnetization effects results in:

$$B = \mu_0(H + J) \qquad (\mathbf{8})$$

Combining equation (7) and (8) results

$$B = \mu_0(1 + k)H \qquad (\mathbf{9})$$

Replacing it with (2), we get

$$B = \mu_0\mu_R H \qquad (\mathbf{10})$$

5.2. Remanent magnetization in magnetic survey

Rocks and minerals can show a remanent or permanent magnetization when after removing them from an applied field. Remanent magnetism in igneous rocks results from magnetization of rocks during their formation, with cooling of these rocks below the Curie temperature leading to acquisition of the magnetic field of that time. The Curie temperature is the value at which the minerals lose their magnetic properties. Magnetic susceptibility is the measure of the magnetic field in response to an external field (Harrison et al., 2015). All materials have magnetic susceptibility, which could be diamagnetic or paramagnetic, ferromagnetic, antiferromagnetic. Diamagnetic materials (e.g. marble, salt, quartz) have all their atomic orbitals full of electrons. When an external field is induced, electrons align in the opposite direction of the applied field. This results in a low and negative susceptibility. Paramagnetic materials (e.g. platinum, aluminum, pyroxenes, biotite) have incomplete atomic orbitals, resulting in an alignment in the same direction of the external field applied. The field produced by these materials is relatively low. Ferromagnetic materials (e.g. cobalt, nickel, magnetite) have positive susceptibility. They show a strong spontaneous magnetization that could exist even in absence of an external field, which can decrease with rising temperature or be completely lost if the Curie temperature is reached. This value varies depending on the mineral composition. Antiferromagnetic materials (e.g. hematite) have divided magnetic domains aligned in opposite directions, with the same quantity of moments in the same directions which results in a magnetic field equal to 0. Ferrimagnetic materials (e.g. garnet, cubic ferrites of iron oxides with other elements such as cobalt, nickel, manganese, zinc) are aligned in opposite directions to the external field, but the magnetic moment is different from 0. This happens because some subdomains have different magnetic components than others. This effect allows a high magnetic susceptibility and a spontaneous magnetization. Figure 9 shows the difference between ferrimagnetism, ferromagnetism and antiferromagnetism.

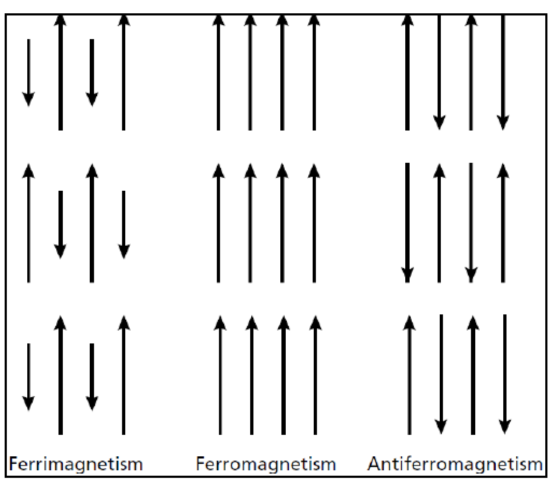

Figure 9: Magnetic moment direction scheme, figure from López Males et al. (2013).

5.3. Magnetic surveying

Magnetic surveys have different applications ranging from micro-scale, archeological studies (detection of metallic objects) to regional-scale studies. It can be used on the ground, air, or sea (İ et al., 2013). The objective of a magnetic survey in a geothermal area is to acquire information about the relationship between geothermal activity, tectonics, and stratigraphy. This will be done with detection and interpretation of the magnetic anomalies of underground rocks and magnetic properties of the ground (Sircar et al., 2015). Magnetic measurements in geothermal exploration are commonly used to detect the location of intrusions, dykes, faults and possibly estimate their depth. It is also possible to locate areas with lower magnetization due geothermal activity (Bjornsson, 1980).

All rocks are magnetic, but, different types of rocks have different amount of magnetic minerals that will create anomalies. What one detects in a magnetometry survey are differences in magnetization of the subsurface rocks, which is a vector sum of the total induced and/or permanent magnetizations within the rock forming minerals. For example, if a ferrous material with an existing permanent magnetization is buried in the ground, it will also acquire an induced magnetization in the direction of the current Earth's magnetic field at that location and most likely in a different direction than the permanent magnetization resulting in a superimposed total magnetization. This will create a magnetic anomaly that is slightly different than what is expected at that location, if there were no magnetic material or if there were only magnetic material with no permanent magnetization. The detectability of such an anomaly depends on the amount of magnetic material, its size, the magnetization contrast between the object and the surroundings and its distance from the sensor. These anomalies can be produced by lithology changes, size of magnetized bodies, faulting and topography (Rivas, 2009). Figure 10 shows the result of the sum of vectors of remanent magnetization (Mr) and induced magnetization (Mi), giving as result the total magnetization (Mt).

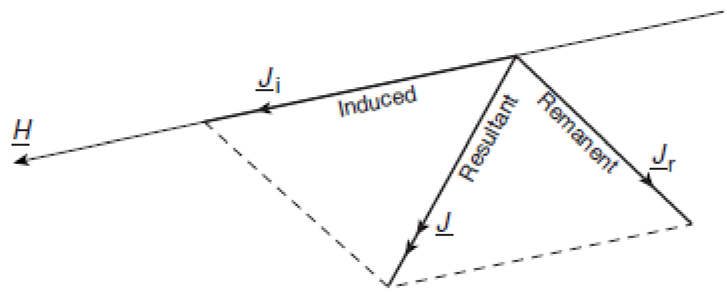

Figure 10: Addition of induced and remnant magnetization.

Several types of magnetometers exist for geophysical exploration, but the most known and the one used in this study is the proton free-precession magnetometer. This kind of magnetometer comprises a recipient filled with hydrogen-rich fluid like kerosene or gasoline that is surrounded by a coil made of copper wire (Figure 11a). The nuclei of hydrogen act like dipoles that are aligned with the Earth's magnetic field (Figure 11b). The equipment form a circuit with a current flowing through the coil and generating a magnetic field 50 – 100 times bigger than the surrounding magnetic field but with a different direction, forcing the protons to realign (Figure 11c) (İ et al., 2013). After this current is turned off, the protons will align back parallel to the surrounding Earth's magnetic field (Figure 11d). However, this aligning back is not direct but happens through precession. The frequency of this precession and the time it requires is related to the strength of the magnetic field at that location.

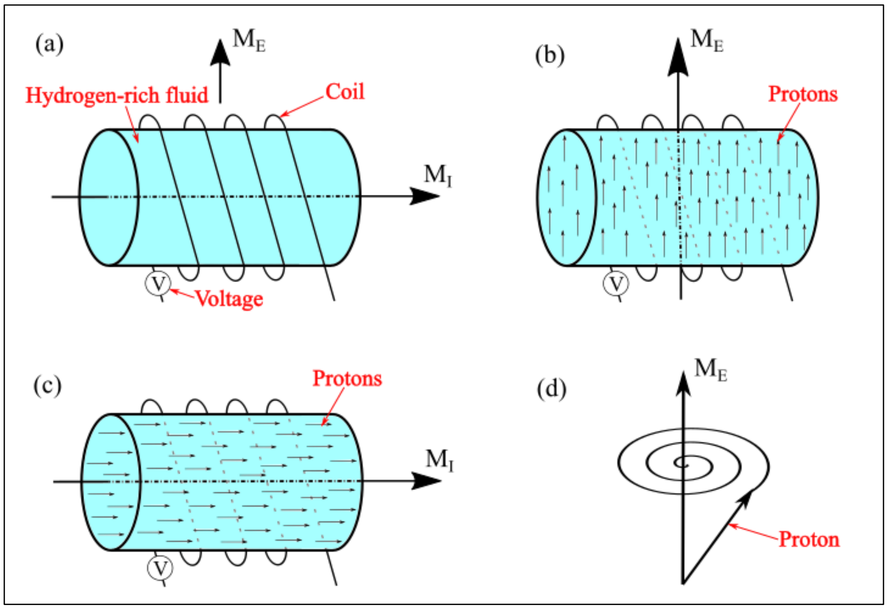

Figure 11: Principle of a proton-precession magnetometer: (a) Sensor with Earth's magnetic field M_E, and magnetic field of instrument coil M_I. (b) Alignment of protons in Earth's magnetic field. (c) Alignment of protons due to applied magnetic field. (d) Precession of protons around Earth's magnetic field after coil current is interrupted. Image from (Gallegos Aguilar, 2020).

5.4. Data collection

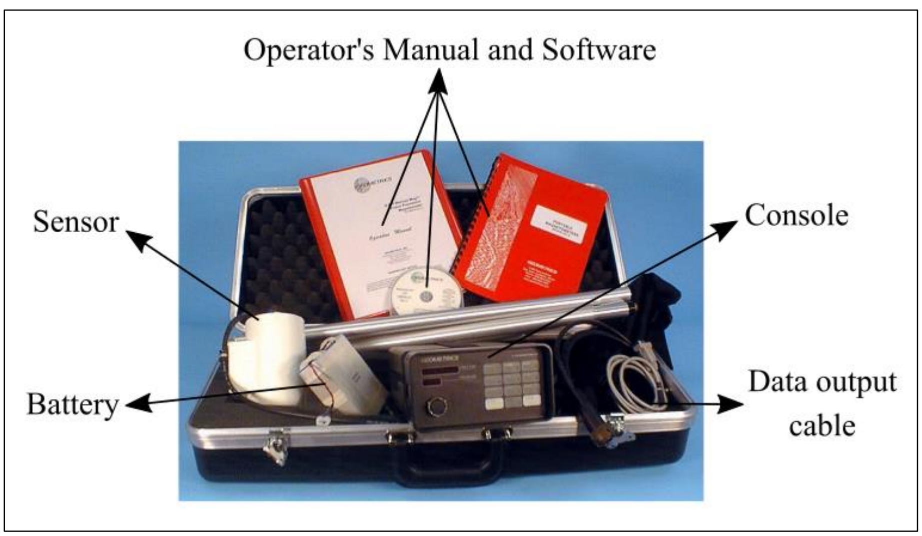

Figure 12: G-856AX proton-precession magnetometer used to take measurements. Image modified from Antennas Manual from Geophysical Survey System, Inc.

The equipment used for this research was a G-856AX proton-precession magnetometer that was provided by the Instituto Nacional de Patrimonio Cultural (INPC) (see Figure 12). This model is a single sensor magnetometer where the user needs to keep the body of the coil perpendicular to the surrounding Earth's magnetic field by approximately pointing the arrow of the magnetometer to the North and always handling the magnetometer in the same way to avoid errors in the measurements.

Magnetic values change during the day due to the interaction between the magnetosphere and the sun location, so corrections need to be applied to the collected data to account for these variations. To realize the corresponding diurnal correction, it is necessary to take "base station" readings every day before starting measuring and throughout the day at certain intervals depending on the size of the anomalies. In our case we were looking for large anomalies so a base station reading every 1 to 2 hours was sufficient to remove the daily variation. For optimal sensitivity the magnetometer was tuned every day to an average value of the magnetic field in the study zone, which in our case was 28500 nT. Then, data correction helped to reduce erratic values of the magnetic field (Telford et al., 1990).

The selected survey area is show in Figure 13. Field work was performed over a duration of one month from November 11th to December 3rd of 2020. The irregularity of the terrain and the presence of a dense forest prevented a regular grid to be applied for the survey. Instead, measurements were taken every ~27 to ~35 m, covering the areas that were the most accessible. Then, two more survey lines (Figure 13) were done across the faults, with a spacing between points of ~5 m. and one additional profile was extracted from the 30 m survey, for a total of three magnetic profiles.

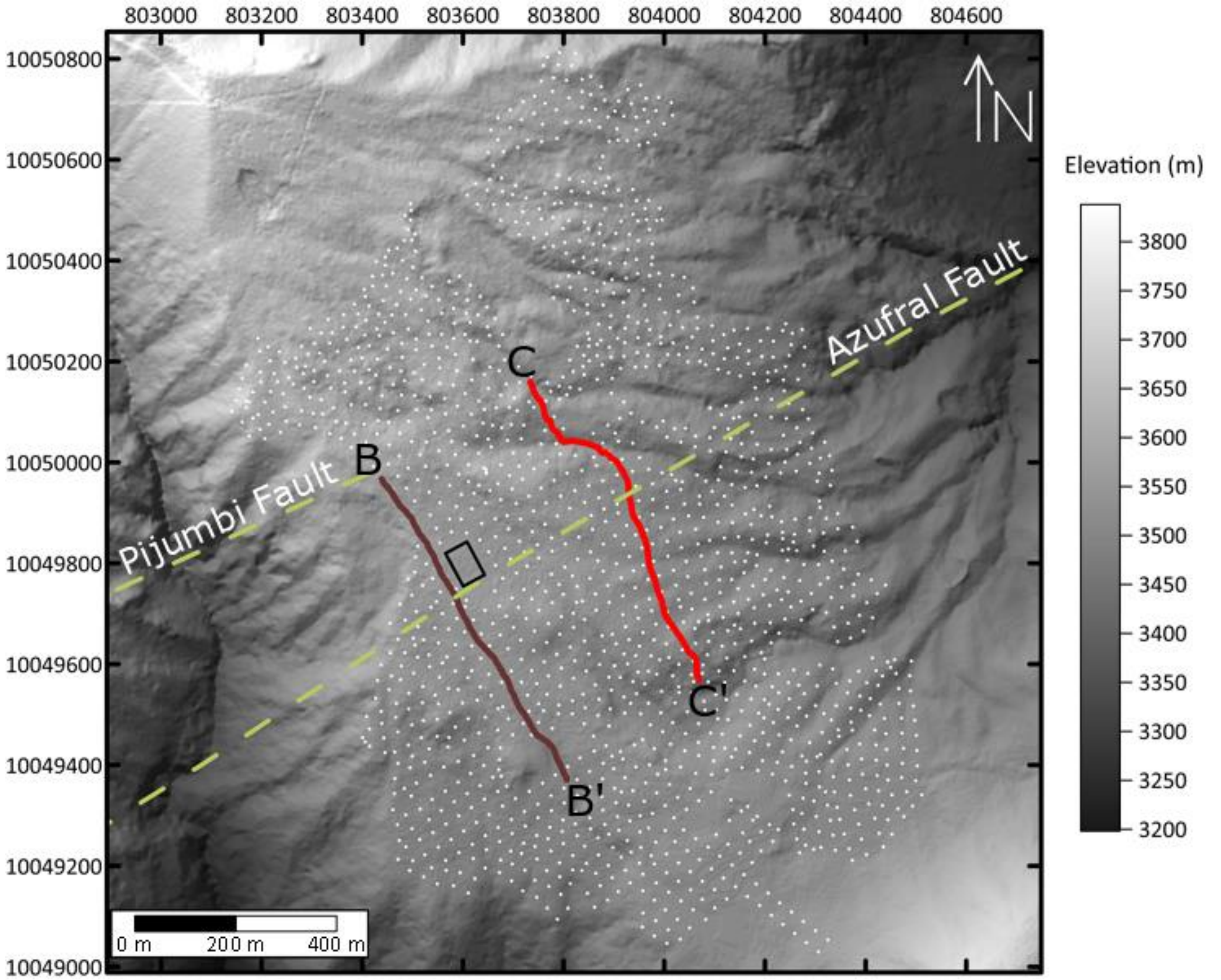

Figure 13: Location map showing the points acquired during the survey. B-B' in brown corresponds to the 5 m step size survey line 1 and C-C' in red corresponds to the 5 m step size survey line 2. Black rectangle is the area of the first drilling, also the two faults crossing the area are shown.

The measured data were noted manually and the location of each point recorded with a Garmin GPS. After fieldwork, the latitudes and longitudes were converted to Universal Transverse Mercator (UTM) coordinates, the base station correction was applied to every data point and the collected data were organized to the required format to be plotted in MagMap software for further processing. After despiking the data in Magmap, the files were exported to be plotted on Surfer GoldenSoftware as a magnetic anomaly map, after that the resultant map was set at the top of the topography map of the area to be compared then.

In addition, some models of a strike-slip fault were done using GravMagSuite app in MATLAB and a model with the clay cap using Mag2dc. This models would help to understand better the resultant magnetic profiles.

6. Results

Data was uploaded to Magmap2000 Software to have an initial filtering. The program shows the survey points' distribution with coordinates, and a profile of the magnetic data, and the user has the option to draw the data in 2D and/or 3D interpolating data in between the points in order to fill the grid. Figure 14 shows the raw data plotted as a color relief map in surfer. It is impossible to interpret, since the outlier values distort the color scale and will not show any details. These outliers are likely either typing errors, instrument errors or interference with unwanted magnetic objects while surveying. It was necessary to use the filter tool called range despike of Magmap2000 to remove these erroneous data that draws very high or very low anomalies that are out of range from the other values.

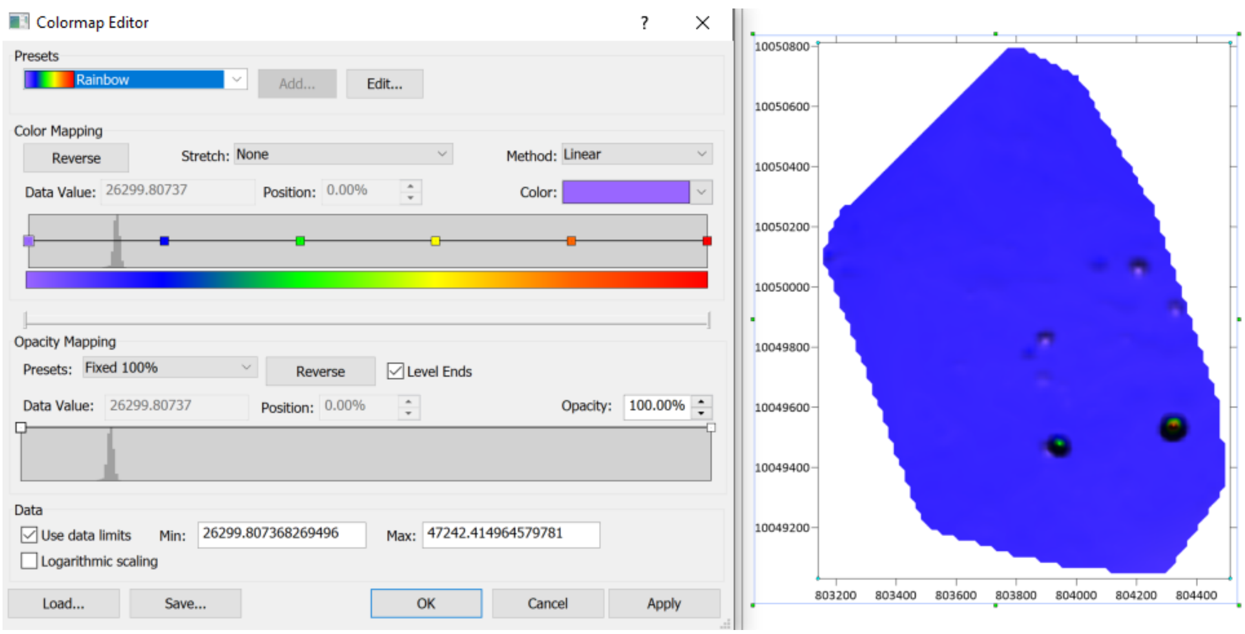

Figure 14: Raw data plotted without filtering in Surfer (i.e. despiking).

After data despiking, the data file was exported and plotted in Surfer GoldenSofware, where, with the obtained results it was possible to create a magnetic anomaly map (Figure 15) of the study area. Also, some parts of the maps were drawn with help of data interpolation. The map shows different distribution of magnetic values in the area. The north part of the map is mainly characterized by high magnetic values and several positive magnetic anomalies, with the highest positive magnetic anomaly at the NW part of the magnetic map. The right southern part of the map is characterized by low magnetic values with several negative magnetic anomalies. Finally, the left lower part is characterized by intermediate magnetic values, with no representative anomalies.

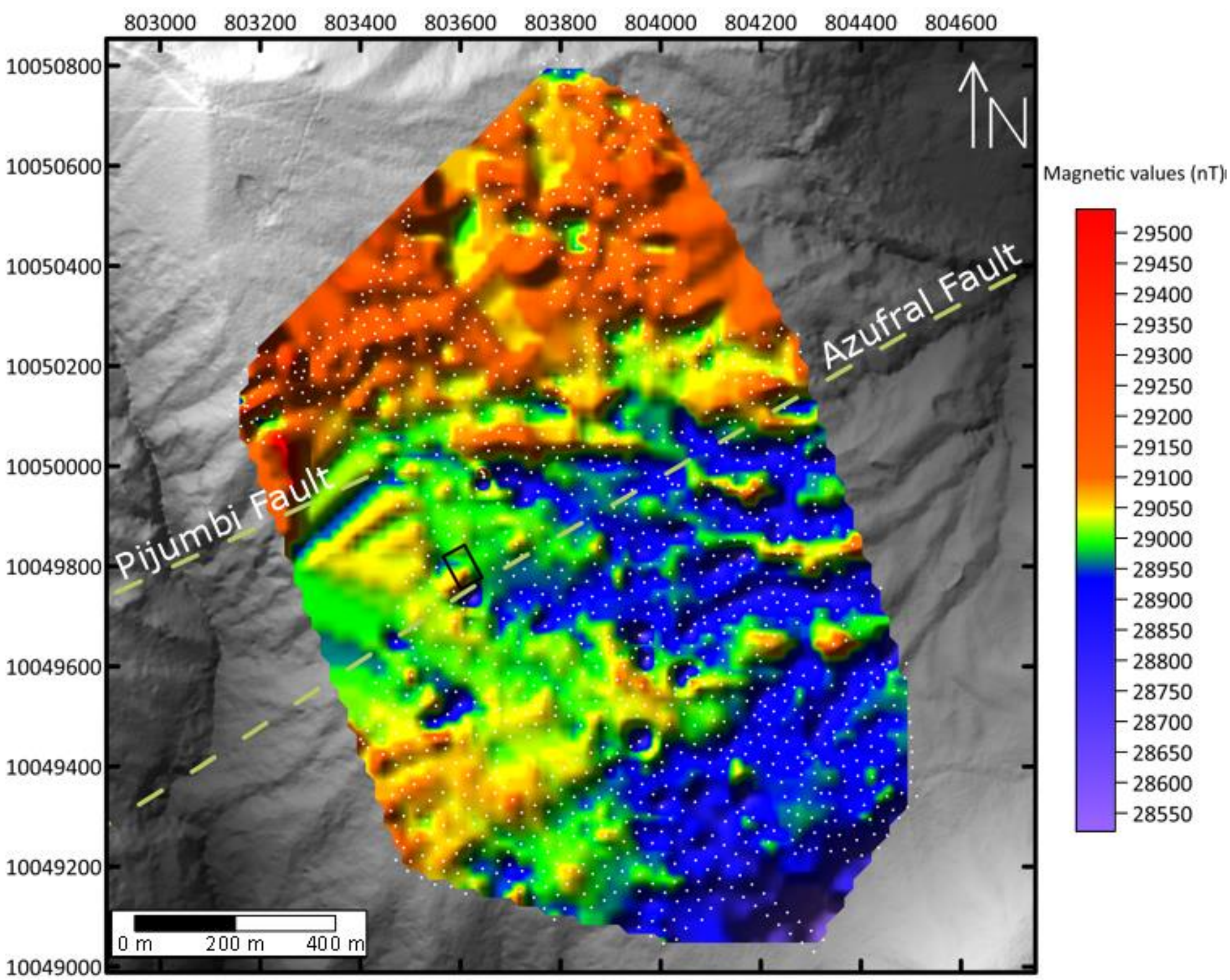

Figure 15: Magnetic anomaly map with survey points. Black rectangle is the area of the first drilling, also the two faults crossing the area are shown.

The resultant magnetic anomaly map was also plotted in 3D format (Figure 16), which helps to recognize the areas with positive or negative anomalies. Then, it is possible to compare the survey data with the study area's elevation map, discussed in the next section.

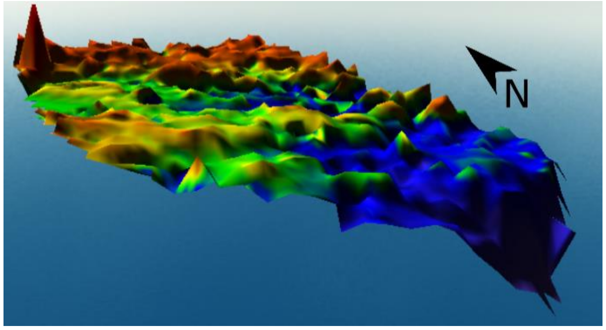

Figure 16: 3D magnetic anomaly map made in Surfer, view from South to North.

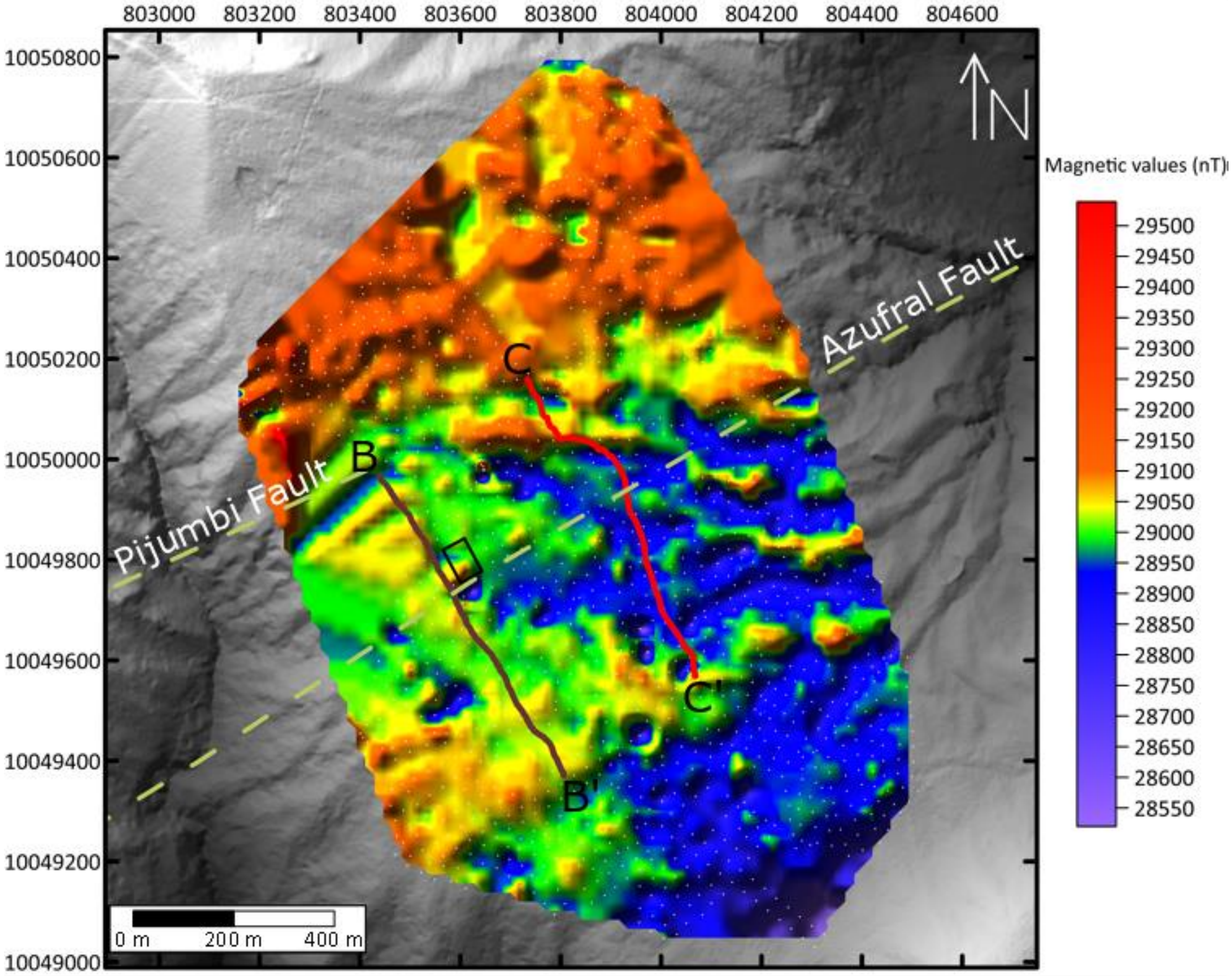

Figure 17: Magnetic map with profile lines. B-B' in brown and C-C' in red. Black rectangle is the area of the first drilling, also the two faults crossing the area are shown.

In addition to the 2D map, two profiles were extracted from the elevation and magnetic maps (Figure 17); the resulting elevation and magnetic profiles are shown in Figure 18.

In the case of B-B’, the elevation profile (Figure 18a) is continuously decreasing from NW to SE, while the 5 m magnetic profile (Figure 18b) initial values increase from values under 28900 nT, then rises and fluctuating between 29100 and 29000 nT at the interval from 0 to 100 m. Then at the interval from 100 to 200 m, values abruptly decrease under 28900 nT, only to rise again between 29100 and 29000 nT. Values fluctuates again between 29100 and ~28950 nT; next to that, values abruptly decrease close to ~28950 nT and increases between 29200 and 29100 nT at the interval 200 to 300 m. After that values keeps fluctuating between 29100 and 29000 nT; close to the end of the profile values increase again close to 29100 nT at the interval 600 to 700 m. The 30 m survey profile (Figure 18c), similar to the last profile values start a values close to 28950 nT from the interval 0 to 100 m. Then values rise close to 29050 nT with a value decreasing of ~50 nT. Next to that values increase again ~50 nT in next interval from 100 to 200 m, followed an abruptly decrease to low magnetic values at interval from 200 to 300 m. After that it keeps fluctuating between 29050 and 29000 nT. Magnetic data from this study is shown on the Appendix chapter (Table A1).

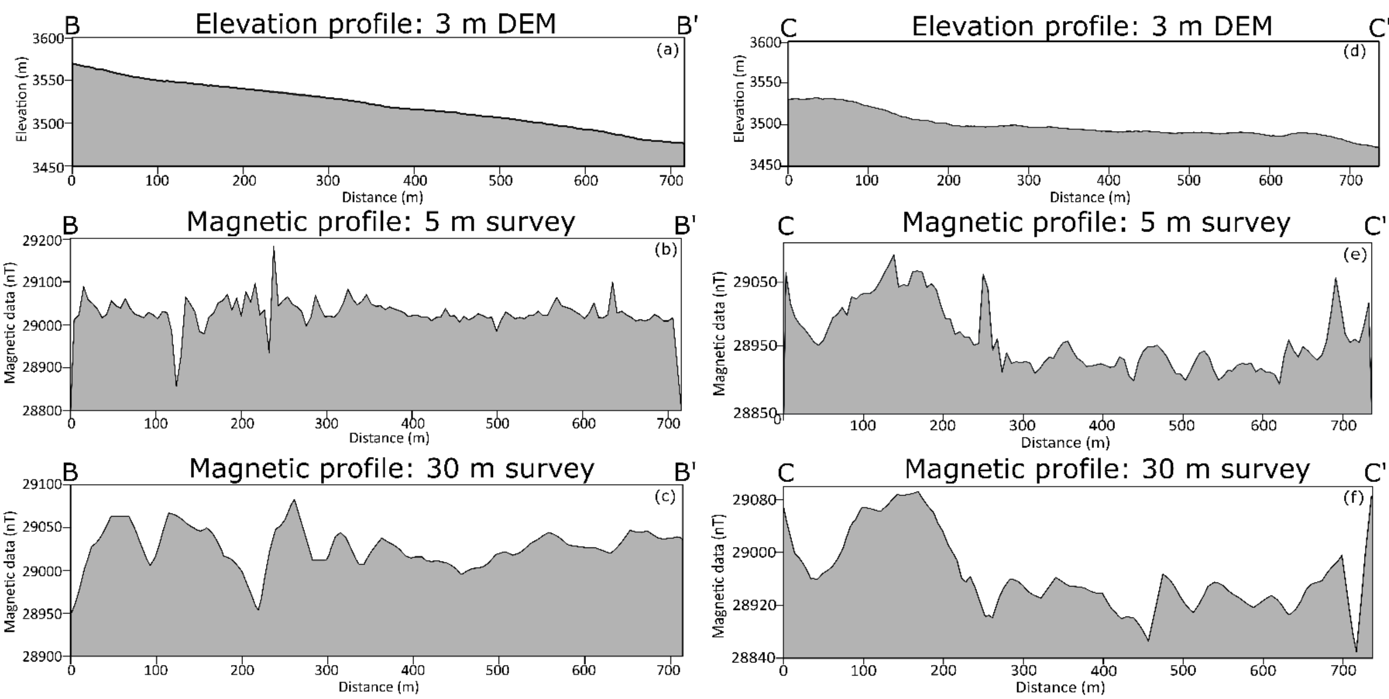

Figure 18: Elevation and magnetic profiles. B-B’ correspond to the fault survey line 1; C-C’ correspond to the fault survey line 2. Profile lines are shown in Figure 17.

For line C-C’, it is possible to observe a little change in the elevation profile, starting with high values and then decrease continuously (Figure 18d). For the magnetic profile for 5 m survey

(Figure 18e), start with high magnetic values, fluctuating a little until it drops a little under 29000 nT at the interval from 0 to 100 m, then, values increase reaching values above 29050 nT. Then values decrease at the start of interval from 200 to 300 m with an abrupt increase in between the interval. Followed values fluctuate in between 29000 and 28900 nT. At the final part of the profile at interval 600 to 700 m, value abruptly rise again. For the magnetic profile for 30 m survey (Figure 18f), at the interval from 0 to 100 m values start at ~29060 nT; next to that values decrease close to ~28960 nT, then values rise again close to 29080 nT. After that, the profile keeps decreasing until it reaches values less than 28920 nT. Values then rise again ~40 nT at the interval from 200 to 300 m. Values continue fluctuating a little with a subsequent decrease again reaching values in between 28920 and 28840 nT, later values rise again in between 29000 and 28920 nT at the interval from 400 to 500 m. Finally, values fluctuate close to 28920 nT until it abruptly decreases close to 28840 nT to rise again at ~29080 nT after the interval from 600 to 700 m.

7. Discussion

7.1. The effects of faulting and hydrothermal alteration on magnetization

According Yang et al. (2020), temperature, stress, and fluids in a fault system may affect iron-bearing minerals because its sensibility to them. Their magnetic properties give an interpretation of the physical and chemical process that affects rocks on faults. Faults go through cycles of creep and seismic slip. A seismic cycle is divided into three periods: 1) coseismic period (Figure 19a), which is the time during an earthquake during seconds to minutes; 2) postseismic period (Figure 19b) which time could be days, months and even years after an earthquake; finally, 3) the interseismic period (Figure 19c) which happens between large earthquakes, taking tens to thousands of years.

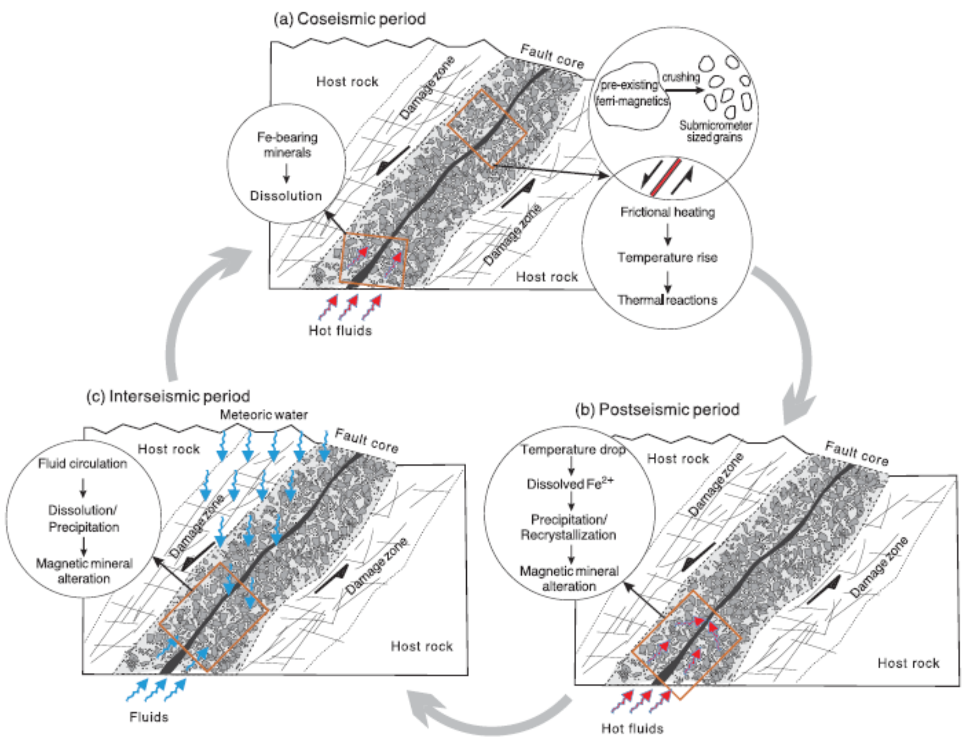

Figure 19: Conceptual model showing the faulting-related physical and chemical processes and the causes of potential magnetic changes in the fault zone during different stage of the earthquake cycle. (a) Coseismic period, (b) Postseismic period and (c) Interseismic period. Image from Yang et al., (2020).

Yang et al. (2020) describe the processes that occur in active fault zones during the seismic cycle, which influence the magnetic properties of the rocks at fault zones. Thermochemical reactions (Figure 19a) take up the largest part of the total energy from an earthquake (~80% to ~90%).

Frictional heat will raise the temperature in the slip zone of rupture. With typical seismic rates (1 m/s) and total slip distance (tens of centimeters to meters) at a fault plane, temperature rises <100 °C at shallow depths close to the surface but it can increase to >1100 °C at higher depths (>5 km). This increased temperature may allow dehydration of some mineral phases and formation of breakdown products; the increased temperature at the slip zone sometimes is enough to melt the host rock minerals. Temperatures inside a geothermal system do not reach Curie temperatures, where minerals get entirely demagnetized. However, hydrothermal alteration may affect mineral magnetization by reducing it or replacing into less magnetic minerals.

Another process that affects the magnetization is the fluid movement in faults: fault zones are formed by dense networks of fractures and secondary faults which act as fluid conduits in the crust. Fluids from several sources, such as meteoric waters, mineral dehydration, trapped formation brines, and volatiles from deep underlying layers infiltrate and percolate along fault zones. Pore fluid pressurization during frictional heating may allow fault weakening. These fluid-related dissolution-precipitation processes are common during all periods of the seismic cycle. Resultant reactions play an important role in physical, chemical, and mechanical evolution of fault rocks.

Magnetic anomalies are useful to delineate high-temperature hydrothermal/geothermal systems; it is possible because several geothermal processes may alter the rock magnetization, going through a demagnetization of minerals or altering them to a less magnetic mineral (Caratori Tontini et al., 2016). Temperatures inside a geothermal system do not reach Curie temperature, where minerals get entirely demagnetized. However, hydrothermal alteration may affect minerals magnetization reducing it or replacing into less magnetic minerals. Magnetic anomalies may be caused by intrusions, flows, or iron-rich sediments. The magnetic method is useful to locate intrusive bodies, tracing individual buried dykes and faults or estimating their deep (Bjornsson, 1980).

7.2. Forward modelling

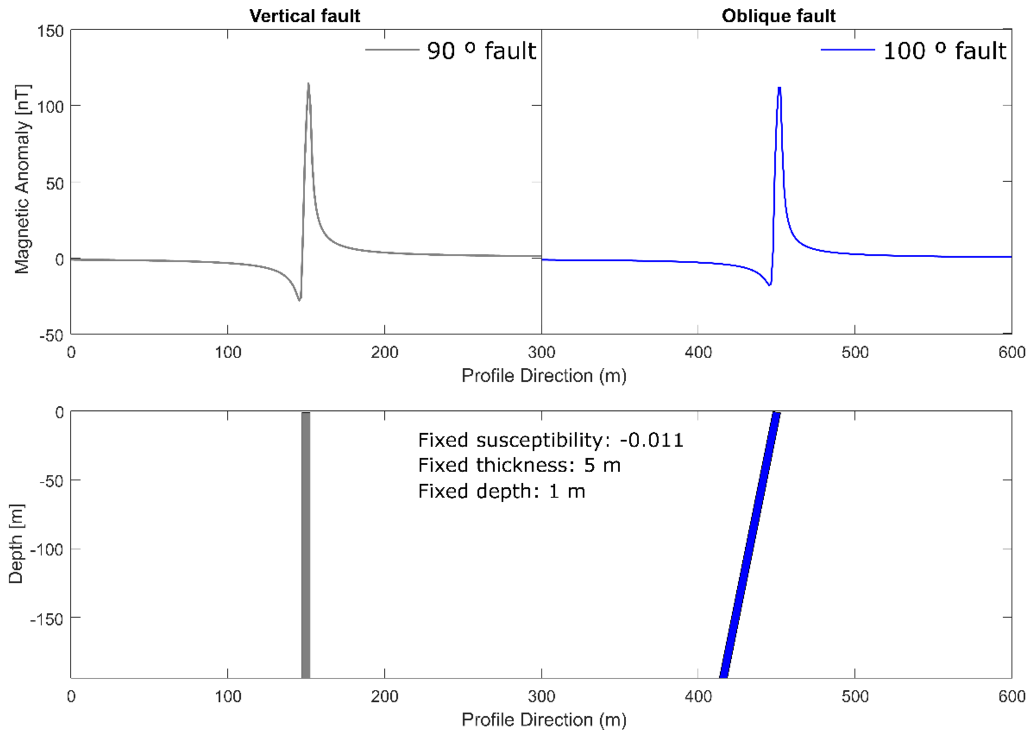

Figure 20: Strike-slip fault model comparison with 90 º and 100 º inclination. Model created with dike-like forward modelling tool from GravMagSuite app.

Models were created at MATLAB with GravMagSuite app, using the modelling feature for dike-like forward modeling tool. Values for inclination of 21.5441 º, a declination of -4.2683 º and a total field of 28859.5 nT correspond to the study area. It was used fixed susceptibility values for andesite, described in (Li and Fu, 2019). Also, other fixed values such as the fault inclination, depth and thickness were used to see it similarity with major anomalies in the profiles. The resultant models help to understand what kind of effect would the fault present in a magnetic survey. The first model (Figure 20) represent the behavior of an strike slip fault, one with a 90 º and other with 100 º inclination. This models show an abruptly variation of magnetic values from low to high values around ~120 nT. Both of them have similar behavior but the 100 º has an slightly variation of ~10 nT in comparison with the 90 º fault.

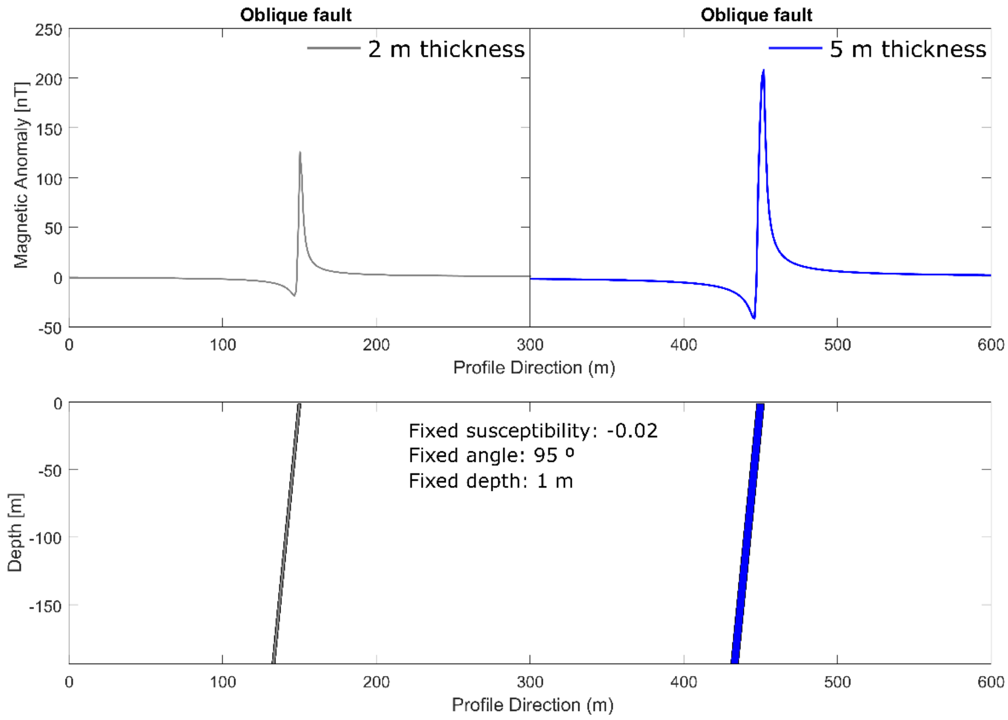

Figure 21: Strike-slip fault model comparison with 2 and 5 m thickness. Model created with dike-like forward modelling tool from GravMagSuite app.

While, the second model (Figure 21) was created with the same total field, inclination and declination configuration, but using a fixed susceptibility, depth and inclination values. In this case, the model compares the effect that the thickness of the fault would have. The first faults show a thickness of 2 m while the second show a thickness of 5 m. Both of the models show to have a similar form for the anomaly but the 2 m thickness show an abruptly change from low to high magnetic values around ~120 nT, while the 5 m thickness show a higher variation in data around ~220 nT.

Finally, the third model was created with the same total field, inclination and declination configuration, but using a fixed susceptibility, thickness and inclination values. In this case, the model compares the effect that the depth of a fault would have. The first model uses a 2 m depth for the fault showing a very abrupt change in the magnetic values around ~200 nT, while the second model uses a 10 m depth, showing a much less effect with a value change around ~50 nT. These models would help to interpret anomalies showed in the magnetic profiles.

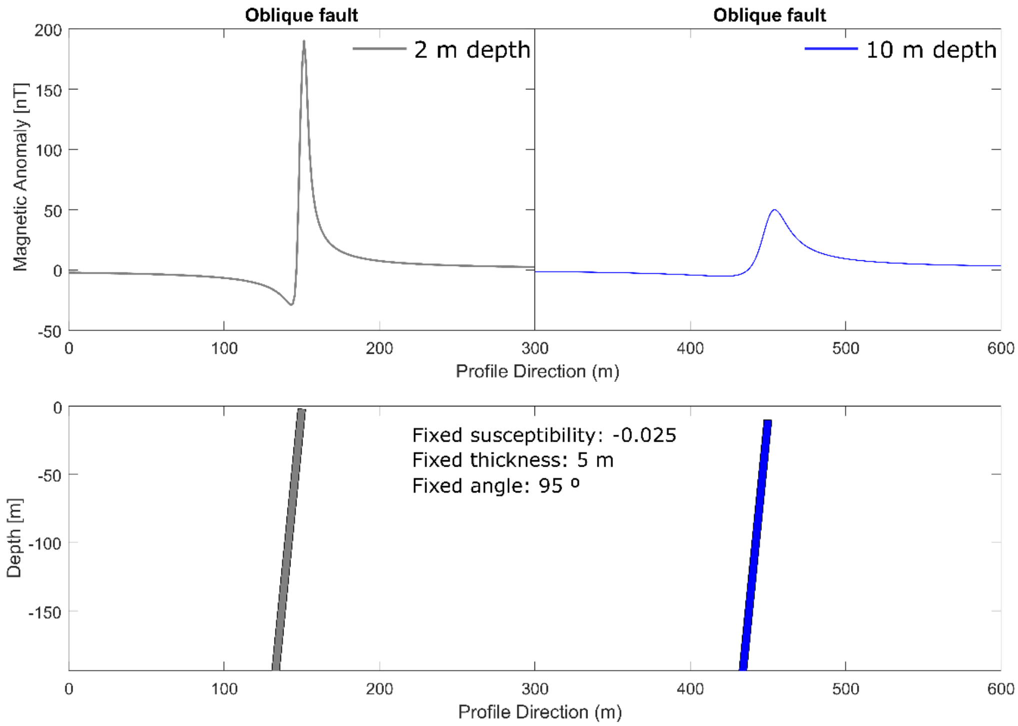

Figure 22: Strike-slip fault model comparison with 2 and 10 m depth. Model created with dike-like forward modelling tool from GravMagSuite app.

The next model (Figure 23) again uses the same configuration of the area for the inclination, declination and magnetic field. This one represents what would be the effect of a clay cap, but using a fixed susceptibility value of -0.05 for andesite to see the effect that a similar body would have. Magnetic values tend to decrease when they are close to the effect of the clay cap as it is expected and increase while they get far from it. Andesite value used is described in (Glen et al., 2007).

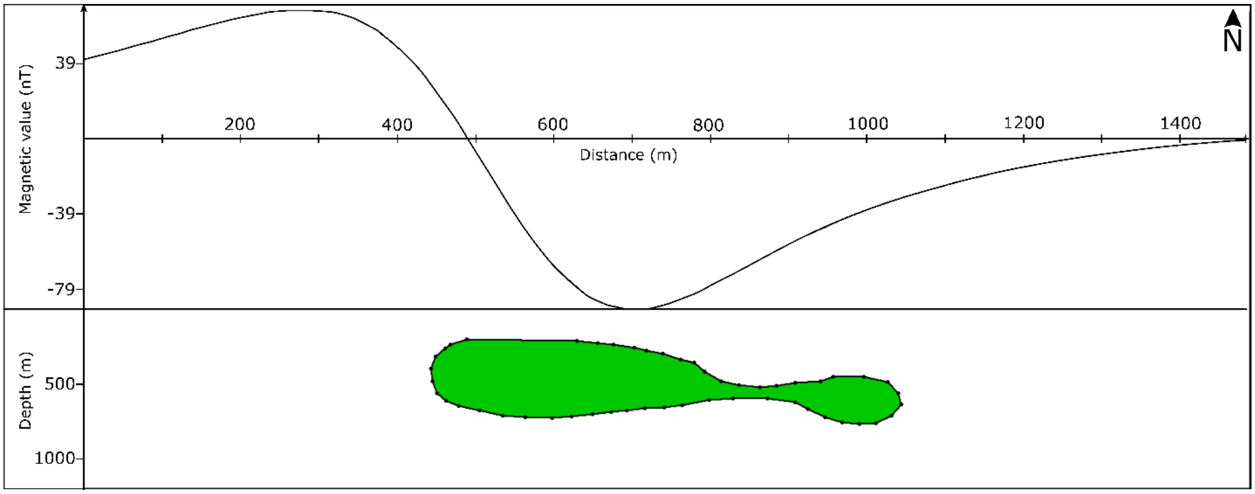

Figure 23: Clay cap model, created on Mag2dc software.

7.3. Interpretation of magnetic anomalies

A geological map of the area is shown in Figure 24A with the major geological units in the zone. These units can be compared with the magnetic anomalies in the study area (Figure 24B). The northern part of the area is characterized by the presence of positive magnetic values with a major positive magnetic anomaly at the NW part of the study area. The whole Chachimbiro's area is comprised of volcanic materials associated with high magnetic values due to its high magnetite content (Kearey et al., 2002); but, this part of the zone may be associated more with materials from the domes Albuji and Huga, composed of dacitic rocks. Likewise, the northwestern area does not show much hydrothermal alteration that may affect rock magnetization and this area comprises the highest elevations registered in the survey.

The western part of the map is associated with the Tumbatu unit, which is composed of pyroclastic flows, ignimbrites, tephras and landslide deposits. This area shows intermediate values with no significant magnetic anomalies; this could be because the area is now covered by pyroclastic deposits of later eruptions of Chachimbiro. These materials have less magnetic susceptibility in comparison to the primary products of a volcanic eruption. Also, the area may be affected by hydrothermal alterations close to the fault zone. Hydrothermal alterations could be caused by carbonization, related to CO_2 emissions; propylitic intermediate temperatures, which may reduce the magnetic properties of the andesites and basaltic andesites, and argillictic alteration, associated with hot springs and fumaroles from the current geothermal activity.

Finally, the central eastern and SE parts are characterized by low values and negative magnetic anomalies. These values may be related to hydrothermal alterations, carbonization, related to CO_2 emissions, and steam heated advanced argillic alteration. These alterations are present in a large area along the Chachimbiro and Azufral faults. Also, the values follow the river valleys, where influence by topography on ground magnetics is very apparent in stream gorges (Telford et al., 1990). Additionally, the lower values could be related with thicker sedimentary deposits filling the area.

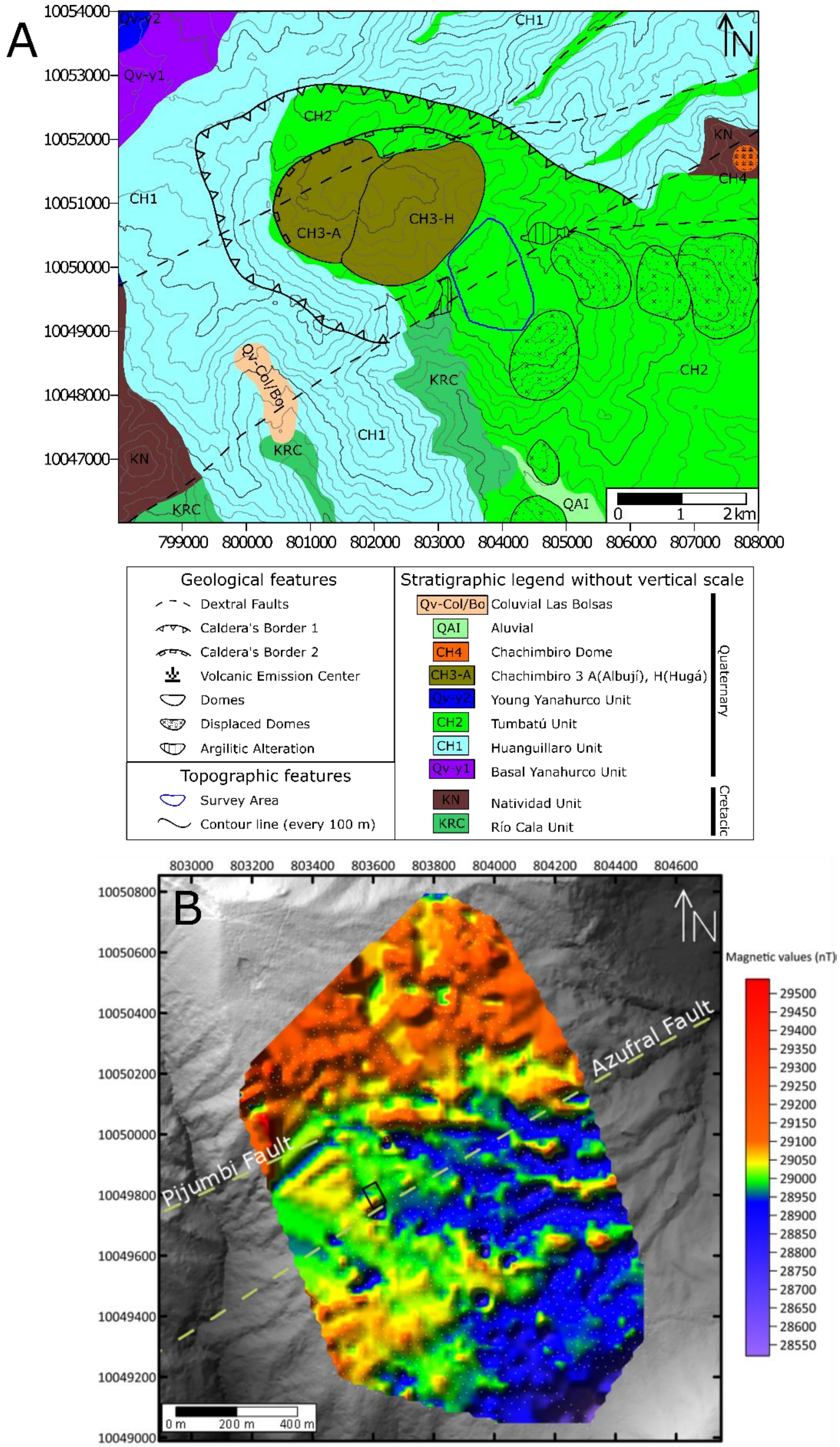

Figure 24: Comparison between the geological map and the magnetic anomaly map. (A) Geological map of Chachimbiro volcanic complex, modified after (SYR, 2012). (B) Resulting magnetic anomaly map.

7.3.1. *Topographic effect on magnetic surveys*

Surfer GoldenSoftware gives the option to create profiles from both elevation and magnetic values from the map, allowing us to see how much the area's topography may affect the magnetic values. The influence of topography in magnetic surveys can be significant, but it is not completely predictable; after diurnal corrections, the variations in magnetic values may only depend on the magnetic properties of topographic features (Kearey et al., 2002). Similar to a dike or fault effect, topography effect will have an associated anomaly but much smaller in comparison to them (Ugalde et al., 2013). In this case, several profiles were created, from survey lines using 5 m spacing survey and one extracted from the 30 m survey.

Figure 24A show the magnetic profiles with some areas circled in black, which correspond to the anomalies that could be related to a topographic effect in the survey, while Figure 24B show the areas related to that effect, circled in black. For B-B' profiles there is only one change that could be related to the topographic effect. In the case of the 5 m survey, the change circled in black seems to be more exaggerated while in the 30 m survey, it is not so appreciable. This difference in the values could be because the 30 m survey does not cover much of the part of the area where the B-B' passes.

For C-C' profiles there are several areas circled in black. For the first circled area, bot profiles show similar changes from low to high magnetic values, corresponding to a change in topography in the area circled in Figure 24B. Values fluctuates more in the 5 m survey while in 30 m are smother, this could related to the distance used to measure the magnetic values. For the next area circled in black at interval from 400 to 500 m, value change from low to high magnetic values of ~60 nT is observed in both profiles, this caused probably by the influence of the quebrada. Finally the last area circled in black at the interval after 700 m, shows and abrupt change to high values and then a decrease to lower values, in the case of the 30 m survey the decreasing is more exaggerated than the 5 m survey, this change could be some values in between the 30 m survey could be interpolated with other distant values with a high difference in topography in comparison to the continuous measuring of 5 m survey.

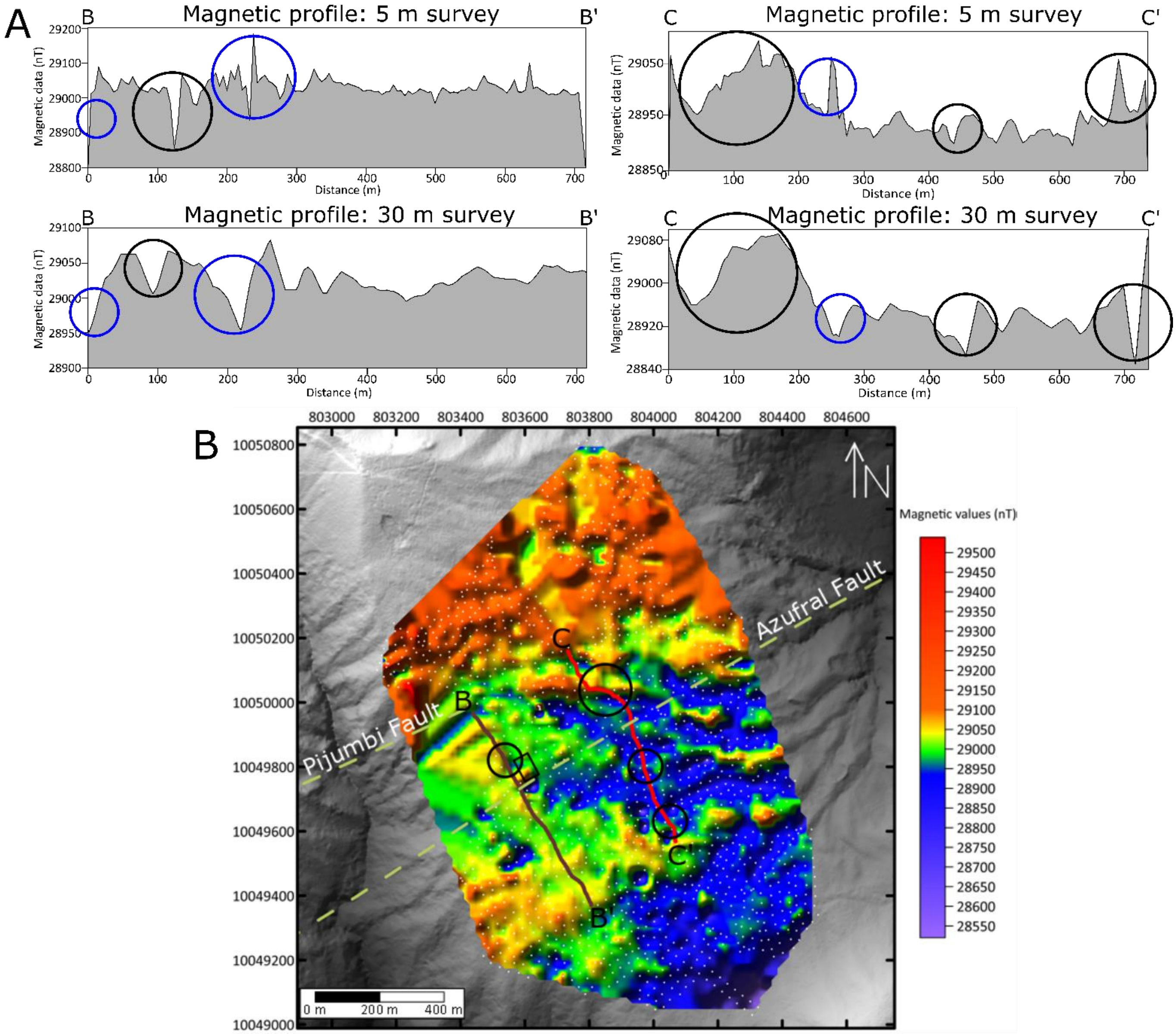

Figure 25: Magnetic profile comparison with the resulting magnetic map. (A) Corresponds to the magnetic profiles. Anomalies in blue circles show the fault effect in magnetic data while black circles the topographic effect. (B) Profile lines B-B' in brown from 30 m survey and C-C' with black circles. Black circles remark the location where topography may affect the magnetic values.

7.4. Faults detection in magnetic survey

Figure 25A shows two abrupt changes circled in blue that may represent the effect of fault in the magnetic survey. First magnetic anomalies circled in blue for B-B' profiles show a similar behavior with the 2 m depth fault model, the 2 m thickness fault model and fits with any of the models showing the inclination effect in a fault. With a difference between low and high magnetic values around ~150 nT. These anomalies and the models named before may represent the interaction of the Pijumbi fault with the magnetic values at the start of both B-B'profiles. While, the next blue circles at both B-B' profiles from 200 to 300 m interval show a similar behavior with 2 m depth fault model, 5 m thickness fault model and any models showing the inclination effect in a fault; with a difference between low and high magnetic values around ~200 nT. These anomalies, due it similarities with the models named before may represent the interaction of the Azufral fault.

For C-C' line it is only possible to see one abruptly change that could be related to a fault. In the case of the 5 m survey the blue circle shows a differentiable abrupt change from low to high magnetic values, while in the 30 m survey the area with the blue circle is not so exaggerated. In the case of the 5 m survey we can relate the anomaly can be compared with any of the models showing the effect of fault inclination, the 2 m depth fault model and the 2 m thickness fault model, while in the 30 m survey the same, except that for this one shows more similarities with the 10 m depth fault model. This difference between the two profiles could be related to the resolution of the survey, the topography related to the quebrada and the presence of the clay cap that is concentrated in the right and right-lower part of the area.

The study showed to be effective in detecting magnetic anomalies in the area, most of the negative anomalies being located in the SE part of the map. We interpret that the low values correspond to the clay cap rock, previously described by Pilicita (2016) that shows that the resistivity anomalies could be related to the presence of the cap rock at the southeast part of the study area. Guillén, (2020) described an estimated depth for a smectite layer around ~200 m and an illite layer around ~250 m; while, Torres Calderón (2014) and Pilicita (2016) studies estimate the clay cap rock at an approximate depth of ~300 to ~600 m.

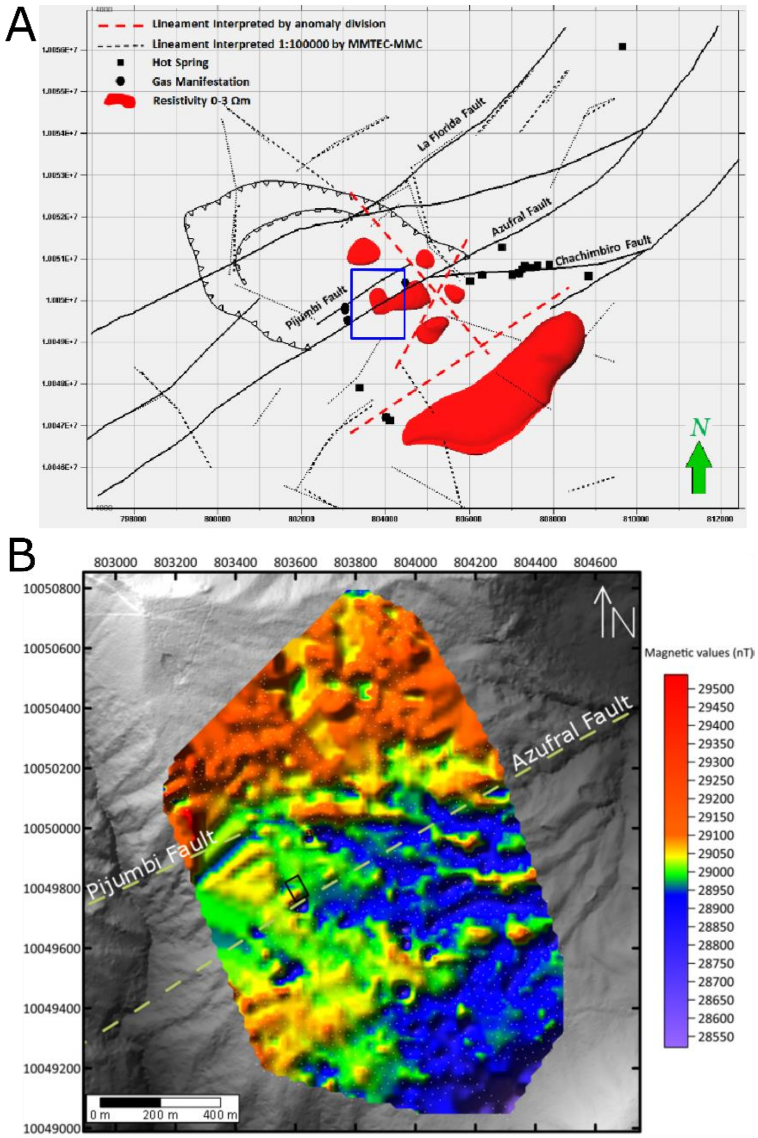

Figure 26: Comparison of the map with previous studies. (A) Resistivity anomaly map from Pilicita (2016), blue rectangle represent the study area. (B) Magnetic anomaly map from this survey.

The magnetic behavior of the geological units is also reflected in the magnetic map. Areas closer to mapped geothermal alterations show a reduced magnetization as expected. The distribution of magnetic anomalies also fit with the resistivity model presented by Pilicita (2016) in Figure 26A, which shows the a resistivity anomaly which correspond to the location of the clay cap at the right most part of the survey area; while in the magnetic map Figure 26B, the right and right-lower part show the major concentration of low magnetic anomalies as is expected for the effect of the clay cap in magnetic values. Finally, faults location and effect seems to slightly offset compared to the area where it was previously mapped.

8. Conclusions

This study used magnetometry applied to geothermal exploration in the Chachimbiro area, using two different approaches: a large scale grid survey with ~30 m spacing, and two high-resolution lines with ~5 m spacing. The survey of the area resulted in a magnetic anomaly map where it is possible to see the distribution of the positive and negative anomalies along the area. Also, elevation and magnetic profiles were compared from ~30 m survey and ~5 m survey lines, showing that topography affects magnetic values; positive anomalies are related to high topographic values and negative anomalies are related to low topographies. Fault effects on the magnetic survey are observable in the magnetic fluctuation values from the profiles, showing the fault effect in magnetization, while the other abrupt changes could be more related with topographic effects. Also, it is possible to see the demagnetization effect of hydrothermal alterations in the area after comparing with the mapped geological units. Comparison with previous model show that the area with major quantity of low magnetic anomalies could be related to the location of the clay cap of the geothermal system. The study shows that it is possible to use the magnetic method in geothermal areas to see the effect of faulting, topography and geothermal alterations on rock magnetization. This study could be used in future studies to contribute with the estimated location of the clay cap in the geothermal area.

To improve the results of this survey, a good option for future work would be to do another magnetic survey taking less resolution, which may help to see if it fits with data from the present work and the fault effect across the area. Also, it would be good to use different geophysical methods, such as resistivity survey along the fault area and see if it shows similar results where the faults are located in this and previous studies.

9. References

Aguilera, E., Cioni, R., Gherardi, F., Magro, G., Marini, L., Pang, Z., 2005. Chemical and isotope characteristics of the Chachimbiro geothermal fluids (Ecuador). Geothermics 34, 495–517. https://doi.org/10.1016/j.geothermics.2005.04.004

Al-Ghussain, L., 2019. Global warming: review on driving forces and mitigation. Environ. Prog. Sustain. Energy 38, 13–21. https://doi.org/10.1002/ep.13041

Beate, B., Urquizo, M., 2015. Geothermal Country Update for Ecuador: 2010 - 2015 Bernardo. World Geotherm. Congr. 2015 14.

Bellver-Baca, M.T., Chiaradia, M., Beate, B., Beguelin, P., Deriaz, B., Mendez-Chazarra, N., Villagómez, D., 2019. Geochemical evolution of the Quaternary Chachimbiro Volcanic Complex (frontal volcanic arc of Ecuador). Lithos 356, 105237. https://doi.org/10.1016/j.lithos.2019.105237

Bernard, B., Hidalgo, S., Robin, C., Beate, B., Quijozaca, J., 2014. The 3640–3510 BC rhyodacite eruption of Chachimbiro compound volcano, Ecuador: a violent directed blast produced by a satellite dome. Bull. Volcanol. 76, 1–20. https://doi.org/10.1007/s00445-014-0849-z

Bernard, B., Robin, C., Beate, B., Hidalgo, S., 2009. Nuevo modelo evolutivo y actividad reciente del volcán Chachimbiro 1988–1991.

Bjornsson, A., 1980. Geophysical methods used in geothermal exploration. Natturufraedingurinn 50, 227–249.

Caratori Tontini, F., de Ronde, C.E.J., Scott, B.J., Soengkono, S., Stagpoole, V., Timm, C., Tivey, M., 2016. Interpretation of gravity and magnetic anomalies at Lake Rotomahana: Geological and hydrothermal implications. J. Volcanol. Geotherm. Res. 314, 84–94. https://doi.org/10.1016/j.jvolgeores.2015.07.002

Chandra, P., 2015. The magnetic method. Groundw. Geophys. Hard Rock 63–85. https://doi.org/10.1201/b19255-6

Córdova Tipantásig, H.H., 2017. Exploración gravimétrica del complejo volcánico Chachimbiro provincia de Imbabura. Quito: UCE.

Dickson, M.H., Fanelli, M., 2004. What Is Geothermal Energy? Flow Heat Transf. Geotherm. Syst. 1–19. https://doi.org/10.1016/b978-0-12-800277-3.00001-3

Dincer, I., Rosen, M.A., 1999. Energy, environment and sustainable development. Appl. Energy 64, 427–440. https://doi.org/10.1016/S0306-2619(99)00111-7

Domra Kana, J., Djongyang, N., Raïdandi, D., Njandjock Nouck, P., Dadjé, A., 2015. A review of geophysical methods for geothermal exploration. Renew. Sustain. Energy Rev. 44, 87–95. https://doi.org/10.1016/j.rser.2014.12.026

Gallegos Aguilar, L.S., 2020. GEOPHYSICAL PROSPECTION OF ARCHAEOLOGICAL SITES FOR THE RECOVERY OF CULTURAL HERITAGE AROUND YACHAY TECH UNIVERSITY, IMBABURA, ECUADOR. Yachay Tech.

Georgsson, L.S., 2009. Geophysical methods used in geothermal exploration. Short Course Surf. Explor. Geotherm. Resour. 50, 227–249.

Gherardi, F., Spycher, N., 2014. Application of Integrated Multicomponent Geothermometry at the Chachimbiro Thermal Area , a Difficult Geothermal Prospection Case. Thirty-Eighth Work. Geotherm. Reserv. Eng. 1–6.

Glen, R.A., Spencer, R., Willmore, A., David, V., Scott, R.J., 2007. Junee – Narromine Volcanic Belt , Macquarie Arc , Lachlan Orogen , New South Wales : components and structure. https://doi.org/10.1080/08120090601146805

Granda, B., 2011. PRECUATERNARIAS DEL PROYECTO GEOTÉRMICO CHACHIMBIRO , FASE DE PREFACTIBILIDAD.

Guillén Pachacama, D.M., 2020. XRD Analysis procedure for clay minerals - application to chachimbiro geothermal system. Yachay Tech.

Gupta, H.K., Roy, S., 2006. Geothermal energy: an alternative resource for the 21st century. Elsevier.

Hammer, S., 1939. TERRAIN CORRECTIONS FOR GRAVIMETER STATIONS. GEOPHYSICS 4, 184–194. https://doi.org/10.1190/1.1440495

Harrison, R.J., Dunin-Borkowski, R.E., Kasama, T., Simpson, E.T., Feinberg, J.M., 2015.

Magnetic Properties of Rocks and Minerals, in: Treatise on Geophysics: Second Edition. pp. 609–660. https://doi.org/10.1016/B978-0-444-53802-4.00048-8

Hochstein, M.P., Hunt, T.M., 1970. Seismic, gravity and magnetic studies, Broadlands geothermal field, New Zealand. Geothermics 2, 333–346. https://doi.org/10.1016/0375-6505(70)90032-5

Hoel, M., 1996. Depletion of fossil fuels and the impacts of global warming. Fuel Energy Abstr. 37, 460. https://doi.org/10.1016/s0140-6701(97)83963-x

İ, K.B.İ.L.G.İ.S.İ.S., López Males, G.G., Zura Quilumbango, C.B., İ, K.B.İ.L.G.İ.S.İ.S., 2013. Correlación de los estudios magnéticos y gravimétricos con la geología del sector de Chachimbiro para prospección geotérmica.

Inguaggiato, S., Hidalgo, S., Beate, B., Bourquin, J., 2010. Geochemical and isotopic characterization of volcanic and geothermal fluids discharged from the Ecuadorian volcanic arc. Geofluids 10, 525–541.

Karl, T.R., Trenberth, K.E., 2003. Modern Global Climate Change. Science (80-.). 302, 1719–1723. https://doi.org/10.1126/science.1090228

Kearey, P., Brooks, M., Hill, I., 2002. An introduction to geophysical exploration. J. African Earth Sci. 4, 46–73. https://doi.org/10.1016/j.jafrearsci.2017.04.031

Li, Z., Fu, G., 2019. Application of Magnetic Susceptibility Parameters in Research of Igneous Rock in Chepaizi Application of Magnetic Susceptibility Parameters in Research of Igneous Rock in Chepaizi. https://doi.org/10.1088/1742-6596/1176/4/042068

Lloret, A., Labus, J., 2014. Geothermal Development in Ecuador: History, Current Status and Future 11.

Lund, J.W., Boyd, T.L., 2016. Direct utilization of geothermal energy 2015 worldwide review. Geothermics 60, 66–93. https://doi.org/10.1016/j.geothermics.2015.11.004

Lund, J.W., Freeston, D.H., Boyd, T.L., 2010. Direct utilization of geothermal energy 2010 worldwide review. Geothermics 40, 159–180. https://doi.org/https://doi.org/10.1016/j.geothermics.2011.07.004

Manzella, A., 1999. Geophysical methods in geothermal exploration. Unpubl. Lect. notes Int. Inst. Geotherm. Res. Pisa, Italy 38:1.

Mohammadzadeh-Moghaddam, M., Oskooi, B., Mirzaei, M., Jouneghani, S.J., 2012. Magnetic studies for geothermal exploration in Mahallat, Iran 1–4. https://doi.org/10.1190/ist092012-001.62

Óskarsson, F., Ármannsson, H., 2015. Geochemical methods in geothermal surface exploration. Short Course X Explor. Dev. Geotherm. Resour. 1–12.

Phuong, N.K., Harijoko, A., Itoi, R., Unoki, Y., 2012. Water geochemistry and soil gas survey at Ungaran geothermal field, central Java, Indonesia. J. Volcanol. Geotherm. Res. 229–230, 23–33. https://doi.org/10.1016/j.jvolgeores.2012.04.004

Piedra Lara, A.L., 2011. Proyecto de una central de generación geotérmica en el Ecuador 6–8. https://doi.org/10.16309/j.cnki.issn.1007-1776.2003.03.004

Pilicita, B., 2016. A 3D model of the Chachimbiro Geothermal System in Ecuador using PETREL. Unu-Gtp 715–750.

Ragnarsson, Á., 2015. Geothermal Development in Iceland. Proc. World Geotherm. Congr. 2015 2010, 19–25.

Rivas, J., 2009. Gravity and magnetic methods. Geophys. Miner. Explor. Geosci. 85–192. https://doi.org/10.1017/cbo9781139024358.005

Saemundsson, K., Axelsson, G., Steingrímsson, B., 2011. Geothermal systems in global perspective. Present. „Short Course Geotherm. Drilling, Resour. Dev. Power Plants“ Organ. by UNU-GTP LaGeo, St. Tecla, El Salvador 16–22, 16–22.

Sircar, A., Shah, M., Sahajpal, S., Vaidya, D., Dhale, S., Chaudhary, A., 2015. Geothermal exploration in Gujarat: case study from Dholera. Geotherm. Energy 3, 22. https://doi.org/10.1186/s40517-015-0041-5

SYR, 2012. Consultoría para el Estudio de Prefactibilidad Inicial para Elaborar el Modelo Geotérmico Conceptual del Proyecto Chachimbiro INFORME FINAL 132.

Syukri, M., Saad, R., Marwan, Tarmizi, Fadhli, Z., Safitri, R., 2018. Volcanic Hazard Implication

Based on Magnetic Signatures Study of Seulawah Agam Geothermal System, Indonesia. J. Phys. Conf. Ser. 1120, 0–9. https://doi.org/10.1088/1742-6596/1120/1/012028

Telford, W.M., Geldart, L.P., Sheriff, R.E., 1990. Applied Geophysics, 2nd ed, Nature. Cambridge University Press. https://doi.org/10.1017/CBO9781139167932

Torres Calderón, M.A., 2014. STUDY OF CHACHIMBIRO AND CHACANA GEOTHERMAL PROJECTS, ECUADOR, AND VOLUMETRIC ASSESSMENT.

Ugalde, H., Yañez, G., Morris, B., Limited, W., Catolica, P.U., 2013. TOPOGRAPHIC EFFECTS ON MAGNETIC DATA : DATA REDUCTION AND APPLICATION TO THE SOUTHERN ANDES, in: 13th SAGA Biennial Conference and Exhibition.

Vallejo Cruz, C., 2007. Evolution of the Western Cordillera in the Andes of Ecuador (Late Cretaceous-Paleogene). Brisk Bin. Robust Invariant Scalable Keypoints 12–19.

Villacreses Baque, S.G., Bravo Cadena, V.A., De, M., 2017. Diseño de generación eléctrica por fuentes geotérmicas en la zona norte del país–Chachimbiro 133.

Williams, L.O., 2002. Fossil fuels. An End to Glob. Warm. 1–31. https://doi.org/10.1016/b978-008044045-3/50007-4

Withagen, C., 1994. Pollution and exhaustibility of fossil fuels. Resour. Energy Econ. 16, 235–242. https://doi.org/10.1016/0928-7655(94)90007-8

Yang, T., Chou, Y.M., Ferré, E.C., Dekkers, M.J., Chen, J., Yeh, E.C., Tanikawa, W., 2020. Faulting Processes Unveiled by Magnetic Properties of Fault Rocks. Rev. Geophys. 58, 1–60. https://doi.org/10.1029/2019RG000690

10. Appendix

Table A1: Measured magnetic data with their coordinates.

Station ID	Latitude	Longitude	UTM_X	UTM_Y	Magnetic_data (nT)
1	0.452391	-78.275829	803237.715	50059.76	29539
2	0.453715	-78.275558	803267.849	50206.279	29470
3	0.452838	-78.276443	803169.298	50109.197	29452
4	0.454074	-78.276233	803192.64	50245.977	29354
5	0.451724	-78.272167	803645.683	49986.105	29353
6	0.453548	-78.275541	803269.749	50187.801	29299
7	0.453918	-78.276052	803212.809	50228.722	29288
8	0.453672	-78.276014	803217.053	50201.502	29286
9	0.453355	-78.276512	803161.59	50166.403	29276
10	0.452929	-78.276106	803206.835	50119.281	29255
11	0.45337	-78.275681	803254.161	50168.098	29255
12	0.45385	-78.276198	803196.548	50221.191	29254
13	0.455834	-78.273483	803498.911	50440.847	29254
14	0.457576	-78.269275	803967.603	50633.789	29252
15	0.455123	-78.269916	803896.299	50362.321	29250
16	0.453831	-78.275852	803235.093	50219.103	29247
17	0.453636	-78.275751	803246.352	50197.529	29238
18	0.453177	-78.27541	803284.358	50146.753	29233
19	0.452936	-78.276389	803175.309	50120.044	29230
20	0.454949	-78.274336	803403.926	50342.88	29227
21	0.453443	-78.275422	803283.01	50176.187	29227
22	0.456945	-78.269973	803889.873	50563.935	29226
23	0.454238	-78.273551	803491.403	50264.237	29224
24	0.458046	-78.269702	803920.016	50685.779	29222
25	0.453252	-78.275605	803262.632	50155.044	29220
26	0.456767	-78.270911	803785.389	50544.198	29220
27	0.453979	-78.275224	803305.044	50235.507	29218
28	0.456482	-78.273511	803495.765	50512.551	29214
29	0.455723	-78.270964	803779.528	50428.671	29210
30	0.458141	-78.269863	803902.076	50696.285	29208
31	0.456736	-78.269547	803937.338	50540.826	29208
32	0.453445	-78.275942	803225.083	50176.386	29207
33	0.458292	-78.268856	804014.249	50713.037	29205
34	0.455649	-78.273901	803452.354	50420.358	29204
35	0.455346	-78.273469	803500.491	50386.847	29204
36	0.453118	-78.276006	803217.967	50140.199	29203
37	0.452642	-78.27632	803183.008	50087.514	29202
38	0.454119	-78.274066	803434.038	50251.047	29201
39	0.45417	-78.273819	803461.551	50256.701	29201
40	0.453663	-78.275041	803325.444	50200.547	29200
41	0.454131	-78.274327	803404.962	50252.364	29200
42	0.453938	-78.274245	803414.105	50231.011	29200
43	0.455824	-78.273622	803483.427	50439.735	29199
44	0.454491	-78.273842	803458.975	50292.221	29199
45	0.45618	-78.269116	803985.374	50479.319	29198
46	0.45347	-78.276191	803197.344	50179.142	29197
47	0.455698	-78.271127	803761.372	50425.897	29195
48	0.455478	-78.270197	803864.981	50401.592	29194

Station ID	Latitude	Longitude	UTM_X	UTM_Y	Magnetic_data (nT)
49	0.456942	-78.271885	803676.879	50563.522	29192
50	0.457917	-78.26899	803999.337	50671.535	29192
51	0.45668	-78.270341	803848.89	50534.595	29191
52	0.455185	-78.274188	803420.403	50369.001	29190
53	0.456542	-78.269262	803969.094	50519.37	29190
54	0.456363	-78.273497	803497.329	50499.384	29189
55	0.455205	-78.274009	803440.342	50371.222	29188
56	0.454398	-78.274305	803407.402	50281.91	29188
57	0.453301	-78.275233	803304.07	50160.481	29188
58	0.454581	-78.273321	803517.01	50302.202	29188
59	0.454251	-78.275302	803296.344	50265.602	29185
60	0.45381	-78.275136	803314.855	50216.809	29184
61	0.454606	-78.272745	803581.175	50304.992	29184
62	0.45434	-78.272729	803582.968	50275.558	29183
63	0.453931	-78.275457	803279.091	50230.185	29181
64	0.453169	-78.27656	803156.25	50145.819	29180
65	0.455009	-78.274188	803420.41	50349.526	29180
66	0.454497	-78.274704	803362.95	50292.848	29179
67	0.453833	-78.274814	803350.724	50219.368	29179
68	0.456196	-78.269024	803995.622	50481.093	29179
69	0.455528	-78.273959	803445.898	50406.966	29178
70	0.453401	-78.274995	803330.579	50171.557	29178
71	0.453911	-78.27444	803392.383	50228.015	29177
72	0.454522	-78.272954	803557.896	50295.688	29176
73	0.45433	-78.266819	804241.335	50274.701	29176
74	0.456271	-78.273606	803485.191	50489.199	29175
75	0.455003	-78.273128	803538.492	50348.907	29175
76	0.453324	-78.266861	804236.698	50163.378	29175
77	0.454413	-78.274982	803331.985	50283.542	29174
78	0.45327	-78.274685	803365.118	50157.074	29174
79	0.457115	-78.270129	803872.488	50582.74	29174
80	0.454937	-78.269354	803958.913	50341.763	29174
81	0.454053	-78.274648	803369.207	50243.719	29172
82	0.456392	-78.270043	803882.098	50502.739	29172
83	0.454682	-78.274506	803384.999	50313.328	29171
84	0.454272	-78.274711	803362.18	50267.95	29171
85	0.453594	-78.276439	803169.712	50192.853	29170
86	0.454746	-78.273998	803441.587	50320.431	29170
87	0.455159	-78.273306	803518.657	50366.162	29170
88	0.457163	-78.272036	803660.049	50587.97	29170
89	0.456032	-78.270338	803849.251	50462.89	29169
90	0.457331	-78.270082	803877.714	50606.644	29169
91	0.455519	-78.270426	803839.469	50406.119	29168
92	0.456539	-78.26948	803944.81	50519.029	29166
93	0.455446	-78.270604	803819.644	50398.034	29165
94	0.453787	-78.275338	803292.353	50214.256	29164
95	0.454023	-78.27245	803614.061	50240.492	29164
96	0.454169	-78.274909	803340.127	50256.545	29162
97	0.45406	-78.273414	803506.672	50244.546	29162
98	0.453932	-78.273128	803538.537	50230.394	29162
99	0.454773	-78.269069	803990.669	50323.627	29162
100	0.452885	-78.274313	803406.574	50114.487	29161
101	0.456729	-78.269801	803909.043	50540.04	29161

Station ID	Latitude	Longitude	UTM_X	UTM_Y	Magnetic_data (nT)
102	0.453309	-78.267141	804205.507	50161.707	29161
103	0.456193	-78.27351	803495.888	50480.572	29160
104	0.455012	-78.273944	803447.591	50349.868	29160
105	0.454146	-78.273179	803532.847	50254.072	29160
106	0.454874	-78.272696	803586.622	50334.65	29160
107	0.456585	-78.271449	803725.464	50524.036	29160
108	0.454383	-78.273197	803530.832	50280.297	29159
109	0.45398	-78.273668	803478.38	50235.683	29159
110	0.456646	-78.271689	803698.726	50530.776	29159
111	0.455758	-78.270254	803858.62	50432.574	29159
112	0.456706	-78.270641	803815.469	50537.46	29159
113	0.45482	-78.274317	803406.048	50328.607	29158
114	0.456811	-78.271634	803704.846	50549.036	29158
115	0.458149	-78.269131	803983.62	50697.201	29158
116	0.457622	-78.269808	803908.225	50638.856	29158
117	0.455684	-78.273745	803469.731	50424.238	29157
118	0.455235	-78.273827	803460.615	50374.549	29157
119	0.454757	-78.272491	803609.463	50321.712	29157
120	0.455147	-78.269666	803924.148	50364.987	29157
121	0.455247	-78.270258	803858.196	50376.028	29157
122	0.454924	-78.269617	803929.616	50340.313	29157
123	0.456486	-78.270943	803781.836	50513.102	29156
124	0.454276	-78.27448	803387.912	50268.403	29155
125	0.455467	-78.273651	803480.212	50400.229	29155
126	0.454243	-78.27411	803429.131	50264.767	29155
127	0.454358	-78.273965	803445.279	50277.498	29155
128	0.456397	-78.269325	803962.082	50503.322	29155
129	0.453299	-78.275886	803231.327	50160.233	29154
130	0.45514	-78.273575	803488.692	50364.048	29154
131	0.454171	-78.2751	803318.85	50256.758	29153
132	0.454648	-78.274252	803413.296	50309.576	29153
133	0.455093	-78.272823	803572.465	50358.879	29153
134	0.452272	-78.271536	803715.953	50046.771	29153
135	0.453482	-78.273685	803476.507	50180.575	29152
136	0.457986	-78.271532	803716.159	50679.062	29151
137	0.455636	-78.273421	803505.826	50418.94	29150
138	0.456486	-78.270559	803824.613	50513.119	29150
139	0.455165	-78.268632	804039.333	50367.023	29150
140	0.455597	-78.270735	803805.044	50414.738	29149
141	0.45372	-78.274372	803399.967	50206.882	29148
142	0.453214	-78.270859	803791.33	50151.038	29148
143	0.455449	-78.274122	803427.744	50398.217	29147
144	0.45538	-78.273958	803446.016	50390.589	29147
145	0.452574	-78.276514	803161.399	50079.981	29146
146	0.456443	-78.270293	803854.247	50508.372	29146
147	0.454882	-78.269891	803899.094	50335.654	29146
148	0.455393	-78.269212	803974.713	50392.228	29145
149	0.45252	-78.275488	803275.696	50074.048	29144
150	0.45451	-78.274078	803432.685	50294.313	29144
151	0.455482	-78.26948	803944.854	50402.065	29144
152	0.455249	-78.270504	803830.792	50376.239	29144
153	0.458385	-78.269081	803989.18	50723.318	29143
154	0.453129	-78.266848	804238.154	50141.801	29143

Station ID	Latitude	Longitude	UTM_X	UTM_Y	Magnetic_data (nT)
155	0.453079	-78.27578	803243.145	50135.893	29142
156	0.458336	-78.270049	803881.348	50717.855	29142
157	0.453985	-78.274952	803335.345	50236.182	29141
158	0.45785	-78.270139	803871.343	50664.072	29141
159	0.444737	-78.273735	803471.298	49212.885	29141
160	0.453571	-78.275383	803287.349	50190.352	29140
161	0.45349	-78.274776	803354.971	50181.415	29140
162	0.454141	-78.27254	803604.031	50253.546	29140
163	0.456167	-78.269755	803914.191	50477.853	29140
164	0.458693	-78.270728	803805.693	50757.33	29140
165	0.445627	-78.273826	803461.125	49311.365	29140
166	0.45523	-78.26946	803947.093	50374.18	29139
167	0.456452	-78.269753	803914.401	50509.39	29138
168	0.455061	-78.270054	803880.929	50355.454	29138
169	0.452183	-78.271187	803754.834	50036.937	29138
170	0.453878	-78.273919	803450.423	50224.385	29137
171	0.455931	-78.271569	803712.124	50451.662	29137
172	0.456498	-78.270821	803795.426	50514.435	29137
173	0.456879	-78.270438	803838.075	50556.612	29137
174	0.455524	-78.2692	803976.044	50406.724	29137
175	0.454717	-78.268454	804059.181	50317.456	29137
176	0.453497	-78.275233	803304.062	50182.17	29136
177	0.45491	-78.273684	803476.559	50338.592	29136
178	0.457531	-78.269435	803949.781	50628.802	29136
179	0.454227	-78.266527	804273.867	50263.315	29136
180	0.452265	-78.272128	803650.005	50045.972	29136
181	0.45817	-78.269342	803960.114	50699.516	29135
182	0.456399	-78.269064	803991.157	50503.555	29135
183	0.454943	-78.273411	803506.969	50342.255	29134
184	0.453486	-78.274511	803384.492	50180.983	29134
185	0.454521	-78.272518	803606.466	50295.596	29134
186	0.458036	-78.269987	803888.268	50684.66	29134
187	0.458174	-78.270211	803863.308	50699.921	29134
188	0.454915	-78.270186	803866.23	50339.293	29134
189	0.456917	-78.2721	803652.93	50560.746	29132
190	0.455418	-78.269958	803891.608	50394.963	29132
191	0.454531	-78.268971	804001.596	50296.852	29132
192	0.453911	-78.266481	804279.005	50228.35	29132
193	0.453122	-78.271011	803774.402	50140.851	29132
194	0.454247	-78.267139	804205.69	50265.503	29131
195	0.454508	-78.274447	803391.579	50294.076	29130
196	0.45639	-78.271212	803751.874	50502.468	29130
197	0.456807	-78.270028	803883.752	50548.662	29130
198	0.446939	-78.273037	803548.964	49456.579	29130
199	0.454497	-78.273597	803486.268	50292.895	29129
200	0.456021	-78.269249	803970.565	50461.719	29129
201	0.45247	-78.271887	803676.844	50068.666	29129
202	0.455954	-78.270141	803871.2	50454.267	29128
203	0.458604	-78.269408	803952.743	50747.538	29128
204	0.454749	-78.27071	803807.864	50320.902	29128
205	0.4562	-78.269301	803964.764	50481.524	29127
206	0.453178	-78.274932	803337.606	50146.883	29126
207	0.454491	-78.272307	803629.972	50292.285	29126

Station ID	Latitude	Longitude	UTM_X	UTM_Y	Magnetic_data (nT)
208	0.454125	-78.272103	803652.712	50251.794	29126
209	0.457802	-78.269481	803944.645	50658.788	29126
210	0.452278	-78.276112	803206.194	50047.244	29125
211	0.454014	-78.272325	803627.987	50239.501	29125
212	0.453182	-78.267365	804180.559	50147.644	29125
213	0.453932	-78.271934	803671.547	50230.444	29125
214	0.446921	-78.274369	803400.582	49454.532	29125
215	0.452843	-78.275749	803246.608	50109.779	29124
216	0.4576	-78.269965	803890.737	50636.415	29124
217	0.454979	-78.270667	803812.645	50346.355	29124
218	0.455417	-78.269683	803922.243	50394.864	29123
219	0.454552	-78.268736	804027.774	50299.186	29123
220	0.453062	-78.270724	803806.375	50134.224	29123
221	0.453488	-78.27193	803672.011	50181.313	29123
222	0.454358	-78.272446	803614.493	50277.562	29122
223	0.44665	-78.273968	803445.264	49424.56	29122
224	0.45602	-78.273555	803490.883	50461.426	29121
225	0.454675	-78.27376	803468.102	50312.585	29121
226	0.454145	-78.272955	803557.8	50253.971	29120
227	0.453589	-78.266495	804277.459	50192.718	29120
228	0.4552	-78.268837	804016.495	50370.887	29119
229	0.453686	-78.271832	803682.92	50203.227	29119
230	0.453565	-78.271586	803710.329	50189.848	29119
231	0.452526	-78.271713	803696.225	50074.871	29119
232	0.454664	-78.269332	803961.375	50311.554	29118
233	0.457627	-78.271947	803669.944	50639.319	29117
234	0.453865	-78.273411	803507.014	50222.968	29116
235	0.453713	-78.273002	803552.583	50206.165	29116
236	0.455932	-78.269607	803930.688	50451.855	29116
237	0.453734	-78.273661	803479.17	50208.462	29115
238	0.446923	-78.272828	803572.247	49454.817	29115
239	0.453689	-78.274577	803377.131	50203.444	29114
240	0.454279	-78.272137	803648.918	50268.833	29114
241	0.458437	-78.270295	803853.94	50729.021	29114
242	0.453292	-78.27618	803198.577	50159.446	29113
243	0.452246	-78.271782	803688.55	50043.884	29113
244	0.454761	-78.273008	803551.87	50322.133	29112
245	0.454797	-78.270961	803779.901	50326.203	29112
246	0.454968	-78.268475	804056.831	50345.23	29112
247	0.453243	-78.273823	803461.144	50154.123	29111
248	0.458528	-78.269634	803927.57	50739.118	29111
249	0.455019	-78.269061	803991.55	50350.849	29111
250	0.447922	-78.268462	804058.573	49565.544	29111
251	0.456923	-78.270674	803811.784	50561.471	29110
252	0.453178	-78.27424	803414.694	50146.912	29109
253	0.453783	-78.272708	803585.331	50213.924	29109
254	0.456114	-78.270126	803872.864	50471.973	29108
255	0.453282	-78.271563	803712.903	50158.533	29108
256	0.453546	-78.273879	803454.893	50187.649	29107
257	0.455822	-78.269446	803948.627	50439.69	29107
258	0.457842	-78.271734	803693.663	50663.119	29106
259	0.458578	-78.27011	803874.543	50744.631	29106
260	0.457807	-78.27208	803655.12	50659.231	29105

Station ID	Latitude	Longitude	UTM_X	UTM_Y	Magnetic_data (nT)
261	0.454673	-78.270361	803846.746	50312.507	29105
262	0.454242	-78.2675	804165.476	50264.934	29105
263	0.445827	-78.271642	803704.411	49333.586	29105
264	0.452861	-78.267886	804122.533	50112.101	29105
265	0.448635	-78.265893	804344.727	49644.549	29105
266	0.4487	-78.265667	804369.901	49651.751	29105
267	0.451398	-78.267546	804160.47	49950.225	29105
268	0.451429	-78.267333	804184.197	49953.664	29105
269	0.452325	-78.276384	803175.892	50052.433	29104
270	0.456295	-78.269542	803937.913	50492.026	29104
271	0.456173	-78.269454	803947.721	50478.53	29104
272	0.454665	-78.270073	803878.829	50311.634	29104
273	0.452515	-78.271492	803720.844	50073.663	29104
274	0.445079	-78.273715	803473.512	49250.73	29104
275	0.450432	-78.265545	804383.42	49843.414	29104
276	0.452775	-78.275457	803279.139	50102.267	29103
277	0.456856	-78.270218	803862.584	50554.076	29103
278	0.458021	-78.271947	803669.927	50682.917	29103
279	0.455236	-78.269078	803989.647	50374.86	29103
280	0.454018	-78.267039	804216.84	50240.167	29103
281	0.444962	-78.273598	803486.551	49237.788	29103
282	0.453114	-78.274678	803365.904	50139.812	29102
283	0.455738	-78.270063	803879.898	50430.368	29102
284	0.453026	-78.273164	803534.565	50130.138	29102
285	0.454039	-78.270116	803874.065	50242.361	29102
286	0.453413	-78.27413	803426.938	50172.921	29101
287	0.45566	-78.269635	803927.58	50421.755	29101
288	0.457948	-78.270469	803834.577	50674.902	29101
289	0.458489	-78.270449	803836.782	50734.768	29101
290	0.45299	-78.272903	803563.641	50126.165	29101
291	0.456638	-78.272499	803608.493	50529.856	29100
292	0.456702	-78.271868	803678.783	50536.965	29100
293	0.455869	-78.271308	803741.201	50444.812	29100
294	0.458034	-78.269485	803944.19	50684.46	29100
295	0.453555	-78.272094	803653.739	50188.72	29100
296	0.452324	-78.272328	803627.723	50052.492	29100
297	0.454772	-78.27351	803495.948	50323.329	29099
298	0.455023	-78.272438	803615.356	50351.149	29099
299	0.45749	-78.271598	803708.828	50624.174	29099
300	0.454475	-78.269938	803893.876	50290.615	29099
301	0.453695	-78.272398	803619.868	50204.199	29099
302	0.454055	-78.270322	803851.116	50244.123	29099
303	0.446007	-78.273624	803483.612	49353.423	29099
304	0.453024	-78.275304	803296.172	50129.827	29098
305	0.454713	-78.269717	803918.485	50316.96	29098
306	0.453456	-78.267138	804205.835	50177.973	29098
307	0.452974	-78.275105	803318.343	50124.302	29097
308	0.45594	-78.271085	803766.04	50452.678	29097
309	0.458166	-78.271734	803693.649	50698.972	29097
310	0.454945	-78.270394	803843.058	50342.604	29097
311	0.455676	-78.269874	803900.955	50423.516	29096
312	0.456666	-78.271117	803762.445	50533.013	29096
313	0.454848	-78.26873	804028.43	50331.94	29096

Station ID	Latitude	Longitude	UTM_X	UTM_Y	Magnetic_data (nT)
314	0.447995	-78.26977	803912.86	49573.567	29096
315	0.447881	-78.269337	803961.1	49560.97	29096
316	0.458371	-78.269309	803963.782	50721.759	29095
317	0.446105	-78.273407	803507.781	49364.276	29095
318	0.452725	-78.275246	803302.646	50096.743	29094
319	0.456476	-78.271777	803688.93	50511.96	29094
320	0.456677	-78.270071	803878.967	50534.275	29093
321	0.457949	-78.269274	803967.698	50675.064	29093
322	0.455003	-78.27089	803787.802	50349.001	29093
323	0.445095	-78.273351	803514.061	49252.515	29093
324	0.454828	-78.273224	803527.805	50329.538	29092
325	0.45407	-78.272742	803581.531	50245.681	29092
326	0.452214	-78.270638	803815.991	50040.391	29092
327	0.453113	-78.276321	803182.877	50139.633	29091
328	0.453438	-78.267386	804178.209	50175.971	29091
329	0.453392	-78.271363	803735.178	50170.714	29091
330	0.453087	-78.269928	803895.048	50137.024	29091
331	0.446786	-78.273552	803491.6	49439.627	29091
332	0.450296	-78.266773	804246.627	49828.313	29091
333	0.454568	-78.270596	803820.571	50300.878	29090
334	0.455192	-78.269247	803970.822	50369.984	29090
335	0.444425	-78.273282	803521.775	49178.379	29090
336	0.45871	-78.270448	803836.884	50759.223	29089
337	0.454447	-78.268396	804065.654	50287.581	29089
338	0.452185	-78.270911	803785.58	50037.17	29089
339	0.452226	-78.269803	803909.008	50041.754	29089
340	0.444174	-78.271512	803718.96	49150.677	29089
341	0.453456	-78.273449	803502.798	50177.708	29088
342	0.456234	-78.270969	803778.95	50485.216	29088
343	0.457415	-78.271854	803680.313	50615.864	29088
344	0.45841	-78.271296	803742.431	50725.99	29088
345	0.454324	-78.270158	803869.374	50273.896	29088
346	0.453926	-78.270536	803827.282	50229.839	29088
347	0.452129	-78.272074	803656.026	50030.925	29088
348	0.446842	-78.274322	803405.821	49445.792	29088
349	0.444715	-78.273474	803500.374	49210.461	29088
350	0.452475	-78.275207	803307.001	50069.081	29087
351	0.448074	-78.273454	803502.464	49582.156	29087
352	0.452657	-78.26708	804212.329	50089.561	29087
353	0.452712	-78.275078	803321.361	50095.312	29086
354	0.456724	-78.27214	803648.482	50539.388	29086
355	0.457719	-78.269146	803981.967	50649.618	29086
356	0.455189	-78.270688	803810.297	50369.592	29085
357	0.454028	-78.268116	804096.863	50241.228	29085
358	0.446244	-78.273157	803535.625	49379.667	29085
359	0.451451	-78.267782	804134.178	49956.079	29085
360	0.456471	-78.272028	803660.969	50511.397	29084
361	0.452502	-78.272569	803600.868	50072.179	29084
362	0.450271	-78.266882	804234.486	49825.542	29084
363	0.449587	-78.2727	803586.396	49749.61	29083
364	0.453544	-78.272988	803554.149	50187.465	29083
365	0.453568	-78.270435	803838.548	50190.228	29083
366	0.445874	-78.273501	803497.319	49338.71	29083

Station ID	Latitude	Longitude	UTM_X	UTM_Y	Magnetic_data (nT)
367	0.452636	-78.26681	804242.408	50087.249	29083
368	0.448809	-78.267185	804200.792	49663.749	29083
369	0.455789	-78.270756	803802.697	50435.983	29082
370	0.457615	-78.271421	803728.54	50638.013	29082
371	0.45868	-78.27118	803755.342	50755.872	29082
372	0.454158	-78.266702	804254.375	50255.673	29082
373	0.452369	-78.274954	803335.189	50057.362	29081
374	0.453283	-78.274398	803397.088	50158.525	29081
375	0.458308	-78.271503	803719.376	50714.695	29081
376	0.453912	-78.269967	803890.669	50228.314	29081
377	0.444721	-78.272887	803565.765	49211.149	29081
378	0.446276	-78.272444	803615.051	49383.238	29081
379	0.457825	-78.269831	803905.655	50661.318	29080
380	0.458165	-78.270915	803784.884	50698.896	29080
381	0.450265	-78.266623	804263.338	49824.889	29080
382	0.452885	-78.274568	803378.167	50114.476	29079
383	0.456208	-78.271178	803755.669	50482.33	29079
384	0.45838	-78.270686	803810.385	50722.697	29079
385	0.454521	-78.27035	803847.978	50295.687	29079
386	0.454229	-78.269245	803971.085	50263.422	29079
387	0.454214	-78.267744	804138.295	50261.826	29079
388	0.449265	-78.272537	803604.568	49713.986	29079
389	0.446661	-78.273796	803464.424	49425.785	29079
390	0.455954	-78.269849	803903.728	50454.279	29078
391	0.458211	-78.27045	803836.683	50704.006	29078
392	0.458066	-78.268838	804016.263	50688.029	29078
393	0.454465	-78.269629	803928.298	50289.521	29078
394	0.453453	-78.26784	804127.633	50177.612	29078
395	0.452514	-78.272048	803658.907	50073.529	29078
396	0.445916	-78.273804	803463.564	49343.346	29078
397	0.44536	-78.27375	803469.602	49281.823	29078
398	0.445812	-78.273128	803538.873	49331.865	29078
399	0.453682	-78.270669	803812.476	50202.833	29077
400	0.448619	-78.267082	804212.274	49642.729	29077
401	0.454429	-78.272002	803663.951	50285.437	29076
402	0.456189	-78.271903	803674.906	50480.197	29076
403	0.457655	-78.270899	803786.688	50642.462	29076
404	0.457977	-78.270317	803851.508	50678.118	29076
405	0.454099	-78.269053	803992.479	50249.045	29076
406	0.453397	-78.267632	804150.806	50171.424	29076
407	0.452178	-78.272535	803604.67	50036.328	29076
408	0.44454	-78.273528	803494.366	49191.094	29076
409	0.452983	-78.267336	804183.798	50125.624	29076
410	0.446717	-78.27318	803533.043	49432.007	29075
411	0.451534	-78.268021	804107.55	49965.254	29075
412	0.453508	-78.274251	803413.455	50183.428	29074
413	0.454207	-78.266873	804235.324	50261.088	29074
414	0.454026	-78.267269	804191.218	50241.042	29074
415	0.449055	-78.27269	803587.532	49690.742	29074
416	0.445594	-78.271484	803722.021	49307.81	29074
417	0.445954	-78.271958	803669.204	49347.627	29074
418	0.44455	-78.270622	803818.09	49192.32	29074
419	0.454821	-78.272267	803634.414	50328.804	29072

Station ID	Latitude	Longitude	UTM_X	UTM_Y	Magnetic_data (nT)
420	0.453604	-78.273267	803523.066	50194.093	29072
421	0.452814	-78.274054	803435.429	50106.641	29072
422	0.45876	-78.270296	803853.815	50764.763	29072
423	0.453778	-78.268727	804028.809	50213.538	29072
424	0.453875	-78.268313	804074.924	50224.289	29072
425	0.452779	-78.273736	803470.855	50102.782	29072
426	0.453333	-78.273301	803519.29	50164.104	29072
427	0.453174	-78.272122	803650.636	50146.559	29072
428	0.44537	-78.272881	803566.407	49282.965	29072
429	0.452929	-78.267612	804153.054	50119.637	29072
430	0.457935	-78.270733	803805.168	50673.452	29071
431	0.454164	-78.27035	803847.992	50256.183	29071
432	0.445916	-78.272503	803608.493	49343.399	29071
433	0.446872	-78.272555	803602.661	49449.185	29071
434	0.452819	-78.268167	804091.232	50107.442	29071
435	0.445186	-78.269977	803889.916	49262.724	29071
436	0.453161	-78.27049	803832.439	50145.189	29070
437	0.452423	-78.271111	803763.291	50063.498	29070
438	0.448241	-78.269642	803927.109	49600.794	29070
439	0.444859	-78.27265	803592.161	49226.429	29070
440	0.454388	-78.269293	803965.731	50281.015	29069
441	0.453058	-78.273671	803478.084	50133.658	29069
442	0.446059	-78.272274	803633.997	49359.233	29069
443	0.450018	-78.266238	804306.237	49797.573	29069
444	0.452593	-78.27573	803248.735	50082.116	29068
445	0.457904	-78.271154	803758.271	50670.004	29068
446	0.452166	-78.273892	803453.502	50034.943	29068
447	0.453275	-78.27107	803767.823	50157.779	29068
448	0.453767	-78.27042	803840.211	50212.249	29068
449	0.452283	-78.274748	803358.141	50047.854	29067
450	0.450712	-78.273419	803506.254	49874.069	29067
451	0.447524	-78.273016	803551.279	49521.313	29067
452	0.446918	-78.273321	803517.328	49454.243	29067
453	0.446456	-78.273736	803471.117	49403.103	29067
454	0.455943	-78.273435	803504.254	50452.911	29066
455	0.444823	-78.273261	803524.098	49222.421	29066
456	0.44605	-78.271799	803686.912	49358.256	29066
457	0.453335	-78.266599	804265.884	50164.607	29065
458	0.453963	-78.270181	803866.827	50233.948	29065
459	0.446102	-78.271157	803758.428	49364.037	29065
460	0.446589	-78.273483	803499.295	49417.83	29065
461	0.452827	-78.274885	803342.856	50108.045	29064
462	0.447681	-78.273076	803544.589	49538.684	29064
463	0.445815	-78.272197	803642.585	49332.236	29064
464	0.450409	-78.26717	804202.397	49840.801	29064
465	0.452584	-78.274836	803348.325	50081.158	29063
466	0.451137	-78.273707	803474.154	49921.085	29063
467	0.452558	-78.274662	803367.709	50078.288	29063
468	0.453251	-78.271801	803686.391	50155.093	29063
469	0.445447	-78.271714	803696.406	49291.534	29063
470	0.445726	-78.271244	803748.752	49322.427	29063
471	0.44564	-78.273344	803514.818	49312.823	29063
472	0.446492	-78.272665	803590.423	49407.131	29063

Station ID	Latitude	Longitude	UTM_X	UTM_Y	Magnetic_data (nT)
473	0.452978	-78.267075	804212.873	50125.082	29063
474	0.45414	-78.271868	803678.89	50253.463	29062
475	0.456846	-78.27235	803625.083	50552.879	29062
476	0.457402	-78.272126	803650.013	50614.413	29062
477	0.453269	-78.272988	803554.161	50157.035	29062
478	0.452206	-78.270372	803845.623	50039.517	29062
479	0.452449	-78.270787	803799.383	50066.389	29062
480	0.44454	-78.272879	803566.664	49191.121	29062
481	0.44596	-78.272895	803564.823	49348.252	29062
482	0.447923	-78.269545	803937.928	49565.609	29062
483	0.456158	-78.27163	803705.319	50476.778	29061
484	0.458497	-78.270976	803778.075	50735.631	29061
485	0.453081	-78.272535	803604.632	50136.25	29061
486	0.445954	-78.271396	803731.81	49347.65	29060
487	0.444955	-78.273019	803551.051	49237.037	29060
488	0.445612	-78.272965	803557.039	49309.741	29060
489	0.446391	-78.272923	803561.686	49395.944	29060
490	0.447746	-78.269035	803994.748	49546.044	29060
491	0.45042	-78.266685	804256.425	49842.038	29060
492	0.456038	-78.270792	803798.676	50463.535	29059
493	0.45175	-78.273555	803491.061	49988.924	29059
494	0.453931	-78.270332	803850.007	50230.401	29059
495	0.453336	-78.270181	803866.853	50164.567	29059
496	0.445694	-78.271875	803678.46	49318.859	29059
497	0.445218	-78.273113	803540.569	49266.136	29059
498	0.44612	-78.272666	803590.327	49365.966	29059
499	0.44879	-78.266942	804227.863	49661.657	29059
500	0.453761	-78.270184	803866.501	50211.595	29058
501	0.452551	-78.272217	803640.079	50077.616	29058
502	0.450346	-78.273383	803510.28	49833.57	29058
503	0.445008	-78.272412	803618.667	49242.927	29058
504	0.446722	-78.269167	803980.086	49432.726	29058
505	0.453313	-78.273618	803483.978	50161.877	29057
506	0.453594	-78.270091	803876.869	50193.12	29057
507	0.447316	-78.270168	803868.551	49498.415	29057
508	0.446185	-78.273794	803464.667	49373.112	29057
509	0.445246	-78.272565	803601.614	49269.257	29057
510	0.452774	-78.271609	803707.8	50102.318	29056
511	0.453764	-78.266759	804248.042	50212.072	29055
512	0.445541	-78.272112	803652.065	49301.919	29055
513	0.445094	-78.272792	803576.333	49252.428	29055
514	0.446599	-78.27239	803621.053	49418.982	29055
515	0.447533	-78.269271	803968.467	49522.465	29055
516	0.443232	-78.268941	804005.405	49046.544	29055
517	0.45463	-78.272143	803648.235	50307.673	29054
518	0.458737	-78.270959	803779.959	50762.189	29054
519	0.457609	-78.269644	803926.495	50637.425	29054
520	0.45305	-78.273435	803504.375	50132.782	29054
521	0.452198	-78.270084	803877.707	50038.643	29054
522	0.448599	-78.269847	803904.257	49640.401	29054
523	0.447398	-78.271139	803760.38	49507.448	29054
524	0.446207	-78.272044	803659.613	49375.619	29054
525	0.446754	-78.272844	803570.472	49436.115	29054

Station ID	Latitude	Longitude	UTM_X	UTM_Y	Magnetic_data (nT)
526	0.447918	-78.268205	804087.202	49565.112	29054
527	0.453703	-78.274098	803430.49	50205.013	29053
528	0.4526	-78.27409	803431.428	50082.959	29053
529	0.450438	-78.271572	803712.019	49843.826	29053
530	0.444299	-78.273038	803548.961	49164.446	29053
531	0.445666	-78.272428	803616.858	49315.738	29053
532	0.447364	-78.269051	803992.982	49503.773	29053
533	0.44772	-78.268506	804053.679	49543.189	29053
534	0.45827	-78.269572	803934.488	50710.572	29052
535	0.453515	-78.268024	804107.133	50184.465	29052
536	0.453426	-78.272198	803642.159	50174.441	29052
537	0.445163	-78.27218	803644.506	49260.088	29052
538	0.447189	-78.26884	804016.494	49484.417	29052
539	0.452439	-78.276193	803197.164	50065.056	29051
540	0.453955	-78.266724	804251.933	50233.208	29051
541	0.453667	-78.270326	803850.687	50201.188	29051
542	0.453479	-78.270611	803818.946	50180.372	29051
543	0.444589	-78.273137	803537.921	49196.532	29051
544	0.445537	-78.2736	803486.304	49301.415	29051
545	0.44642	-78.272209	803641.223	49399.182	29051
546	0.450485	-78.273266	803523.308	49848.956	29050
547	0.458281	-78.271109	803763.268	50711.724	29050
548	0.453982	-78.269046	803993.264	50236.098	29050
549	0.453705	-78.267915	804119.268	50205.494	29050
550	0.453734	-78.269934	803894.352	50208.618	29050
551	0.452836	-78.271749	803692.201	50109.172	29050
552	0.449794	-78.272876	803566.782	49772.509	29049
553	0.45319	-78.270666	803812.831	50148.39	29049
554	0.447695	-78.271078	803767.163	49540.316	29049
555	0.447526	-78.271228	803750.46	49521.609	29049
556	0.446381	-78.273522	803494.959	49394.812	29049
557	0.458099	-78.271302	803741.776	50691.576	29048
558	0.451436	-78.272814	803573.62	49954.209	29048
559	0.447441	-78.271951	803669.922	49512.173	29048
560	0.452001	-78.271397	803731.448	50016.789	29047
561	0.449779	-78.269757	803914.234	49770.979	29047
562	0.447673	-78.272076	803655.988	49537.84	29047
563	0.448768	-78.269914	803896.787	49659.099	29047
564	0.446401	-78.270711	803808.099	49397.142	29047
565	0.446226	-78.271895	803676.211	49377.728	29047
566	0.445288	-78.273488	803498.791	49273.866	29047
567	0.444304	-78.270666	803813.198	49165.097	29047
568	0.454306	-78.268881	804011.631	50271.958	29046
569	0.453724	-78.267682	804145.223	50207.606	29046
570	0.447148	-78.273489	803498.603	49479.687	29046
571	0.44552	-78.272652	803591.911	49299.573	29046
572	0.453915	-78.272861	803568.281	50228.524	29045
573	0.449885	-78.273436	803504.395	49782.555	29045
574	0.452193	-78.269548	803937.416	50038.113	29045
575	0.447393	-78.271402	803731.082	49506.884	29045
576	0.448094	-78.269453	803948.169	49584.535	29045
577	0.446477	-78.27326	803524.141	49405.446	29045
578	0.457597	-78.271172	803756.279	50636.032	29044

Station ID	Latitude	Longitude	UTM_X	UTM_Y	Magnetic_data (nT)
579	0.450032	-78.273231	803527.225	49798.83	29044
580	0.453419	-78.270416	803840.671	50173.741	29044
581	0.448808	-78.27255	803603.138	49663.415	29044
582	0.447173	-78.271502	803719.951	49482.536	29044
583	0.446315	-78.270319	803851.771	49387.641	29044
584	0.44577	-78.272735	803582.655	49327.234	29044
585	0.445483	-78.271241	803749.096	49295.537	29044
586	0.45356	-78.269312	803963.649	50189.39	29043
587	0.451343	-78.272093	803653.942	49943.948	29043
588	0.447256	-78.272487	803610.22	49491.679	29043
589	0.447768	-78.269932	803894.823	49548.441	29043
590	0.453779	-78.268925	804006.752	50213.64	29042
591	0.453846	-78.26748	804167.72	50221.115	29042
592	0.452371	-78.269862	803902.43	50057.796	29042
593	0.451468	-78.271952	803669.644	49957.786	29042
594	0.447707	-78.269484	803944.732	49541.71	29042
595	0.453988	-78.268831	804017.214	50236.771	29041
596	0.452715	-78.272429	803616.455	50095.755	29041
597	0.449181	-78.273406	803507.766	49704.654	29041
598	0.449762	-78.273556	803491.032	49768.94	29041
599	0.447283	-78.273775	803466.738	49494.614	29041
600	0.446738	-78.272131	803649.899	49434.374	29041
601	0.447906	-78.267909	804120.177	49563.796	29041
602	0.450262	-78.265757	804359.81	49824.593	29041
603	0.453659	-78.268349	804070.922	50200.386	29040
604	0.452015	-78.272297	803631.189	50018.301	29040
605	0.44588	-78.271006	803775.258	49339.477	29040
606	0.452791	-78.273404	803507.839	50104.124	29039
607	0.450384	-78.270076	803878.673	49837.913	29039
608	0.450896	-78.27179	803687.715	49894.497	29039
609	0.446165	-78.270545	803826.601	49371.034	29039
610	0.446677	-78.270237	803860.891	49427.702	29039
611	0.447529	-78.269588	803933.154	49522.009	29039
612	0.446378	-78.267603	804154.328	49394.725	29039
613	0.45178	-78.274172	803422.327	49992.218	29038
614	0.453596	-78.268248	804082.176	50193.419	29038
615	0.447256	-78.271771	803689.982	49491.709	29038
616	0.446346	-78.271941	803671.081	49391.005	29038
617	0.45263	-78.266416	804286.299	50086.601	29038
618	0.450255	-78.266134	804317.813	49823.803	29038
619	0.455188	-78.27264	803592.847	50369.399	29037
620	0.447392	-78.274038	803437.436	49506.664	29037
621	0.446765	-78.27424	803414.959	49437.275	29037
622	0.447358	-78.269693	803921.464	49503.082	29037
623	0.453908	-78.268578	804045.402	50227.93	29036
624	0.453617	-78.267486	804167.061	50195.774	29036
625	0.453496	-78.272684	803588.016	50182.166	29036
626	0.447022	-78.273741	803470.536	49465.734	29036
627	0.447224	-78.273284	803521.437	49488.105	29036
628	0.454261	-78.269952	803892.325	50266.933	29035
629	0.453733	-78.267045	804216.183	50208.629	29035
630	0.448777	-78.272251	803636.448	49659.997	29035
631	0.450154	-78.273424	803505.72	49812.322	29035

Station ID	Latitude	Longitude	UTM_X	UTM_Y	Magnetic_data (nT)
632	0.453328	-78.272417	803617.767	50163.587	29034
633	0.452222	-78.272778	803577.598	50041.186	29034
634	0.446557	-78.270494	803832.266	49414.413	29034
635	0.447726	-78.268723	804029.506	49543.844	29034
636	0.444535	-78.270457	803836.471	49190.667	29034
637	0.456991	-78.270885	803788.276	50568.986	29033
638	0.449357	-78.27305	803547.416	49724.145	29033
639	0.447345	-78.269408	803953.213	49501.655	29033
640	0.452692	-78.267357	804181.47	50093.422	29033
641	0.453996	-78.269686	803921.968	50237.621	29032
642	0.454081	-78.269456	803947.586	50247.036	29032
643	0.453964	-78.269261	803969.314	50234.098	29032
644	0.447075	-78.274245	803414.389	49471.578	29032
645	0.444501	-78.272628	803594.626	49186.815	29032
646	0.44844	-78.267258	804192.676	49622.914	29032
647	0.453746	-78.267246	804193.792	50210.059	29031
648	0.452515	-78.269992	803887.942	50073.725	29031
649	0.447468	-78.271605	803708.465	49515.175	29031
650	0.448205	-78.269876	803901.043	49596.801	29031
651	0.444392	-78.272367	803623.706	49174.765	29031
652	0.447056	-78.271958	803669.158	49469.57	29031
653	0.44783	-78.268729	804028.833	49555.352	29031
654	0.448023	-78.268837	804016.794	49576.704	29031
655	0.45116	-78.27344	803503.896	49923.642	29030
656	0.458958	-78.271137	803760.12	50786.637	29030
657	0.45425	-78.269683	803922.292	50265.728	29030
658	0.452792	-78.27314	803537.248	50104.245	29030
659	0.447192	-78.271231	803750.14	49484.649	29030
660	0.44711	-78.272715	803584.827	49475.514	29030
661	0.452531	-78.276036	803214.65	50075.243	29029
662	0.453565	-78.266821	804241.144	50190.048	29029
663	0.453235	-78.272752	803580.452	50153.282	29029
664	0.451374	-78.271701	803697.609	49947.395	29029
665	0.449471	-78.273489	803498.508	49736.741	29029
666	0.446945	-78.27025	803859.432	49457.358	29029
667	0.445397	-78.272338	803626.895	49285.975	29029
668	0.447646	-78.269709	803919.67	49534.951	29029
669	0.445621	-78.270086	803877.756	49310.855	29029
670	0.451373	-78.273833	803460.108	49947.195	29028
671	0.456338	-78.271508	803718.902	50496.701	29028
672	0.455762	-78.269202	803975.811	50433.061	29028
673	0.448564	-78.272421	803617.519	49636.421	29028
674	0.446251	-78.270932	803783.486	49380.534	29028
675	0.451517	-78.268247	804082.374	49963.363	29028
676	0.453583	-78.269068	803990.83	50191.946	29027
677	0.452952	-78.27229	803631.93	50121.986	29027
678	0.448863	-78.272833	803571.61	49669.49	29027
679	0.449142	-78.272942	803559.456	49700.358	29027
680	0.447431	-78.273543	803492.576	49511	29027
681	0.448111	-78.270378	803845.125	49586.378	29027
682	0.444266	-78.27275	803581.045	49160.806	29027
683	0.447001	-78.272292	803631.954	49463.47	29027
684	0.44697	-78.271694	803698.571	49460.064	29027

Station ID	Latitude	Longitude	UTM_X	UTM_Y	Magnetic_data (nT)
685	0.446967	-78.271359	803735.89	49459.746	29027
686	0.453489	-78.266994	804221.875	50181.631	29026
687	0.447472	-78.271869	803679.056	49515.607	29026
688	0.448884	-78.273076	803544.54	49671.803	29026
689	0.448541	-78.270664	803813.247	49633.948	29026
690	0.453762	-78.269281	803967.094	50211.744	29025
691	0.448898	-78.265957	804337.587	49673.649	29025
692	0.450351	-78.266325	804296.532	49834.418	29025
693	0.451386	-78.273583	803487.957	49948.644	29024
694	0.452663	-78.270951	803781.105	50090.062	29024
695	0.449252	-78.273147	803536.615	49712.522	29024
696	0.44754	-78.268796	804021.381	49523.259	29024
697	0.45193	-78.274381	803399.038	50008.808	29023
698	0.452361	-78.274512	803384.427	50056.495	29023
699	0.454295	-78.268132	804095.069	50270.772	29023
700	0.44953	-78.272984	803554.761	49743.291	29023
701	0.448623	-78.271085	803766.345	49643.005	29023
702	0.447173	-78.274026	803438.782	49482.431	29023
703	0.447931	-78.267553	804159.834	49566.577	29023
704	0.45286	-78.272676	803588.934	50111.789	29022
705	0.447702	-78.271702	803697.65	49541.065	29022
706	0.448408	-78.270905	803786.405	49619.221	29022
707	0.448744	-78.270095	803876.624	49656.435	29022
708	0.450585	-78.272515	803606.964	49860.053	29021
709	0.451441	-78.272294	803631.547	49954.784	29021
710	0.448478	-78.271318	803740.395	49626.95	29021
711	0.447912	-78.271534	803716.356	49564.309	29021
712	0.447344	-78.270876	803789.68	49501.484	29021
713	0.445305	-78.27195	803670.121	49275.811	29021
714	0.444975	-78.27041	803841.689	49239.358	29021
715	0.458322	-78.269799	803909.198	50716.316	29020
716	0.452718	-78.272885	803565.658	50096.067	29020
717	0.448228	-78.268727	804029.039	49599.393	29020
718	0.452465	-78.266624	804263.135	50068.334	29020
719	0.453534	-78.269764	803913.298	50186.494	29019
720	0.453816	-78.269466	803946.483	50217.712	29019
721	0.451779	-78.273241	803526.039	49992.146	29019
722	0.447993	-78.272493	803609.522	49573.233	29019
723	0.447532	-78.273767	803467.619	49522.167	29019
724	0.447864	-78.27022	803862.736	49559.052	29019
725	0.447083	-78.270986	803777.437	49472.598	29019
726	0.446523	-78.271925	803672.856	49410.592	29019
727	0.445334	-78.271466	803724.037	49279.04	29019
728	0.451584	-78.267174	804201.903	49970.822	29019
729	0.453897	-78.267854	804126.055	50226.743	29018
730	0.44844	-78.273611	803484.96	49622.65	29018
731	0.447547	-78.2733	803519.641	49523.847	29018
732	0.447025	-78.269017	803996.783	49466.262	29018
733	0.447581	-78.268506	804053.685	49527.808	29018
734	0.44865	-78.267431	804173.395	49646.145	29018
735	0.449197	-78.272183	803644.005	49706.476	29017
736	0.448909	-78.273381	803510.562	49674.557	29017
737	0.446913	-78.27399	803442.803	49453.662	29017

Station ID	Latitude	Longitude	UTM_X	UTM_Y	Magnetic_data (nT)
738	0.445108	-78.271062	803769.052	49254.048	29017
739	0.450235	-78.273158	803535.349	49821.296	29016
740	0.454265	-78.268658	804036.475	50267.431	29016
741	0.452571	-78.2739	803452.594	50079.758	29016
742	0.452368	-78.270255	803858.65	50057.448	29016
743	0.448565	-78.272105	803652.721	49636.544	29016
744	0.449646	-78.273295	803520.112	49756.114	29016
745	0.448108	-78.269271	803968.443	49586.092	29016
746	0.451622	-78.268401	804065.215	49974.976	29016
747	0.452215	-78.273226	803527.692	50040.393	29015
748	0.45074	-78.271113	803763.138	49877.263	29015
749	0.450831	-78.271553	803714.119	49887.315	29015
750	0.448299	-78.270583	803822.28	49607.173	29015
751	0.448167	-78.270822	803795.661	49592.556	29015
752	0.447695	-78.270434	803838.904	49540.343	29015
753	0.445261	-78.2698	803909.63	49271.031	29015
754	0.453554	-78.269502	803942.484	50188.718	29014
755	0.453652	-78.268564	804046.972	50199.602	29014
756	0.451508	-78.272481	803610.713	49962.19	29014
757	0.448336	-78.272578	803600.039	49611.184	29014
758	0.447629	-78.274135	803426.62	49532.886	29014
759	0.4475	-78.270869	803790.453	49518.747	29014
760	0.448001	-78.269976	803889.912	49574.223	29014
761	0.447256	-78.268033	804106.39	49491.864	29014
762	0.444427	-78.270853	803792.362	49178.7	29014
763	0.453378	-78.270794	803798.564	50169.188	29013
764	0.453052	-78.271902	803675.148	50133.068	29013
765	0.45083	-78.272609	803596.482	49887.16	29013
766	0.447298	-78.274296	803408.699	49496.252	29013
767	0.444676	-78.270858	803791.795	49206.253	29013
768	0.444805	-78.27062	803818.302	49220.538	29013
769	0.449322	-78.272754	803580.392	49720.284	29012
770	0.44805	-78.272117	803651.405	49579.556	29012
771	0.445451	-78.273187	803532.315	49291.916	29012
772	0.447433	-78.269951	803892.72	49511.371	29012
773	0.450479	-78.266875	804235.257	49848.559	29012
774	0.454095	-78.268489	804055.308	50248.626	29011
775	0.453968	-78.267643	804149.557	50234.608	29011
776	0.447829	-78.27227	803634.37	49555.094	29011
777	0.448702	-78.273463	803501.436	49651.648	29011
778	0.447283	-78.272179	803644.53	49494.68	29011
779	0.447146	-78.269236	803972.382	49479.642	29011
780	0.445056	-78.271927	803672.694	49248.259	29011
781	0.448273	-78.271957	803669.22	49604.239	29010
782	0.447907	-78.271886	803677.144	49563.742	29010
783	0.449309	-78.273699	803475.121	49718.806	29010
784	0.448202	-78.273677	803477.617	49596.311	29010
785	0.446012	-78.270775	803800.986	49354.094	29010
786	0.450546	-78.267144	804205.288	49855.962	29010
787	0.452537	-78.274338	803403.803	50075.978	29009
788	0.45618	-78.270688	803810.255	50479.252	29009
789	0.456128	-78.271416	803729.159	50473.467	29009
790	0.445891	-78.264928	804452.341	49340.946	29009

Station ID	Latitude	Longitude	UTM_X	UTM_Y	Magnetic_data (nT)
791	0.448366	-78.267553	804159.816	49614.713	29009
792	0.454137	-78.267924	804118.247	50253.297	29008
793	0.452019	-78.271678	803700.145	50018.769	29008
794	0.448816	-78.273615	803484.499	49664.256	29008
795	0.445021	-78.270788	803799.578	49244.433	29008
796	0.451158	-78.266221	804308.084	49923.722	29008
797	0.452419	-78.27283	803571.797	50062.983	29007
798	0.449029	-78.272394	803620.507	49687.877	29007
799	0.448584	-78.272708	803585.547	49638.622	29007
800	0.448109	-78.272714	803584.898	49586.06	29007
801	0.44877	-78.270852	803792.295	49659.281	29007
802	0.448434	-78.273869	803456.219	49621.975	29007
803	0.447455	-78.270398	803842.924	49513.787	29007
804	0.445373	-78.270575	803823.292	49283.392	29007
805	0.450921	-78.273555	803491.095	49897.19	29006
806	0.453045	-78.274021	803439.095	50132.204	29006
807	0.452382	-78.273079	803544.06	50058.879	29006
808	0.448257	-78.272945	803559.159	49602.427	29006
809	0.443667	-78.270896	803787.603	49094.599	29006
810	0.445076	-78.269649	803926.459	49250.566	29006
811	0.451436	-78.266024	804330.018	49954.493	29006
812	0.44977	-78.273118	803539.824	49769.843	29005
813	0.451126	-78.272985	803554.584	49919.898	29005
814	0.452586	-78.273545	803492.14	50081.433	29005
815	0.450606	-78.271342	803737.633	49862.426	29005
816	0.448892	-78.271676	803700.497	49672.747	29005
817	0.448614	-78.273016	803551.235	49641.929	29005
818	0.448468	-78.270061	803880.423	49625.896	29005
819	0.448051	-78.269122	803985.044	49579.791	29005
820	0.445313	-78.271029	803772.719	49276.734	29005
821	0.45008	-78.265996	804333.193	49804.444	29005
822	0.450834	-78.272815	803573.534	49887.594	29004
823	0.450373	-78.271248	803748.114	49836.647	29004
824	0.449035	-78.270409	803841.633	49688.623	29004
825	0.446459	-78.270078	803878.612	49403.586	29004
826	0.445481	-78.270316	803852.14	49295.354	29004
827	0.444473	-78.269371	803957.453	49183.851	29004
828	0.444344	-78.268738	804027.974	49169.603	29004
829	0.452031	-78.274095	803430.894	50019.996	29003
830	0.450389	-78.270752	803803.367	49838.438	29003
831	0.450757	-78.272244	803637.146	49879.097	29003
832	0.44812	-78.272422	803617.426	49587.289	29003
833	0.44778	-78.273896	803453.238	49549.605	29003
834	0.447343	-78.270631	803816.973	49501.383	29003
835	0.446586	-78.269921	803896.097	49417.646	29003
836	0.446735	-78.271913	803674.185	49434.051	29003
837	0.448217	-78.268297	804076.941	49598.194	29003
838	0.444816	-78.270163	803869.211	49221.774	29003
839	0.444128	-78.27036	803847.294	49145.634	29003
840	0.45283	-78.271984	803666.023	50108.499	29002
841	0.450981	-78.271321	803739.957	49903.923	29002
842	0.450837	-78.272	803664.323	49887.96	29002
843	0.448516	-78.271775	803689.484	49631.136	29002

Station ID	Latitude	Longitude	UTM_X	UTM_Y	Magnetic_data (nT)
844	0.450468	-78.267415	804175.102	49847.319	29002
845	0.456153	-78.270408	803841.448	50476.276	29001
846	0.456477	-78.272318	803628.663	50512.048	29001
847	0.448365	-78.272864	803568.177	49614.382	29001
848	0.448962	-78.272048	803659.054	49680.477	29001
849	0.448404	-78.273188	803532.083	49618.684	29001
850	0.451187	-78.269192	803977.116	49926.807	29001
851	0.447605	-78.270149	803870.656	49530.395	29001
852	0.446989	-78.26861	804042.124	49462.295	29001
853	0.447416	-78.268062	804103.153	49509.568	29001
854	0.447412	-78.268258	804081.319	49509.117	29001
855	0.444912	-78.272161	803646.632	49232.314	29001
856	0.444844	-78.271535	803716.371	49224.816	29001
857	0.444665	-78.270378	803845.266	49205.056	29001
858	0.452121	-78.274567	803378.31	50029.935	29000
859	0.451586	-78.273045	803547.881	49970.798	29000
860	0.44768	-78.271427	803728.285	49538.642	29000
861	0.445611	-78.271	803775.938	49309.711	29000
862	0.444885	-78.271012	803774.631	49229.374	29000
863	0.44769	-78.26807	804102.251	49539.887	29000
864	0.451541	-78.273384	803510.119	49965.804	28999
865	0.45315	-78.271271	803745.437	50143.939	28999
866	0.453355	-78.269913	803896.707	50166.68	28999
867	0.451059	-78.272695	803586.892	49912.497	28999
868	0.450604	-78.272784	803576.997	49862.144	28999
869	0.450114	-78.270533	803827.775	49808.017	28999
870	0.451656	-78.270722	803806.657	49978.641	28999
871	0.448672	-78.27328	803521.823	49648.336	28999
872	0.449914	-78.268822	804018.387	49785.957	28999
873	0.447577	-78.270625	803817.631	49527.277	28999
874	0.445167	-78.271262	803746.769	49260.569	28999
875	0.444252	-78.271047	803770.758	49159.327	28999
876	0.451863	-78.271088	803765.876	50001.531	28998
877	0.449028	-78.273607	803485.381	49687.716	28998
878	0.444135	-78.272488	803610.237	49146.321	28998
879	0.444885	-78.271725	803695.203	49229.345	28998
880	0.445239	-78.270812	803796.896	49268.555	28998
881	0.446236	-78.265193	804422.806	49379.112	28997
882	0.450909	-78.273162	803534.875	49895.879	28997
883	0.450246	-78.27212	803650.98	49822.557	28997
884	0.451999	-78.270844	803793.052	50016.591	28997
885	0.447943	-78.274102	803430.284	49567.633	28997
886	0.448417	-78.269706	803919.972	49620.267	28997
887	0.452662	-78.267649	804148.943	50090.09	28997
888	0.444948	-78.269905	803897.946	49236.391	28997
889	0.444499	-78.268949	804004.462	49186.746	28997
890	0.45067	-78.273051	803547.251	49869.436	28996
891	0.448023	-78.273853	803458.018	49576.496	28996
892	0.448111	-78.268011	804108.806	49586.476	28996
893	0.445163	-78.270546	803826.531	49260.156	28996
894	0.448558	-78.269429	803950.824	49635.881	28995
895	0.450451	-78.268178	804090.105	49845.406	28995
896	0.449063	-78.265276	804413.443	49691.936	28995

Station ID	Latitude	Longitude	UTM_X	UTM_Y	Magnetic_data (nT)
897	0.450558	-78.266666	804258.536	49857.31	28995
898	0.452651	-78.273198	803530.793	50088.64	28994
899	0.450243	-78.270303	803853.391	49822.301	28994
900	0.448289	-78.268474	804057.221	49606.154	28994
901	0.45273	-78.269577	803934.163	50097.534	28994
902	0.445362	-78.270049	803881.888	49282.197	28994
903	0.447981	-78.270607	803819.62	49571.983	28993
904	0.452211	-78.274303	803407.716	50039.905	28992
905	0.452223	-78.273494	803497.837	50041.267	28992
906	0.451272	-78.272602	803597.243	49936.07	28992
907	0.451296	-78.272379	803622.084	49938.735	28992
908	0.447957	-78.273693	803475.845	49569.199	28992
909	0.447887	-78.271262	803746.658	49561.554	28992
910	0.448277	-78.27113	803761.346	49604.716	28992
911	0.450889	-78.268552	804048.424	49893.858	28992
912	0.450516	-78.267665	804147.25	49852.62	28992
913	0.447379	-78.268574	804046.118	49505.452	28992
914	0.448828	-78.265433	804395.963	49665.925	28992
915	0.450261	-78.27099	803776.86	49824.264	28991
916	0.450655	-78.271764	803690.621	49867.83	28991
917	0.451017	-78.272415	803618.086	49907.861	28991
918	0.45118	-78.271903	803675.115	49925.919	28991
919	0.448968	-78.273879	803455.083	49681.065	28991
920	0.44839	-78.269497	803943.255	49617.288	28991
921	0.448349	-78.268902	804009.539	49612.776	28991
922	0.445748	-78.270773	803801.219	49324.88	28991
923	0.444315	-78.269132	803984.084	49166.377	28991
924	0.448827	-78.271304	803741.94	49665.57	28990
925	0.448113	-78.271716	803696.073	49586.544	28990
926	0.447126	-78.269973	803890.282	49477.398	28990
927	0.450409	-78.272988	803554.279	49840.558	28989
928	0.448337	-78.272259	803635.575	49611.308	28989
929	0.44842	-78.270336	803849.791	49620.573	28989
930	0.45275	-78.275962	803222.884	50099.479	28988
931	0.451634	-78.272652	803591.659	49976.126	28988
932	0.451044	-78.268937	804005.529	49910.994	28988
933	0.444743	-78.271256	803747.455	49213.651	28988
934	0.444535	-78.271087	803766.29	49190.641	28988
935	0.454246	-78.268396	804065.662	50265.339	28987
936	0.452101	-78.266363	804292.226	50028.066	28987
937	0.451819	-78.273908	803451.734	49996.545	28986
938	0.447704	-78.266491	804278.149	49541.502	28986
939	0.452935	-78.2714	803731.075	50120.142	28986
940	0.450461	-78.272275	803633.704	49846.342	28986
941	0.448801	-78.268122	804096.412	49662.825	28986
942	0.448933	-78.267736	804139.406	49677.448	28986
943	0.444967	-78.271295	803743.101	49238.436	28986
944	0.444488	-78.270208	803864.211	49185.477	28986
945	0.45375	-78.269706	803919.75	50210.398	28985
946	0.451315	-78.273177	803533.188	49940.804	28985
947	0.452838	-78.271311	803740.994	50109.412	28985
948	0.448227	-78.270141	803871.521	49599.224	28985
949	0.452386	-78.267682	804145.279	50059.548	28985

Station ID	Latitude	Longitude	UTM_X	UTM_Y	Magnetic_data (nT)
950	0.447169	-78.268375	804068.295	49482.223	28985
951	0.446031	-78.270316	803852.117	49356.215	28985
952	0.445425	-78.269603	803931.569	49289.187	28985
953	0.444266	-78.270131	803872.798	49160.914	28985
954	0.450521	-78.271998	803664.559	49852.993	28984
955	0.4528	-78.272193	803642.742	50105.17	28984
956	0.446431	-78.269252	803970.629	49400.522	28984
957	0.445754	-78.269852	803903.817	49325.582	28984
958	0.447796	-78.264808	804465.63	49551.753	28984
959	0.450626	-78.270756	803802.912	49864.663	28983
960	0.451123	-78.272174	803644.928	49919.6	28983
961	0.449197	-78.271223	803750.948	49706.516	28983
962	0.448967	-78.267374	804179.731	49681.225	28983
963	0.445062	-78.267055	804215.429	49249.124	28983
964	0.445472	-78.265234	804418.27	49294.568	28982
965	0.451967	-78.273714	803473.34	50012.93	28982
966	0.448318	-78.271536	803716.117	49609.236	28982
967	0.44819	-78.273171	803533.985	49595.004	28982
968	0.44812	-78.271354	803736.399	49587.333	28982
969	0.448063	-78.264853	804460.606	49581.296	28982
970	0.450005	-78.271995	803664.915	49795.894	28981
971	0.451112	-78.271627	803705.864	49918.406	28981
972	0.451809	-78.272475	803611.369	49995.498	28981
973	0.446788	-78.269523	803940.425	49440.015	28981
974	0.452305	-78.268939	804005.254	50050.532	28981
975	0.4518	-78.272856	803568.926	49994.486	28980
976	0.446666	-78.269767	803913.249	49426.505	28980
977	0.448312	-78.269068	803991.049	49608.674	28980
978	0.452211	-78.268692	804032.773	50040.14	28980
979	0.447238	-78.267851	804126.666	49489.88	28980
980	0.44512	-78.270169	803868.53	49255.413	28980
981	0.444111	-78.270835	803794.38	49143.733	28980
982	0.451121	-78.271094	803765.239	49919.424	28979
983	0.450494	-78.267916	804119.29	49850.175	28979
984	0.452704	-78.267967	804113.517	50094.725	28979
985	0.450495	-78.270999	803775.848	49850.157	28978
986	0.448363	-78.273385	803510.139	49614.139	28978
987	0.44588	-78.27054	803827.17	49339.497	28978
988	0.44544	-78.26741	804175.866	49290.937	28978
989	0.444866	-78.26958	803934.154	49227.331	28978
990	0.45167	-78.267431	804173.269	49980.328	28978
991	0.458971	-78.270874	803789.418	50788.087	28977
992	0.452365	-78.274113	803428.875	50056.954	28977
993	0.449545	-78.272007	803663.597	49744.992	28977
994	0.447842	-78.270842	803793.447	49556.592	28977
995	0.450321	-78.268682	804033.966	49831	28977
996	0.452391	-78.267419	804174.576	50060.112	28977
997	0.44388	-78.270231	803861.674	49118.196	28977
998	0.450309	-78.271828	803683.506	49829.541	28976
999	0.450164	-78.269611	803930.483	49813.588	28976
1000	0.447717	-78.273542	803492.676	49542.648	28976
1001	0.449388	-78.26873	804028.657	49727.755	28976
1002	0.447	-78.268161	804092.142	49463.531	28976

Station ID	Latitude	Longitude	UTM_X	UTM_Y	Magnetic_data (nT)
1003	0.451522	-78.270084	803877.735	49963.84	28975
1004	0.447571	-78.268281	804078.75	49526.711	28975
1005	0.449153	-78.266097	804321.98	49701.861	28975
1006	0.445583	-78.270566	803824.286	49306.631	28975
1007	0.444629	-78.269989	803888.602	49201.088	28975
1008	0.454351	-78.269459	803947.241	50276.913	28974
1009	0.450116	-78.271731	803694.32	49808.188	28974
1010	0.451702	-78.270456	803836.287	49983.742	28974
1011	0.449052	-78.271451	803725.555	49690.461	28974
1012	0.447836	-78.273293	803520.409	49555.827	28974
1013	0.445284	-78.270305	803853.373	49273.555	28974
1014	0.448025	-78.271056	803769.6	49576.833	28973
1015	0.453794	-78.268113	804097.207	50215.334	28972
1016	0.446832	-78.268379	804067.864	49444.931	28972
1017	0.452587	-78.269007	803997.667	50081.734	28972
1018	0.448868	-78.26763	804151.217	49670.259	28972
1019	0.445559	-78.269199	803976.569	49304.031	28972
1020	0.450136	-78.271224	803750.798	49810.422	28971
1021	0.448669	-78.269171	803979.56	49648.175	28971
1022	0.45264	-78.26775	804137.693	50087.652	28971
1023	0.448602	-78.267727	804140.423	49640.821	28971
1024	0.446178	-78.27009	803877.287	49372.491	28971
1025	0.444315	-78.269597	803932.283	49166.358	28971
1026	0.447753	-78.264596	804489.248	49547.003	28971
1027	0.449106	-78.265509	804387.485	49696.684	28970
1028	0.450018	-78.266496	804277.496	49797.562	28970
1029	0.455817	-78.270497	803831.548	50439.092	28969
1030	0.445559	-78.266535	804273.336	49304.142	28969
1031	0.445503	-78.266279	804301.856	49297.955	28969
1032	0.450511	-78.27051	803830.321	49851.948	28969
1033	0.448667	-78.271546	803714.988	49647.854	28969
1034	0.452331	-78.266858	804237.074	50053.496	28969
1035	0.445521	-78.26942	803951.951	49299.817	28969
1036	0.44544	-78.270794	803798.893	49290.797	28969
1037	0.445505	-78.269823	803907.058	49298.03	28969
1038	0.447609	-78.267438	804172.658	49530.951	28969
1039	0.454068	-78.269818	803907.261	50245.582	28968
1040	0.44705	-78.265633	804373.756	49469.168	28968
1041	0.4511	-78.269827	803906.382	49917.153	28968
1042	0.450076	-78.269175	803979.056	49803.868	28968
1043	0.445202	-78.271703	803697.641	49264.424	28968
1044	0.445711	-78.269626	803928.995	49320.834	28968
1045	0.444364	-78.271297	803742.903	49171.71	28968
1046	0.444669	-78.269433	803950.538	49205.537	28968
1047	0.448604	-78.268428	804062.332	49641.013	28967
1048	0.451361	-78.268696	804032.363	49946.082	28967
1049	0.444951	-78.269406	803953.534	49236.744	28967
1050	0.444776	-78.269758	803914.329	49217.364	28967
1051	0.447596	-78.26788	804123.42	49529.494	28967
1052	0.446219	-78.265975	804335.692	49377.198	28966
1053	0.451318	-78.269908	803897.349	49941.273	28966
1054	0.45169	-78.269555	803936.658	49982.452	28966
1055	0.452039	-78.269971	803890.301	50021.054	28966

Station ID	Latitude	Longitude	UTM_X	UTM_Y	Magnetic_data (nT)
1056	0.450865	-78.268285	804078.168	49891.214	28966
1057	0.452451	-78.2688	804020.732	50066.693	28966
1058	0.447692	-78.267696	804143.914	49540.124	28966
1059	0.450659	-78.265894	804344.532	49868.518	28966
1060	0.449936	-78.265785	804356.704	49788.518	28966
1061	0.452211	-78.266124	804318.845	50040.248	28966
1062	0.450648	-78.270266	803857.496	49867.118	28965
1063	0.450244	-78.271487	803721.495	49822.362	28965
1064	0.448756	-78.271914	803673.99	49657.688	28965
1065	0.448675	-78.269617	803929.876	49648.82	28965
1066	0.446997	-78.264749	804472.235	49463.34	28965
1067	0.448114	-78.267746	804138.326	49586.819	28965
1068	0.446577	-78.266264	804303.483	49416.801	28964
1069	0.447311	-78.265327	804407.834	49498.062	28964
1070	0.453005	-78.271663	803701.775	50127.877	28964
1071	0.449774	-78.271866	803679.295	49770.338	28964
1072	0.450887	-78.270892	803787.751	49893.539	28964
1073	0.452572	-78.269378	803956.338	50080.059	28964
1074	0.452446	-78.267848	804126.784	50066.18	28964
1075	0.44406	-78.271265	803746.48	49138.072	28964
1076	0.444411	-78.269919	803896.409	49176.968	28964
1077	0.44401	-78.27	803887.402	49132.591	28964
1078	0.448059	-78.266952	804226.779	49580.766	28963
1079	0.445275	-78.266497	804277.581	49272.717	28963
1080	0.449814	-78.270626	803817.427	49774.816	28963
1081	0.448576	-78.273432	803504.894	49637.706	28963
1082	0.448221	-78.274036	803437.624	49598.398	28963
1083	0.450913	-78.269191	803977.239	49896.487	28963
1084	0.44454	-78.26968	803923.028	49191.252	28963
1085	0.45151	-78.266258	804303.947	49962.672	28963
1086	0.451015	-78.270062	803880.206	49907.738	28962
1087	0.447167	-78.270418	803840.708	49481.917	28962
1088	0.448968	-78.26571	804365.099	49681.405	28962
1089	0.444753	-78.272397	803620.349	49214.71	28962
1090	0.444724	-78.271906	803675.047	49211.522	28962
1091	0.444158	-78.269811	803908.45	49148.976	28962
1092	0.446956	-78.264495	804500.533	49458.814	28962
1093	0.447483	-78.264546	804494.829	49517.128	28962
1094	0.451164	-78.269605	803931.11	49924.245	28961
1095	0.448143	-78.267379	804179.209	49590.044	28961
1096	0.449974	-78.270762	803802.271	49792.515	28960
1097	0.451789	-78.270197	803865.135	49993.38	28960
1098	0.451973	-78.270573	803823.242	50013.725	28960
1099	0.451989	-78.272714	803584.737	50015.406	28960
1100	0.451163	-78.269444	803949.045	49924.141	28960
1101	0.45017	-78.268921	804007.348	49814.281	28960
1102	0.449648	-78.268781	804022.965	49756.524	28960
1103	0.448072	-78.268309	804075.61	49582.148	28960
1104	0.443865	-78.271077	803767.431	49116.502	28960
1105	0.447528	-78.264802	804466.309	49522.097	28960
1106	0.449845	-78.270998	803775.986	49778.231	28959
1107	0.451626	-78.26983	803906.026	49975.359	28959
1108	0.449502	-78.268507	804053.494	49740.379	28959

Station ID	Latitude	Longitude	UTM_X	UTM_Y	Magnetic_data (nT)
1109	0.445863	-78.2701	803876.186	49337.634	28959
1110	0.444655	-78.269164	803980.505	49203.999	28959
1111	0.451652	-78.266225	804307.617	49978.387	28959
1112	0.447518	-78.265139	804428.768	49520.976	28958
1113	0.45293	-78.269709	803919.451	50119.66	28958
1114	0.44925	-78.271589	803710.174	49712.365	28958
1115	0.447591	-78.272324	803628.364	49528.756	28958
1116	0.446775	-78.270025	803884.504	49438.556	28958
1117	0.445029	-78.271496	803720.708	49245.289	28958
1118	0.446723	-78.264722	804475.255	49433.021	28958
1119	0.451693	-78.267702	804143.079	49982.862	28958
1120	0.449992	-78.271432	803727.633	49794.479	28957
1121	0.449869	-78.271624	803706.249	49780.86	28957
1122	0.445626	-78.266693	804255.732	49311.549	28957
1123	0.445369	-78.266679	804257.302	49283.111	28957
1124	0.44694	-78.26587	804347.359	49456.986	28956
1125	0.446506	-78.268969	804002.152	49408.833	28956
1126	0.452482	-78.269121	803984.972	50070.11	28956
1127	0.446308	-78.266229	804307.393	49387.036	28955
1128	0.451215	-78.270155	803869.838	49929.865	28955
1129	0.448895	-78.270604	803819.916	49673.123	28955
1130	0.448	-78.272995	803553.599	49573.987	28955
1131	0.449528	-78.269034	803994.786	49743.234	28955
1132	0.4462	-78.269687	803922.18	49374.942	28955
1133	0.446011	-78.269875	803901.245	49354.02	28955
1134	0.445706	-78.266079	804324.128	49320.427	28955
1135	0.448327	-78.267197	804199.476	49610.412	28955
1136	0.445781	-78.266321	804297.166	49328.716	28954
1137	0.451134	-78.270407	803841.769	49920.891	28954
1138	0.450084	-78.270169	803868.325	49804.712	28954
1139	0.448643	-78.268199	804087.841	49645.338	28954
1140	0.445944	-78.269754	803914.727	49346.611	28954
1141	0.447406	-78.265481	804390.674	49508.569	28953
1142	0.449703	-78.271242	803748.811	49762.507	28953
1143	0.44628	-78.268427	804062.539	49383.847	28953
1144	0.446329	-78.26732	804185.856	49389.315	28953
1145	0.448025	-78.26461	804487.677	49577.101	28953
1146	0.447797	-78.272833	803571.654	49551.53	28952
1147	0.448487	-78.268667	804035.712	49628.056	28952
1148	0.448344	-78.267872	804124.281	49612.265	28952
1149	0.444503	-78.271929	803672.494	49187.066	28952
1150	0.444803	-78.269223	803973.926	49220.374	28952
1151	0.451563	-78.274027	803438.489	49968.212	28951
1152	0.447854	-78.265175	804424.744	49558.156	28951
1153	0.458959	-78.270634	803816.154	50786.769	28951
1154	0.450831	-78.268824	804018.126	49887.429	28951
1155	0.448057	-78.2672	804199.152	49580.535	28951
1156	0.452373	-78.273704	803474.437	50057.857	28950
1157	0.451752	-78.272204	803641.56	49989.202	28950
1158	0.450034	-78.26984	803904.978	49799.193	28950
1159	0.448974	-78.267096	804210.7	49682.011	28950
1160	0.448287	-78.264581	804490.897	49606.095	28950
1161	0.448148	-78.265984	804334.61	49590.655	28950

Station ID	Latitude	Longitude	UTM_X	UTM_Y	Magnetic_data (nT)
1162	0.450027	-78.273009	803551.956	49798.286	28949
1163	0.44727	-78.267211	804197.96	49493.447	28949
1164	0.452948	-78.271096	803764.94	50121.593	28949
1165	0.451987	-78.273337	803515.336	50015.159	28949
1166	0.451433	-78.270335	803849.777	49953.981	28949
1167	0.449487	-78.270786	803799.617	49738.624	28949
1168	0.450006	-78.269361	803958.339	49796.115	28949
1169	0.451103	-78.268627	804040.06	49917.536	28949
1170	0.450779	-78.268028	804106.801	49881.708	28949
1171	0.449394	-78.268264	804080.569	49728.438	28949
1172	0.452052	-78.268164	804091.598	50022.568	28949
1173	0.446981	-78.267955	804115.091	49461.437	28949
1174	0.445713	-78.270325	803851.128	49321.026	28949
1175	0.445435	-78.266026	804330.043	49290.441	28949
1176	0.446687	-78.264483	804501.88	49429.048	28949
1177	0.447615	-78.265315	804409.158	49531.703	28948
1178	0.450967	-78.269583	803933.568	49902.446	28948
1179	0.450779	-78.270529	803828.193	49881.603	28948
1180	0.451524	-78.270952	803781.041	49964.025	28948
1181	0.44977	-78.270312	803852.408	49769.96	28948
1182	0.449261	-78.268699	804032.116	49713.703	28948
1183	0.449023	-78.266545	804272.079	49687.456	28948
1184	0.45	-78.267345	804182.919	49795.535	28948
1185	0.44415	-78.268911	804008.71	49148.128	28948
1186	0.447225	-78.26452	804497.736	49488.58	28948
1187	0.447889	-78.265923	804341.416	49561.997	28948
1188	0.447398	-78.26761	804153.506	49507.595	28948
1189	0.446033	-78.266221	804308.296	49356.606	28947
1190	0.445668	-78.265906	804343.401	49316.229	28947
1191	0.449872	-78.267565	804158.417	49781.362	28947
1192	0.444836	-78.268951	804004.225	49224.037	28947
1193	0.45058	-78.266149	804316.128	49859.766	28947
1194	0.451703	-78.265995	804333.237	49984.04	28947
1195	0.447778	-78.272663	803590.593	49549.435	28946
1196	0.445925	-78.269122	803985.132	49344.535	28946
1197	0.444353	-78.271712	803696.673	49170.476	28946
1198	0.445832	-78.266513	804275.775	49334.352	28945
1199	0.449658	-78.270864	803790.921	49757.543	28945
1200	0.450173	-78.268329	804073.295	49814.637	28945
1201	0.446803	-78.268878	804012.277	49441.701	28945
1202	0.452275	-78.267801	804132.027	50047.26	28945
1203	0.44548	-78.268816	804019.238	49295.305	28945
1204	0.444176	-78.26937	803957.576	49150.986	28945
1205	0.4451	-78.266628	804262.994	49253.346	28945
1206	0.447841	-78.267354	804182.006	49556.626	28945
1207	0.449418	-78.271702	803697.579	49730.951	28944
1208	0.452057	-78.273003	803552.54	50022.919	28944
1209	0.444584	-78.272181	803644.418	49196.018	28944
1210	0.446142	-78.266825	804241.006	49368.642	28944
1211	0.447277	-78.266782	804245.749	49494.24	28943
1212	0.447451	-78.266581	804268.133	49513.502	28943
1213	0.446097	-78.266461	804281.557	49363.678	28943
1214	0.451342	-78.270579	803822.6	49943.901	28943

Station ID	Latitude	Longitude	UTM_X	UTM_Y	Magnetic_data (nT)
1215	0.449124	-78.269726	803917.715	49698.5	28943
1216	0.451103	-78.268355	804070.361	49917.547	28943
1217	0.446006	-78.268528	804051.299	49353.523	28943
1218	0.443863	-78.270706	803808.76	49116.296	28943
1219	0.449365	-78.27045	803837.052	49725.138	28942
1220	0.448648	-78.270409	803841.649	49645.799	28942
1221	0.443637	-78.269141	803983.109	49091.352	28942
1222	0.451605	-78.273737	803470.792	49972.871	28941
1223	0.446863	-78.267377	804179.484	49448.403	28941
1224	0.4509	-78.270291	803854.701	49895.003	28941
1225	0.446533	-78.269727	803917.71	49411.789	28941
1226	0.444991	-78.266468	804280.823	49241.291	28940
1227	0.449538	-78.271104	803764.19	49744.255	28940
1228	0.449339	-78.269971	803890.413	49722.281	28940
1229	0.448986	-78.268646	804038.031	49683.275	28940
1230	0.450385	-78.268387	804066.826	49838.094	28940
1231	0.452901	-78.266767	804247.187	50116.574	28940
1232	0.452638	-78.269779	803911.665	50087.345	28939
1233	0.449403	-78.269253	803970.395	49729.393	28939
1234	0.450865	-78.269434	803950.171	49891.166	28939
1235	0.449805	-78.268568	804046.686	49773.906	28939
1236	0.446742	-78.268111	804097.722	49434.983	28939
1237	0.446348	-78.268963	804002.827	49391.349	28939
1238	0.445945	-78.266111	804320.553	49346.873	28939
1239	0.45009	-78.266788	804244.965	49805.517	28939
1240	0.446504	-78.267237	804195.095	49408.683	28938
1241	0.447139	-78.267461	804170.115	49478.941	28938
1242	0.447194	-78.265655	804371.3	49485.102	28938
1243	0.452985	-78.270859	803791.34	50125.698	28938
1244	0.449144	-78.27061	803819.238	49700.677	28938
1245	0.449457	-78.269727	803917.59	49735.349	28938
1246	0.448905	-78.269675	803923.405	49674.269	28938
1247	0.448559	-78.267957	804114.803	49636.053	28938
1248	0.449513	-78.267991	804110.976	49741.618	28938
1249	0.446264	-78.267059	804214.934	49382.133	28938
1250	0.445883	-78.26676	804248.258	49339.985	28938
1251	0.449086	-78.270824	803795.401	49694.25	28937
1252	0.449602	-78.269506	803942.203	49751.403	28937
1253	0.449203	-78.270201	803864.797	49707.222	28937
1254	0.449261	-78.26949	803943.999	49713.67	28937
1255	0.443775	-78.269368	803957.816	49106.613	28937
1256	0.450943	-78.26981	803908.282	49899.781	28936
1257	0.451904	-78.269738	803916.263	50006.125	28936
1258	0.448951	-78.269137	803983.336	49679.381	28936
1259	0.448596	-78.26895	804004.182	49640.106	28936
1260	0.445966	-78.269547	803937.785	49349.054	28936
1261	0.446425	-78.265013	804442.85	49400.033	28935
1262	0.449276	-78.271929	803672.297	49715.228	28935
1263	0.449402	-78.27135	803736.792	49729.195	28935
1264	0.449901	-78.270077	803878.582	49784.466	28935
1265	0.451628	-78.268858	804014.305	49975.621	28935
1266	0.45213	-78.268435	804061.406	50031.188	28935
1267	0.45247	-78.268094	804099.379	50068.826	28935

Station ID	Latitude	Longitude	UTM_X	UTM_Y	Magnetic_data (nT)
1268	0.445942	-78.265956	804337.82	49346.547	28934
1269	0.446258	-78.265455	804393.618	49381.535	28934
1270	0.451943	-78.270241	803860.228	50010.419	28934
1271	0.451805	-78.271901	803675.312	49995.079	28934
1272	0.446336	-78.267872	804124.363	49390.067	28934
1273	0.448835	-78.267852	804126.488	49666.599	28934
1274	0.445109	-78.268427	804062.587	49254.268	28934
1275	0.446078	-78.268895	804010.413	49361.475	28934
1276	0.445297	-78.269268	803968.893	49275.036	28934
1277	0.447125	-78.266623	804263.468	49477.426	28933
1278	0.44659	-78.266533	804273.516	49418.229	28933
1279	0.446786	-78.265214	804420.444	49439.972	28933
1280	0.449571	-78.271491	803721.078	49747.89	28933
1281	0.450718	-78.269659	803925.112	49874.89	28933
1282	0.452173	-78.26733	804184.5	50035.993	28933
1283	0.446262	-78.269105	803987.012	49381.827	28933
1284	0.450194	-78.267335	804184.025	49817.003	28933
1285	0.450377	-78.26971	803919.445	49837.154	28932
1286	0.449295	-78.268981	804000.7	49717.454	28932
1287	0.451329	-78.268945	804004.626	49942.531	28932
1288	0.451766	-78.267981	804111.996	49990.928	28932
1289	0.447904	-78.266774	804246.615	49563.622	28931
1290	0.45142	-78.269657	803925.306	49952.571	28931
1291	0.449493	-78.270217	803863.003	49739.312	28931
1292	0.446728	-78.267909	804120.225	49433.442	28931
1293	0.446392	-78.269492	803943.895	49396.196	28931
1294	0.447265	-78.264758	804471.222	49492.996	28931
1295	0.459178	-78.270568	803823.497	50811.005	28930
1296	0.446803	-78.265505	804388.026	49441.841	28930
1297	0.448906	-78.268915	804008.068	49674.411	28930
1298	0.447303	-78.266451	804282.621	49497.131	28929
1299	0.452793	-78.266519	804274.818	50104.634	28929
1300	0.451661	-78.266913	804230.975	49979.354	28929
1301	0.447841	-78.266263	804303.542	49556.672	28928
1302	0.445231	-78.26623	804307.326	49267.859	28928
1303	0.446535	-78.265472	804391.713	49412.187	28928
1304	0.451246	-78.270833	803794.309	49933.267	28928
1305	0.451933	-78.269425	803951.129	50009.347	28928
1306	0.452375	-78.266341	804294.665	50058.387	28928
1307	0.449587	-78.267672	804146.509	49749.82	28928
1308	0.44419	-78.268518	804052.488	49152.571	28928
1309	0.44761	-78.266757	804248.521	49531.089	28927
1310	0.445699	-78.2651	804433.188	49319.693	28927
1311	0.44639	-78.268696	804032.568	49396.008	28927
1312	0.449041	-78.266835	804239.772	49689.436	28927
1313	0.450853	-78.266385	804289.827	49889.965	28927
1314	0.450687	-78.265626	804374.386	49871.628	28927
1315	0.45064	-78.269299	803965.219	49866.273	28926
1316	0.451421	-78.269499	803942.907	49952.688	28926
1317	0.45065	-78.268424	804062.693	49867.417	28926
1318	0.451243	-78.26836	804069.798	49933.039	28926
1319	0.449917	-78.267085	804211.886	49786.361	28926
1320	0.449071	-78.267939	804116.787	49692.71	28926

Station ID	Latitude	Longitude	UTM_X	UTM_Y	Magnetic_data (nT)
1321	0.445629	-78.268594	804043.962	49311.802	28926
1322	0.445965	-78.265168	804425.602	49349.125	28925
1323	0.451782	-78.271575	803711.629	49992.548	28925
1324	0.445777	-78.269347	803960.073	49328.148	28925
1325	0.445623	-78.265593	804378.271	49311.263	28924
1326	0.44616	-78.265686	804367.889	49370.681	28924
1327	0.451027	-78.270669	803812.587	49909.04	28924
1328	0.449095	-78.271806	803686.007	49695.205	28924
1329	0.451725	-78.269265	803968.962	49986.337	28924
1330	0.451463	-78.269197	803976.548	49957.348	28924
1331	0.446681	-78.268623	804040.689	49428.212	28924
1332	0.444543	-78.271475	803723.067	49191.51	28924
1333	0.446791	-78.267131	804206.891	49440.446	28923
1334	0.446664	-78.26688	804234.858	49426.403	28923
1335	0.448271	-78.265005	804443.665	49604.307	28923
1336	0.446616	-78.266204	804310.165	49421.12	28923
1337	0.44628	-78.266468	804280.77	49383.928	28923
1338	0.449334	-78.270983	803777.678	49721.686	28923
1339	0.449057	-78.269449	803948.575	49691.098	28923
1340	0.452183	-78.267608	804153.531	50037.087	28923
1341	0.449387	-78.266896	804232.963	49727.721	28923
1342	0.450931	-78.265894	804344.52	49898.617	28923
1343	0.445881	-78.265668	804369.906	49339.809	28922
1344	0.446	-78.265396	804400.201	49352.988	28922
1345	0.447249	-78.273035	803549.174	49490.882	28922
1346	0.450684	-78.269046	803993.401	49871.153	28922
1347	0.450075	-78.268597	804043.445	49803.782	28922
1348	0.449677	-78.26824	804083.231	49759.755	28922
1349	0.445358	-78.267112	804209.067	49281.876	28922
1350	0.44665	-78.267468	804169.356	49424.829	28921
1351	0.447489	-78.266291	804300.438	49517.719	28921
1352	0.446493	-78.266452	804282.543	49407.498	28921
1353	0.450385	-78.269197	803976.593	49838.06	28921
1354	0.4464	-78.266716	804253.138	49397.196	28920
1355	0.446495	-78.265999	804333.007	49407.739	28920
1356	0.449169	-78.268932	804006.164	49703.513	28919
1357	0.448401	-78.26822	804085.511	49618.558	28919
1358	0.450233	-78.268037	804105.821	49821.289	28919
1359	0.445451	-78.265859	804348.646	49292.219	28918
1360	0.449645	-78.269995	803887.727	49756.141	28918
1361	0.45109	-78.268039	804105.563	49916.122	28918
1362	0.446827	-78.266394	804288.991	49444.46	28917
1363	0.447056	-78.265886	804345.572	49469.822	28917
1364	0.449753	-78.269278	803967.595	49768.122	28917
1365	0.450433	-78.268931	804006.223	49843.383	28917
1366	0.446108	-78.269322	803962.844	49364.777	28917
1367	0.444853	-78.266577	804268.686	49226.016	28917
1368	0.447423	-78.266959	804226.026	49510.388	28916
1369	0.448344	-78.265277	804413.361	49612.373	28916
1370	0.446159	-78.264999	804444.42	49370.599	28916
1371	0.450736	-78.267437	804172.64	49876.974	28916
1372	0.452205	-78.266564	804269.83	50039.566	28916
1373	0.444889	-78.267263	804192.265	49229.971	28916

Station ID	Latitude	Longitude	UTM_X	UTM_Y	Magnetic_data (nT)
1374	0.44643	-78.26571	804365.204	49400.558	28915
1375	0.446512	-78.265207	804421.235	49409.653	28915
1376	0.446984	-78.265036	804440.264	49461.89	28915
1377	0.449339	-78.270552	803825.691	49722.257	28915
1378	0.446255	-78.268142	804094.289	49381.092	28915
1379	0.451955	-78.267611	804153.206	50011.858	28915
1380	0.449748	-78.267784	804134.026	49767.631	28915
1381	0.443993	-78.268691	804033.224	49130.764	28915
1382	0.446145	-78.264504	804499.563	49369.071	28915
1383	0.45199	-78.266614	804264.269	50015.772	28915
1384	0.445848	-78.268749	804026.687	49336.03	28914
1385	0.445229	-78.267259	804192.696	49267.595	28914
1386	0.4458	-78.267799	804132.517	49330.758	28914
1387	0.449664	-78.265607	804376.545	49758.427	28914
1388	0.4479	-78.265377	804402.239	49563.237	28913
1389	0.452319	-78.268428	804062.178	50052.102	28913
1390	0.449785	-78.266856	804237.402	49771.764	28913
1391	0.444566	-78.268147	804093.801	49194.193	28913
1392	0.446965	-78.266941	804228.05	49459.708	28912
1393	0.444951	-78.266195	804311.236	49236.876	28912
1394	0.45077	-78.26777	804135.543	49880.723	28912
1395	0.4462	-78.264756	804471.488	49375.146	28912
1396	0.446701	-78.265729	804363.076	49430.545	28911
1397	0.445729	-78.26534	804406.451	49323.003	28911
1398	0.446703	-78.265024	804441.613	49430.796	28911
1399	0.450077	-78.267546	804160.525	49804.047	28911
1400	0.449744	-78.268009	804108.961	49767.179	28911
1401	0.445255	-78.268972	804001.869	49270.401	28911
1402	0.445507	-78.267331	804184.664	49298.354	28911
1403	0.446456	-78.264741	804473.149	49403.475	28911
1404	0.448174	-78.264952	804449.573	49593.575	28910
1405	0.45079	-78.270033	803883.446	49882.841	28910
1406	0.450872	-78.267071	804213.406	49892.039	28910
1407	0.446594	-78.268373	804068.542	49418.595	28910
1408	0.450227	-78.26778	804134.451	49820.636	28910
1409	0.44521	-78.267588	804156.047	49265.479	28910
1410	0.447053	-78.265237	804417.87	49469.517	28909
1411	0.449244	-78.267384	804178.606	49711.877	28909
1412	0.44772	-78.266947	804227.35	49543.254	28908
1413	0.448104	-78.265518	804386.524	49585.806	28908
1414	0.449189	-78.269213	803974.86	49705.714	28908
1415	0.449213	-78.266341	804294.796	49708.49	28908
1416	0.44523	-78.269422	803951.74	49267.616	28908
1417	0.449844	-78.265527	804385.449	49778.348	28908
1418	0.451736	-78.27131	803741.151	49987.469	28907
1419	0.44922	-78.268495	804054.843	49709.175	28907
1420	0.445056	-78.268795	804021.595	49248.388	28907
1421	0.449741	-78.265295	804411.298	49766.96	28907
1422	0.448066	-78.266426	804285.375	49581.563	28906
1423	0.447188	-78.267044	804216.567	49484.38	28906
1424	0.447348	-78.266141	804317.153	49502.123	28906
1425	0.449627	-78.270544	803826.57	49754.126	28906
1426	0.44874	-78.268697	804032.36	49656.051	28906

Station ID	Latitude	Longitude	UTM_X	UTM_Y	Magnetic_data (nT)
1427	0.448996	-78.268375	804068.22	49684.392	28906
1428	0.451661	-78.269027	803995.477	49979.265	28906
1429	0.449333	-78.265374	804402.514	49721.809	28906
1430	0.444518	-78.268525	804051.694	49188.866	28906
1431	0.445602	-78.267615	804153.023	49308.855	28906
1432	0.446571	-78.267788	804133.711	49416.074	28905
1433	0.449258	-78.26673	804251.46	49713.453	28905
1434	0.44383	-78.268969	804002.261	49112.716	28905
1435	0.44517	-78.265979	804335.29	49261.119	28905
1436	0.446877	-78.266729	804251.67	49449.979	28904
1437	0.44519	-78.265781	804357.346	49263.34	28904
1438	0.44982	-78.269081	803989.538	49775.544	28904
1439	0.446473	-78.266972	804224.617	49405.264	28903
1440	0.449244	-78.26582	804352.834	49711.942	28903
1441	0.444674	-78.268735	804028.294	49206.119	28903
1442	0.443833	-78.268476	804057.181	49113.068	28903
1443	0.443364	-78.269166	803980.335	49061.141	28903
1444	0.452289	-78.268173	804090.586	50048.793	28902
1445	0.445266	-78.268645	804038.296	49271.632	28902
1446	0.445946	-78.264666	804481.525	49347.043	28902
1447	0.447517	-78.267119	804208.198	49520.783	28901
1448	0.452035	-78.267884	804122.791	50020.699	28901
1449	0.445059	-78.267466	804169.644	49248.775	28901
1450	0.449907	-78.269536	803938.848	49785.152	28900
1451	0.449123	-78.268211	804086.484	49698.453	28900
1452	0.448128	-78.266678	804257.3	49588.413	28899
1453	0.447854	-78.26659	804267.114	49558.097	28899
1454	0.452077	-78.266804	804243.1	50025.392	28899
1455	0.448216	-78.266215	804308.874	49598.17	28899
1456	0.449732	-78.266569	804269.376	49765.911	28899
1457	0.445365	-78.265521	804386.302	49282.716	28898
1458	0.449286	-78.267107	804209.462	49716.536	28898
1459	0.451853	-78.266834	804239.767	50000.603	28898
1460	0.447007	-78.267228	804196.077	49464.344	28897
1461	0.44726	-78.26506	804437.579	49492.43	28897
1462	0.451502	-78.268667	804035.587	49961.686	28897
1463	0.451003	-78.267386	804178.31	49906.522	28897
1464	0.44772	-78.265722	804363.814	49543.305	28897
1465	0.451391	-78.271188	803754.756	49949.297	28896
1466	0.450547	-78.269498	803943.055	49855.974	28896
1467	0.448681	-78.273733	803471.359	49649.313	28896
1468	0.444917	-78.266322	804297.09	49233.109	28896
1469	0.450624	-78.266394	804288.834	49864.624	28896
1470	0.446499	-78.268107	804098.178	49408.094	28895
1471	0.445044	-78.269141	803983.051	49247.046	28895
1472	0.451829	-78.267123	804207.574	49997.935	28895
1473	0.45169	-78.266633	804262.165	49982.575	28895
1474	0.44671	-78.267715	804141.838	49431.459	28894
1475	0.451524	-78.268779	804023.11	49964.116	28894
1476	0.444733	-78.26836	804070.066	49212.664	28894
1477	0.443475	-78.26892	804007.735	49073.434	28894
1478	0.44641	-78.264474	804502.894	49398.396	28894
1479	0.448023	-78.265098	804433.315	49576.86	28893

Station ID	Latitude	Longitude	UTM_X	UTM_Y	Magnetic_data (nT)
1480	0.449778	-78.26607	804324.962	49771.022	28893
1481	0.449661	-78.266206	804309.817	49758.07	28893
1482	0.449268	-78.26799	804111.097	49714.507	28893
1483	0.449143	-78.267672	804146.527	49700.688	28893
1484	0.445269	-78.266957	804226.337	49272.034	28893
1485	0.446833	-78.266038	804328.649	49445.139	28892
1486	0.44737	-78.272811	803574.123	49504.281	28892
1487	0.450924	-78.267538	804161.381	49897.774	28892
1488	0.449499	-78.266363	804292.334	49740.137	28892
1489	0.445179	-78.268063	804103.134	49262.029	28892
1490	0.443659	-78.268251	804082.253	49093.823	28891
1491	0.451831	-78.266392	804289.006	49998.187	28891
1492	0.449616	-78.26583	804351.705	49753.106	28890
1493	0.447445	-78.265663	804370.398	49512.877	28889
1494	0.450064	-78.267728	804140.251	49802.601	28889
1495	0.449749	-78.267188	804200.419	49767.766	28889
1496	0.45246	-78.268605	804042.454	50067.698	28888
1497	0.444462	-78.267568	804158.306	49182.708	28888
1498	0.444348	-78.268312	804075.429	49170.063	28888
1499	0.449639	-78.26741	804175.693	49755.585	28887
1500	0.444794	-78.267998	804110.39	49219.429	28887
1501	0.450537	-78.269864	803902.283	49854.852	28886
1502	0.447595	-78.267203	804198.837	49529.411	28885
1503	0.447231	-78.266009	804331.863	49489.182	28885
1504	0.443661	-78.268755	804026.108	49094.023	28884
1505	0.450893	-78.26726	804192.351	49894.355	28883
1506	0.449361	-78.266549	804271.619	49724.858	28883
1507	0.447489	-78.265924	804341.321	49517.735	28882
1508	0.451865	-78.269928	803895.099	50001.801	28882
1509	0.450842	-78.266098	804321.799	49888.76	28882
1510	0.451924	-78.266205	804309.834	50008.486	28882
1511	0.447661	-78.2655	804388.547	49536.785	28881
1512	0.445891	-78.264401	804511.048	49340.968	28880
1513	0.459111	-78.27107	803767.578	50803.57	28879
1514	0.449014	-78.268196	804088.16	49686.392	28879
1515	0.451911	-78.267403	804176.379	50006.997	28879
1516	0.447829	-78.267062	804214.535	49555.311	28878
1517	0.449453	-78.265614	804375.774	49735.078	28878
1518	0.444655	-78.2717	803697.998	49203.895	28878
1519	0.443509	-78.268537	804050.399	49077.213	28878
1520	0.447355	-78.267306	804187.373	49502.849	28877
1521	0.451245	-78.267916	804119.259	49933.279	28877
1522	0.444019	-78.268311	804075.554	49133.657	28877
1523	0.451612	-78.271745	803692.698	49973.729	28875
1524	0.445944	-78.268154	804092.965	49346.677	28875
1525	0.451549	-78.271513	803718.545	49966.768	28873
1526	0.451041	-78.266209	804309.425	49910.776	28873
1527	0.446951	-78.267636	804150.628	49458.13	28872
1528	0.450784	-78.266897	804232.793	49882.308	28872
1529	0.444891	-78.268577	804045.886	49230.138	28872
1530	0.451967	-78.266038	804328.436	50013.251	28872
1531	0.451243	-78.271399	803731.257	49932.912	28871
1532	0.444007	-78.269164	803980.531	49132.294	28871

Station ID	Latitude	Longitude	UTM_X	UTM_Y	Magnetic_data (nT)
1533	0.4495	-78.265192	804422.782	49740.296	28871
1534	0.447541	-78.272587	803599.069	49523.212	28870
1535	0.449527	-78.266776	804246.325	49743.218	28870
1536	0.447929	-78.265682	804368.262	49566.434	28869
1537	0.451082	-78.267776	804134.861	49915.247	28869
1538	0.450824	-78.266651	804260.196	49886.745	28869
1539	0.452079	-78.26708	804212.353	50025.601	28868
1540	0.444632	-78.267778	804134.905	49201.511	28868
1541	0.451061	-78.267109	804209.165	49912.951	28867
1542	0.444956	-78.268208	804086.99	49237.346	28867
1543	0.445787	-78.268373	804068.575	49329.295	28867
1544	0.450318	-78.269385	803955.652	49830.638	28866
1545	0.449475	-78.267223	804196.532	49737.445	28866
1546	0.444402	-78.267934	804117.536	49176.054	28866
1547	0.443526	-78.26938	803956.489	49079.059	28866
1548	0.452706	-78.276226	803193.477	50094.6	28864
1549	0.44935	-78.267748	804138.052	49723.591	28864
1550	0.444851	-78.26764	804150.269	49225.751	28864
1551	0.445007	-78.267851	804126.757	49243.005	28864
1552	0.446362	-78.269892	803899.337	49392.86	28864
1553	0.448963	-78.271055	803769.673	49680.629	28861
1554	0.443869	-78.268089	804100.291	49117.067	28861
1555	0.449648	-78.265042	804439.486	49756.68	28857
1556	0.449927	-78.268265	804080.435	49787.418	28856
1557	0.450595	-78.266879	804234.806	49861.395	28853
1558	0.443306	-78.268707	804031.469	49054.742	28850
1559	0.4449	-78.265939	804339.757	49231.243	28850
1560	0.445435	-78.267829	804129.19	49290.367	28848
1561	0.445097	-78.265471	804391.883	49253.062	28847
1562	0.449562	-78.266976	804224.044	49747.082	28843
1563	0.447009	-78.266174	804313.491	49464.609	28841
1564	0.449426	-78.266008	804331.883	49732.074	28841
1565	0.444193	-78.268093	804099.832	49152.92	28840
1566	0.448117	-78.265212	804420.611	49587.257	28839
1567	0.444679	-78.267424	804174.338	49206.727	28835
1568	0.444296	-78.267351	804182.486	49164.348	28835
1569	0.449393	-78.267488	804167.014	49728.36	28834
1570	0.450594	-78.268706	804031.281	49861.208	28833
1571	0.451326	-78.268134	804094.97	49942.233	28833
1572	0.45919	-78.270845	803792.639	50812.322	28830
1573	0.445641	-78.264821	804464.271	49313.286	28830
1574	0.449974	-78.267977	804112.516	49792.631	28829
1575	0.4457	-78.268972	804001.851	49319.643	28829
1576	0.444926	-78.265694	804367.048	49234.13	28825
1577	0.444245	-78.267719	804141.493	49158.69	28823
1578	0.444028	-78.267875	804124.124	49134.671	28821
1579	0.445445	-78.265002	804444.115	49291.59	28820
1580	0.448046	-78.268506	804053.666	49579.263	28806
1581	0.448872	-78.268442	804060.761	49670.668	28805
1582	0.445692	-78.264561	804493.232	49318.941	28803
1583	0.445501	-78.264715	804476.085	49297.799	28802
1584	0.44688	-78.269374	803957.02	49450.202	28796
1585	0.445681	-78.267502	804165.608	49317.602	28795

Station ID	Latitude	Longitude	UTM_X	UTM_Y	Magnetic_data (nT)
1586	0.445204	-78.265159	804426.636	49264.915	28794
1587	0.448309	-78.264878	804457.811	49608.517	28790
1588	0.444071	-78.267507	804165.117	49139.444	28789
1589	0.444718	-78.265635	804373.629	49211.116	28780
1590	0.443912	-78.26729	804189.297	49121.859	28780
1591	0.444134	-78.267138	804206.221	49146.431	28779
1592	0.443956	-78.26693	804229.399	49126.742	28759
1593	0.452961	-78.276625	803149.018	50122.8	28747
1594	0.445184	-78.264928	804452.37	49262.712	28735
1595	0.444821	-78.265385	804401.475	49222.524	28734
1596	0.449379	-78.272517	803606.791	49726.601	28723
1597	0.444962	-78.265084	804435	49238.139	28722
1598	0.443736	-78.26708	804212.698	49102.392	28715
1599	0.452762	-78.276703	803140.337	50100.776	28708
1600	0.448385	-78.269225	803973.556	49616.746	28672
1601	0.443791	-78.266718	804253.022	49108.493	28665
1602	0.44357	-78.266872	804235.876	49084.031	28643
1603	0.448801	-78.269367	803957.72	49662.773	28631
1604	0.450229	-78.267495	804166.2	49820.869	28627
1605	0.443407	-78.266663	804259.165	49066.003	28626
1606	0.451671	-78.272157	803646.799	49980.241	28620
1607	0.451649	-78.272161	803646.355	49977.806	28600
1608	0.443623	-78.266507	804276.534	49089.911	28581
1609	0.443246	-78.266454	804282.454	49048.196	28539
1610	0.44346	-78.266293	804300.38	49071.883	28530
1611	0.443296	-78.266075	804324.672	49053.744	28520
1612	0.443082	-78.266242	804306.077	49030.057	28477
1613	0.452944	-78.276441	803169.516	50120.927	28465